AFRL-OSR-VA-TR-2013-0615

DEVELOPING IONIC LIQUID KNOW-HOW FOR THE DESIGN OF MODULAR FUNCTIONALITY, VERSATILE PLATFORMS, AND NEW SYNTHETIC METHODOLOGIES FOR ENERGETIC MATERIALS

ROBIN ROGERS

UNIV OF ALABAMA

12/05/2013
Final Report

AIR FORCE RESEARCH LABORATORY
AF OFFICE OF SCIENTIFIC RESEARCH (AFOSR)/RSA
ARLINGTON, VIRGINIA 22203
AIR FORCE MATERIEL COMMAND

REPORT DOCUMENTATION PAGE

1. REPORT DATE *(DD-MM-YYYY)*	2. REPORT TYPE	3. DATES COVERED *(From - To)*

4. TITLE AND SUBTITLE

5a. CONTRACT NUMBER

5b. GRANT NUMBER

5c. PROGRAM ELEMENT NUMBER

6. AUTHOR(S)

5d. PROJECT NUMBER

5e. TASK NUMBER

5f. WORK UNIT NUMBER

7. PERFORMING ORGANIZATION NAME(S) AND ADDRESS(ES)

8. PERFORMING ORGANIZATION REPORT NUMBER

9. SPONSORING / MONITORING AGENCY NAME(S) AND ADDRESS(ES)

10. SPONSOR/MONITOR'S ACRONYM(S)

11. SPONSOR/MONITOR'S REPORT NUMBER(S)

12. DISTRIBUTION / AVAILABILITY STATEMENT

13. SUPPLEMENTARY NOTES

14. ABSTRACT

15. SUBJECT TERMS

16. SECURITY CLASSIFICATION OF:			17. LIMITATION OF ABSTRACT	18. NUMBER OF PAGES	19a. NAME OF RESPONSIBLE PERSON
a. REPORT	b. ABSTRACT	c. THIS PAGE			19b. TELEPHONE NUMBER *(include area code)*

FINAL REPORT

Project Title:
Developing Ionic Liquid Know-How for the Design of Modular Functionality, Versatile Platforms, and New Synthetic Methodologies for Energetic Materials

Principal Investigator:
Robin D. Rogers
Center for Green Manufacturing and Department of Chemistry,
The University of Alabama, Tuscaloosa, AL 35487
Tel: (205) 348-4323; Email: **rdrogers@as.ua.edu**

Report Prepared by: Robin D. Rogers and Parker D. McCrary

Table of Contents

I. Objectives

The overall goal of our program is to develop an understanding of Energetic Ionic Liquids (EILs) at a modular level and share this data and understanding with those working to model, predict, or prepare Energetic Materials (EMs). The dual-functional nature of ILs and their inherent design flexibility allows for the custom synthesis of targeted structures tuned to exhibit the desirable chemical and physical properties sought by the Air Force in EMs. While *energetic* ILs are the specific goals of the AFOSR program, our role remains to guide the program with respect to design and control of *ionic liquid* behavior by developing new modular functionality, new versatile platforms, and new synthetic methodologies. We will pursue five distinct research objectives, emphasizing the first three.

Objective 1: Create a conceptual tool-box that can be accessed to modify IL structure through *either ion* to achieve target properties. Particular attention in this grant cycle will be paid to introduction of "trigger" (sensitive to external stimuli) and hypergolic groups. We will also work to relate <u>solid state</u> structures to the interactions in the liquid by developing the capability to crystallize very low melting ILs *in situ* on the diffractometer and focusing on <u>deliberate crystallization</u> of EILs, thus providing an entire new range of data for predictive efforts.

Objective 2: Develop and showcase new multicyclic platforms for the synthetic design of IL-based structures that are currently unknown or underutilized. A new design platform will be utilized for symmetric and asymmetric bridged multicyclic targets. We will investigate the capacity of these platforms to provide a link between solid polymeric energetic materials and ILs.

Objective 3: Introduce novel, post-synthetic methods for the modification of bulk properties *via* unique IL formulations. We will invoke the ionic nature of ILs to enhance performance of target materials using 'non-synthetic' techniques such as multiple ion mixtures, dissolution of neutral additives, and preparation of non-stoichiometric mixtures of EILs with their ion precursors.

Objective 4: Investigate IL-based synthetic strategies which might address scale-up and transitional issues. We will be cognizant of pertinent scale up and transition issues when synthesizing ILs.

Objective 5: Provide IL-based solutions that enable responsible custody with respect to current safety and detection needs. We will collect and organize the physical/chemical data to make it readily accessible should the need arise for new technologies for detection of EIL components.

Fundamental insight into IL chemistry will be gained, as well as a deeper understanding of how specific properties may be established in more advanced materials from IL-based synthetic strategies.

II. *Status of Effort*

To address **Objective 1** of the proposed work, the dual-functional nature of ILs has been exploited towards selective formation of new salts, where cation/anions are varied by structural modification and or ion exchange techniques. New classes of azolium azolate salts featuring nitro functional groups, nitrate anions, and dicyanamide anions have been synthesized and their energetic properties have been determined. As electron-withdrawing groups (*e.g.*, nitro, nitrile) directly appended to the azole core tends to deactivate the nucleophilicity of the ring for further substitution (*e.g.*, *N*-alkylation to form quaternized azolium cation), the synthesis of ILs with either stable azolate anions or cations with energetic group appended to *N*-alkyl chains both represented strategies for EIL synthesis to circumvent synthetic obstacles.

Special attention has also been placed in developing new crystallographic methods for obtaining solid state structures of low melting EILs. Full details on the crystallographic results have been included in Appendix D. These solid state structures have served as models for the development of new synthetic pathways, achieving target properties, and understanding the interactions in the liquid state.

In order to address **Objective 2**, we developed a generalized synthetic platform that allowed us to construct *singly charged* multi-heterocycle cations and anions with design flexibility in (i) the identity and/or number of incorporated heterocycles, (ii) their charges, (iii) bridging units (*e.g.*, alkylene, alkylene ethers, etc.), and (iv) type and length of substituents appended to each heterocyclic core. Such a degree of synthetic flexibility provided a systematic approach to control symmetry, charge, and structure in the final product, while at the same time increasing the number of energetic azole cores per cation or anion. Such a strategy might be considered as intermediate between the well-studied single-azole ion ILs and solid state energetic polymers that utilize azole building blocks; thus allowing multi-heterocycle design while retaining the properties of a liquid.

Objective 3 was approached by preparing non-stoichiometric mixtures of nitric acid and hydroxyethylhydrazine, which provided a lower melting salt without sacrificing any energetic monopropellant performance. Additionally, nanoparticles were incorporated into EILs, which provided an increased energetic density, improved viscosity, or improved solution density based on the specific nanoparticle surface-IL interaction. These interactions were guided by typical metal-ligand binding theory or hydrogen bonding.

New synthetic methods were developed in response to **Objective 4** to synthesize azolium azolate salts to avoid potentially hazardous and expensive intermediates. Combining the concepts developed during our previous studies: (i) the utilization of azolate-based anions in the synthesis of ILs, (ii) the use of the zwitterionic 1,3-dimethyl-imidazolium-2-carboxylate IL precursors for the clean synthesis of 1,3-dimethyl-imidazolium salts, and (iii) the development of new [HCO$_3$]$^-$ IL precursors ([1,2,3-triMe-im]$^+$ and [*N,N*-diMe-Pyr]$^+$), it was possible to prepare a new family of azolate-based ILs in a fast and efficient fashion by reacting neutral azoles with the developed IL precursors. These routes provided an alternative for the formation of azolate salts, overcoming the previously experienced limitations related to ion exchange processes and allowing for much faster and more efficient routes to such compounds.

Additional care was also given to the development and report of energetic, physical, and chemical properties of our synthesized salts as proposed in **Objective 5**, which will allow the

data to remain freely accessible. Such key properties included: thermal stability, melting transitions, density, viscosity, impact sensitivity, ignition delay, and reactivity with oxidizers.

III. Major Achievements

1. Development of a systematic and versatile multi-heterocyclic synthetic platform combining a) classic alkylation reactions, b) Click Chemistry, and c) IL strategies to obtain highly variable anions, cations, and zwitterions for potential application as novel energetic ILs.
2. Demonstrated the safer use of an IL as a monopropellant.
3. Explored the synthesis of combustible protic EILs based on simple acid-base reactions.
4. Designed new halide and metal-free synthetic pathway to azolium azolate salts based on acid-base reaction between hydrogen carbonate salts or zwitterionic 1,3-dimethyl-imidazolium-2-carboxylate IL precursors and acidic azoles.
5. Prepared new composite IL-nanoparticle systems, which provided an increased energetic density, improved viscosity, or improved density based on the specific nanoparticle surface-IL interaction.

IV. Technical Summary of the Work Accomplished

4.1. <u>A General Design Platform for Ionic Liquid Ions Based on Bridged Multi-Heterocycles With Flexible Symmetry and Charge</u>

While others have been pursuing new examples of ILs that are energetic,[1] where the primary driver for the synthesis of these materials has been to include energetic ions with targeted physical properties, it has been our interest to understand the underlying science behind how proper combinations of performance and physicochemical characteristics might be incorporated into energetic ILs.[2-5] We have not tried to make energetic materials *per se*, but to understand the influence of added energetic components on IL behavior, and thus we have investigated structural modifications that afford predictable changes in both the properties and reactivity of the final materials,[6] while at the same time exploring new ion platforms and improved synthetic routes to them.[7]

We were interested in developing a generalized synthetic platform that would allow us to construct *singly charged* multi-heterocycle cations and anions with design flexibility in (i) the identity and/or number of incorporated heterocycles, (ii) their charges, (iii) bridging units (e.g., alkylene, alkylene ethers, etc.), and (iv) type and length of substituents appended to each heterocyclic core. Such a degree of synthetic flexibility would provide a systematic approach to control symmetry, charge, and structure in the final product, while at the same time increasing the number of energetic azole cores per cation or anion. Such a strategy might be considered as intermediate between the well-studied single-azole ion ILs and solid state energetic polymers that utilize azole building blocks;[8] thus allowing multi-heterocycle design while retaining the properties of a liquid.

To address this challenge, we propose a systematic and versatile multi-heterocyclic synthetic platform combining a) classic alkylation reactions, b) Click Chemistry, and c) IL strategies (Figure 4.1.1) to obtain highly variable anions, cations, and zwitterions for potential application as novel energetic ILs. Such a generalized approach, allows (i) simple formation of functionalized azoles capable of further cyclization, (ii) facile cyclization of functionalized azoles to form bridged multi-heterocyclic compounds, and (iii) utilization of IL-based strategies to access zwitterions, neutral molecules, anions, and cations from common multi-heterocyclic precursors. Here we illustrate the utility of this approach with the synthesis and characterization of bicyclic and tricyclic precursors and their use in the formation of ILs.

Synthetic Design Strategy. The overall design strategy begins (Step A, Figure 4.1.1) with selection of a starting azole core (Az) which is alkylated one or more times with one or more alkylating agents containing a "clickable" unit (RX and/or R′X, where X = cyano, azo, etc.). (Although the core heterocycle could itself be formed via Click chemistry, a general class of 3+2 dipolar cycloaddition reactions that occur with fast reaction times, mild conditions, and good to excellent yields,[9] we have chosen to start the discussion of our platform approach from the point where most IL researchers entered the field; by alkylation of an azole core.) The number of alkylations corresponds to the number of desired heterocycles to be appended to the core; the alkyl group (R) in the alkylating agent determines the length and nature of the bridges between

the heterocycles; and the clickable reagent (X) determines the identity of the appended heterocyles after 'Clicking' (Step B Figure 4.1.1).
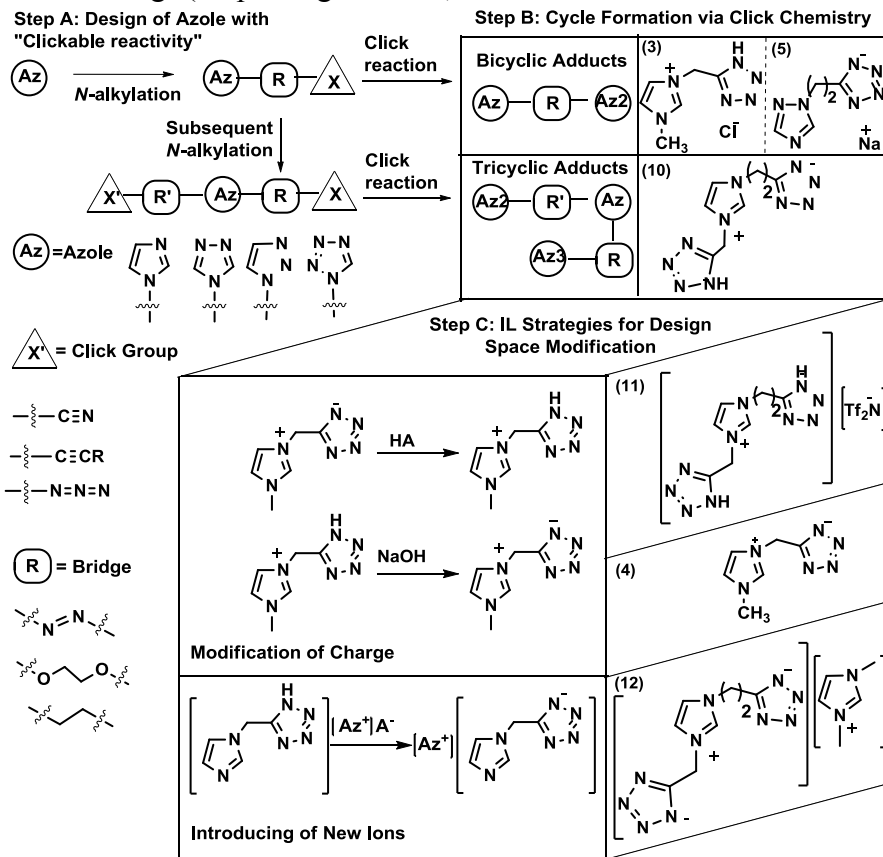
Figure 4.1.1 A flexible IL design platform for the synthesis of multi-heterocyclic targets.

Step C implements IL-based strategies to obtain the final products. For example, the overall *charge* may be altered through simple protonation/deprotonation, alkylation, etc., resulting in anionic, cationic, zwitterionic, or even neutral products. Additional modification (e.g., alkylation/acylation) of the new heterocyclic cores can introduce new functionalities to tune the final properties of the product or introduce new reactive sites for additional synthetic operations.

The design strategy for a systematic and versatile multi-heterocyclic synthetic platform, allows for formation of highly variable anions, cations, and zwitterions for potential application as novel IL components or precursors. We believe that the ability to extend the number, identity, and bridging of heterocycles, especially to *asymmetric, singly charged molecular ions* will be a more useful strategy to make ILs than any of the known oligomeric approaches to multi-heterocyclic IL ions. We have demonstrated this here with low-valent, bridged bi- and tricyclic compounds including the synthesis of the crystalline zwitterion 1-(2-(5-tetrazolidyl)ethyl)-3-(5-1*H*-tetrazolyl)methylimidazolium and its conversion into room temperature ionic liquids as either the cation or the anion. Given the richness of this design space – from available multi-heterocyclic precursors to the diversity enabled by IL-based modifications – we foresee this platform as a powerful tool that may be utilized towards new multi-heterocyclic IL targets of yet unlimited scope or even as an alternative to some of the polymer synthesis approaches to energetic oligomers.

7

4.2. Catalytic ignition of ionic liquids for propellant applications

Shamshina, J. L.; Smiglak, M.; Drab, D. M.; Parker, T. G.; Dykes, Jr., H. W. H.; Di Salvo, R.; Reich, A. J.; Rogers, R. D. "Catalytic ignition of ionic liquids for propellant applications," *Chem. Commun.* **2010**, *46*, 8965-8967.

Numerous studies have now been conducted on ILs for propellant applications, where it has been shown that IL salts can perform quite well with the addition of a suitable oxidizer.[10] On the contrary, the literature provides virtually no information about the catalytic decomposition of *pure* ILs on solid catalysts. We were thus curious to know if it was possible to find an IL that would decompose when in contact with a catalyst as observed for neutral molecular propellants such as hydrazine.

There are only a few known classes of hypergolic fuels that do not require use of an external oxidant (so-called *monopropellants*).[11] Moreover, current understanding of hypergolic processes does not yet allow one to predict which compounds will be hypergolic on contact with a particular catalyst.[12] Hydrazine, NH_2NH_2, and it's derivatives (e.g., monomethylhydrazine and dimethylhydrazine) are the most popular examples due to their ready exothermic decomposition on alumina supported iridium catalysts (Shell-405, S-405, KC-12 GA)[13,14] to produce a 1000 °C mixture of nitrogen, hydrogen, and ammonia gases.[15] However, the acute vapor toxicity of hydrazine, high vapor pressure, and small liquidus range (mp = 1 °C, bp = 113.5 °C) are severe drawbacks that have prompted studies towards hydrazine substitutes. Hydrazine's high vapor pressure restricts the safe working concentration to 0.01 ppm.

In contrast, 2-hydroxyethylhydrazinium (HEH) salts are ILs that are thermally stable, possess substantially lower toxicity than that of other hydrazinium salts,[16] and have been predicted to provide higher performance.[17] Nonetheless, the available literature on HEH salts is limited to the use of these salts with the addition of NTO or RFNA.[18] For monopropellant applications of HEH, the addition of oxidizers is necessary to achieve total combustion since HEH contains carbon and the oxygen balance is below zero.

Given the suggested promising properties of HEH-derivatives and the limited available data[19] for nitrate salts of HEH, we chose this platform to test our hypothesis that a neutral propellant when converted to an IL could still ignite when placed in contact with the catalyst. (Catalysts were chosen for study based on their use in the propellant field with particular emphasis on Shell 405, with its ability to rapidly and reliably ignite and decompose hydrazine at relatively low temperatures.[20])

Synthesis and Characterization (Scheme 4.2.1). 2-Hydroxyethylhydrazinium nitrate ([HEH][NO$_3$]) and 2-hydroxyethylhydrazinium dinitrate ([HEH][NO$_3$]$_2$) were prepared as reported by Drake by reaction of aqueous nitric acid and HEH followed by removal of the solvent. Differential Scanning Calorimetry (DSC) analysis of [HEH][NO$_3$] indicated a glass transition temperature (T_g) of −56.9 °C and no other observable transition, while [HEH][NO$_3$]$_2$ was found to have a melting point of 67 °C and when supercooled a T_g of -47.9 °C. [HEH][NO$_3$] was the most thermally stable with $T_{5\%dec}$ (onset to 5% decomposition) = 193 °C, versus $T_{5\%dec}$ for [HEH][NO$_3$]$_2$ (a solid) = 62 °C. Under these experimental conditions, $T_{5\%dec}$ for HEH was determined to be 102 °C, however, this is associated with its boiling point (113 °C) rather than

thermal decomposition. These data indicate substantial improvement (ca. 100 $^{\circ}$C) in the range of use for [HEH][NO$_3$] over HEH, while the thermal stability of [HEH][NO$_3$]$_2$ was found to be substantially lower than that of [HEH][NO$_3$] or HEH.
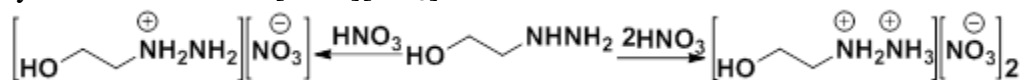
Scheme 4.2.1 Synthesis of salts based on hydroxyethylhydrazine

The longer term stability (measured by heating each sample to 75 $^{\circ}$C for 24 h[21]) decreases in the order [HEH][NO$_3$] > [HEH][NO$_3$]$_2$ > HEH. [HEH][NO$_3$] lost 24% of its mass after 24 h, with ca. 8% of this from loss of water (Karl-Fisher titration). [HEH][NO$_3$]$_2$ lost 43% of its mass, of which ca. 4% was water. (It should be noted that even substantial dilution of hydrazine with water results in mixtures that function satisfactorily as rocket fuels, and the resultant systems retain the characteristics of hydrazine.[22]) By comparison, HEH lost 88% mass under these conditions, underscoring the anticipated improvements in lowering the volatility of HEH by converting to its salt forms.

Catalyst Selection. The initial screening for catalytic reactivity was conducted at ambient temperature and pressure. Approximately 50 mg of [HEH][NO$_3$] or [HEH][NO$_3$]$_2$ was added to test tubes loaded with 10 mg of catalyst, which included Pd, Sm, Fe, Raney Ni, Pt foil, In foil, oxygen-free Cu (OFC), stainless steel, and Shell 405 (Ir on alumina 32%). Changes were visually monitored over a 3 h period and then examined again after 24 h. The only catalyst with observable activity (the formation of bubbles) was Shell 405.

Reactivity to Shell 405 (Fig. 4.2.1). Reactions of HEH, [HEH][NO$_3$], and [HEH][NO$_3$]$_2$ with preheated Shell 405 (20-30 mesh, 32 wt. % Ir) were conducted by adding an exact amount of each to preweighted catalyst on a Fischer watch glass. Shell 405 was preheated in a sand bath, at atmospheric pressure, to temperatures of 50, 100, 150, or 200 $^{\circ}$C. The HEH, [HEH][NO$_3$], and [HEH][NO$_3$]$_2$ were preheated to the same temperatures as the catalyst and added dropwise to the preheated Shell 405 via Pauster pipettes. ([HEH][NO$_3$]$_2$ at 50 $^{\circ}$C was added as a solid since this is below its melting point.) A high speed camera (Redlake's MotionPro® HS 4) recording 500 frames/s was used to determine the ignition delay times (ID).
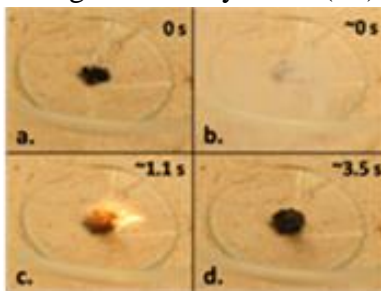
Figure 4.2.1 Drop test: a) addition of [HEH][NO$_3$]$_2$ to Shell 405 at 200 $^{\circ}$C, b) smoke, c) flame, d) residual catalyst.

First Drop (Clean Catalyst) Tests. At 50 $^{\circ}$C, the reactions proceeded extremely slowly with only formation of bubbles to indicate any reaction at all. Virtually all of the mass of sample added remained on the catalyst after ~4 h. The reactions were substantially faster at 100 $^{\circ}$C and above where, after a delay, visible white smoke and in the case of [HEH][NO$_3$]$_2$, flame were observed. HEH had the shortest delay time to smoke evolution when compared to either salt. [HEH][NO$_3$]$_2$ had shorter smoke delay than [HEH][NO$_3$], though longer than HEH. However,

[HEH][NO$_3$]$_2$ catalytically ignited at 100 ^{o}C after ~1100 ms. The major differences observed between experiments included the time delay to and duration of smoke or flame after addition of IL to the catalyst and the mass of IL consumed in the reaction (measured as the residual mass left on the catalyst).

At temperatures of 150 ^{o}C and above, all three reactions were immediate, with the smoke delay below 100 ms, and formation of a visible caramel-like brown char, that most likely is the result of incomplete combustion or decomposition and formation of soot. This residue may be responsible for poisoning of the catalyst during consecutive ignition cycles.

Multiple Drop (Catalyst Recycle) Tests. Addition of a second and third drop to each catalyst was studied at 50, 100, and 150 ^{o}C. Approximately 10 min after each first or second drop test, and after reheating each catalyst to the required temperature, an additional portion was added and the results noted. In general, the qualitative results follow those reported above for the addition of the first drop.

At 150 ^{o}C, upon addition of the 2nd and 3rd drop of [HEH][NO$_3$] or [HEH][NO$_3$]$_2$, smoke and ignition were observed, however, the delay times for appearance of both smoke and flame increased with every subsequent IL addition. The results suggest that although the catalyst is still active after initial reaction, activity is decreased. This might be due to the interference of possible char which was noted by color, although as noted in Table 1, in most cases no char mass could be measured.

Catalytic Ignition. Catalytic ignition, with an observable flame, was noted for [HEH][NO$_3$] and [HEH][NO$_3$]$_2$. [HEH][NO$_3$]$_2$ appeared the most reactive with catalytic ignition for all drops at 100 ^{o}C and above (although longer delay times were noted during each recycling run). [HEH][NO$_3$] was less reactive, but did demonstrate catalytic ignition at 150 ^{o}C with addition of the 1st, 2nd, and 3rd portions. In comparison, HEH showed no such reactivity toward Shell 405 at either temperature.

Summary. Two ILs, 2-hydroxyethylhydrazinium nitrate (a room temperature liquid, T$_g$ = −56.9 ^{o}C) and hydroxyethylhydrazinium dinitrate (a white solid, T$_m$ = 67 ^{o}C), catalytically decompose on Shell 405 catalyst, suggesting potential applications as hydrazine alternatives in monopropellant applications. Compared with the parent molecular liquid, hydroxyethylhydrazine, total reactivity decreases in the order [HEH][NO$_3$]$_2$ ~ [HEH][NO$_3$] >> HEH. Catalytic ignition with an observable flame was noted for both [HEH][NO$_3$] and [HEH][NO$_3$]$_2$ at 150 ^{o}C and above, while HEH showed no such reactivity at either temperature. It was noted that the Shell 405 catalyst remains active after the initial reaction, although catalytic activity decreases.

Use of ILs in propellant applications could possibly increase safety by reducing the hazards currently associated with handling of neutral, volatile forms of commonly used propellants. The ILs studied here possess relatively high thermal stabilities (>100 ^{o}C above the boiling point of hydrazine) and substantially decreased volatility. However, optimization of these salts and discovery of new catalytically ignitable derivatives could produce even better results. Along those lines, we intend to study the use of 'oligomeric anions'[23] in nonstoichiometric mixtures of HEH and HNO$_3$ (as we have suggested for pharmaceuticals[24]) to increase liquidity while allowing fine tuning of the oxygen content.

4.3 <u>**Synthesis of N-cyanoalkyl-functionalized imidazolium nitrate and dicyanamide ionic liquids with a comparison of their thermal properties for energetic applications**</u>

Work in our group has been focused not on the synthesis of EMs per se but, rather, on the understanding of IL chemistry at a deeper level. It has long been an interest to identify IL structural patterns with the goal of accessing targeted properties in a systematic and predictable fashion. Previously, we have synthesized azole-based ILs with energetic substituents (e.g., nitro-, amino-, cyano- groups) to identify the effect of azole type and ring substituents on thermal properties of resultant ILs.[25-27] In another study, we established a strategy to incorporate energetic functional groups into either cation or anion, with the consequence that electron-withdrawing nitro and cyano- groups were observed to deactivate azoles toward formation of cations.[28][29][30]

Continuing the above efforts, in this paper, we report systematic studies of thermal properties for two series of N-cyanoalkyl-functionalized imidazolium salts. Although there have been reported examples of N-cyanoalkyl-functionalized imidazolium halides, nitrates, and dicyanamides, to the best of our knowledge these classes have not been examined systematically or comparatively with respect to homologous changes in structure.

Synthetic Design. Three types of systematic modifications to N-cyanoalkylfunctionalized imidazoliums have been made here. First, we believed that the length and branching of the alkyl chains in the N-cyanoalkyl-functionalized imidazolium cation would influence the liquid state, as others have reported melting point reduction as alkyl length increases.[31] We also hypothesized that the melting points of N-cyanoalkyl-functionalized imidazolium salts would be higher when compared with 1,3-dialkylimidazolium analogs, due to possible intra- and intermolecular organization from the p-electron system and lone pair electrons available in the cyano group.

Secondly, for the same reason, we varied the N-alkyl substituent on the imidazole ring to probe for trends similar to those reported in the literature, where melting points typically decrease and thermal stabilities remain largely unaffected from N-methyl to N-butyl substitution.[32] Lastly, we investigated the effect of different energetic anions—nitrate and dicyanamide. Nitrate was chosen because of the oxidizing nature of the $[NO_3]^-$ anion, which facilitates thermal decomposition of the salt.[33] In turn, dicyanamide anions were expected to decrease melting points and increase thermal stability when compared to halide analogs.[34] In addition, the nitrate and dicyanamide anions were selected for their reputed IL-forming abilities and physicochemical properties suitable for EILs. These nitrile-functionalized salts are also excellent precursors to novel mixed heterocyclic species, as we have recently illustrated.[35]
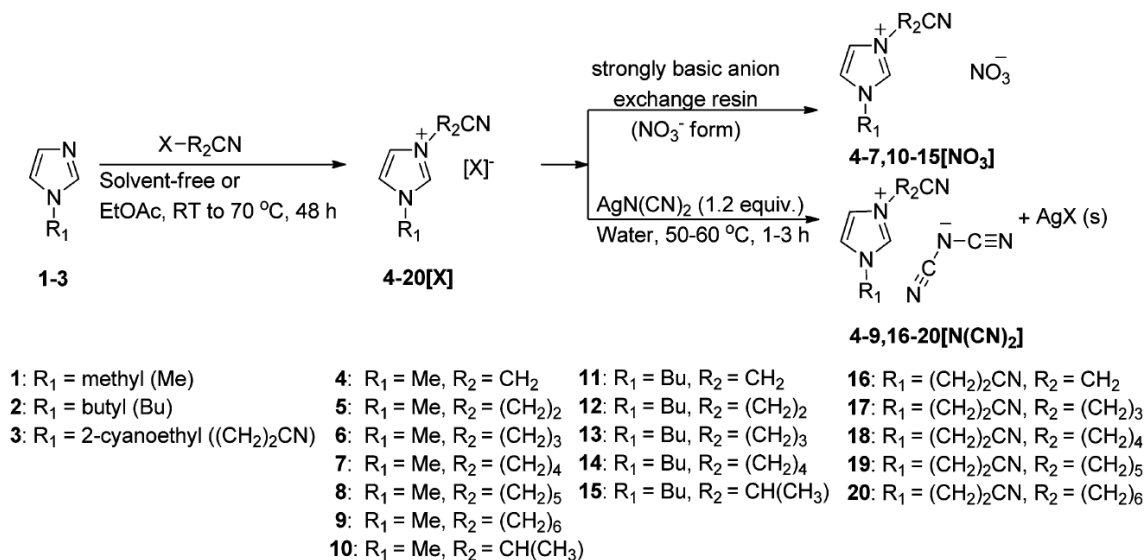
Scheme 4.3.1 Overall Synthetic Scheme

1: R_1 = methyl (Me)
2: R_1 = butyl (Bu)
3: R_1 = 2-cyanoethyl (($CH_2)_2CN$)

4: R_1 = Me, R_2 = CH_2
5: R_1 = Me, R_2 = $(CH_2)_2$
6: R_1 = Me, R_2 = $(CH_2)_3$
7: R_1 = Me, R_2 = $(CH_2)_4$
8: R_1 = Me, R_2 = $(CH_2)_5$
9: R_1 = Me, R_2 = $(CH_2)_6$
10: R_1 = Me, R_2 = $CH(CH_3)$

11: R_1 = Bu, R_2 = CH_2
12: R_1 = Bu, R_2 = $(CH_2)_2$
13: R_1 = Bu, R_2 = $(CH_2)_3$
14: R_1 = Bu, R_2 = $(CH_2)_4$
15: R_1 = Bu, R_2 = $CH(CH_3)$

16: R_1 = $(CH_2)_2CN$, R_2 = CH_2
17: R_1 = $(CH_2)_2CN$, R_2 = $(CH_2)_3$
18: R_1 = $(CH_2)_2CN$, R_2 = $(CH_2)_4$
19: R_1 = $(CH_2)_2CN$, R_2 = $(CH_2)_5$
20: R_1 = $(CH_2)_2CN$, R_2 = $(CH_2)_6$

The starting halide salts were obtained by alkylating commercially available methyl-, butyl-, or 2-cyanoethyl-substituted imidazole (Scheme 4.3.1: **1**, **2**, **3**, respectively) with haloalkylnitriles via a classical quaternization reaction. Given the wide variety of commercially available haloalkylnitriles, this was considered a logical starting point for the synthesis of imidazolium salts with variable N-cyanoalkyl side-chain lengths as described here. The N-cyanoalkyl-functionalized imidazolium nitrate (**4–7**, **10-15**[NO_3]), and dicyanamide (**4–9**, **16-20**[DCA]) salts were prepared by metathesis of the analogous halides (**4-20**[X]), either by using an ion exchange resin (nitrate salts) or a silver salt (dicyanamide salts).

Halide Precursor Synthesis. The 17 N-cyanoalkyl-functionalized imidazolium halide salts (4-20[X]) were synthesized according to literature protocols,[36,37] where 1-alkylimidazole starting materials (1–3) were alkylated with haloalkylnitriles generally under solvent-free conditions at 70 $^\circ$C for 48 h in a sealed, high-pressure vial (except as noted below).

Nitrate Salt Synthesis. Nitrate salts **4–7**, **10-15**[NO_3] were prepared from the halide precursors using the strongly basic anion exchange resin BioRad AG 1-X8 (100–200 mesh with 8% divinylbenzene copolymer cross-linkage). The resin has an exchange capacity of 2.6 meq/g dry resin and an appropriate amount of resin was prepared to exchange 3.2 to 6.4 mmol of halide precursor. The commercially available chloride resin was converted to (NO_3^-) -form following the manufacturer's protocol, where the resin was loaded into a column (1 cm diameter - 10 cm tall) and washed with 5 bed volumes of 0.5 N sodium nitrate solution. To check for the completeness of the nitrate exchange, the presence of halide in the eluted solution was spot checked frequently with a 1.0 M silver nitrate solution. When no halide was indicated as evident by the lack of white, cloudy precipitate, final conditioning of the nitrate-exchanged resin column was completed by washing with 2 bed volumes of deionized water.

With the (NO_3^-)-form of the resin in hand, halide samples were dissolved in 100 mL of deionized water and eluted through the column followed by an additional 2 bed volumes of deionized water in the final rinse. For both nitrate loading and sample elution, the linear flow rate was maintained at approximately 2 cm min^{-1} through the bed volume. Each of the eluted

fractions was qualitatively screened for the presence of halide by spot-testing each eluted fraction with 1.0 M silver nitrate solution. Once separated, the 'halide-free' fractions were then purified by removal of water from the nitrate salts using an air stream followed by final drying under high vacuum for 24 h. The final 10 products **4–7**, **10-15**[NO$_3$] were obtained in fair to excellent yields (76–95%).

Dicyanamide Salt Synthesis. The dicyanamide salts **4–9**, **16-20**[DCA] were obtained by metathesis using silver dicyanamide. Each of the halide precursors (**4–9**, **16-20**[X]) was combined with a 10% excess of Ag[DCA] in deionized water and heated at 50 °C for 1 h. At the end of the metathesis reaction, the silver halide by-product was filtered, and subsequent evaporation of water from the filtrate using an air stream resulted in the 11 dicyanamide salts in fair to good yields (75–92%).

The focus for this work was to explore the synthesis of new 1-alkyl-3-cyanoalkylimidazolium ILs and to examine the effects of different cation substituent lengths (N-alkyl, N-cyanoalkyl), as well as energetic anions (nitrate, dicyanamide) on the observed thermal properties for each salt reported. Most of the 41 compounds prepared were ILs by definition (melting point below 100 °C). DSC analyses indicated several distinct classes of thermal behavior, including liquid–liquid transitions from failed attempts for the salt to crystallize from a supercooled phase within the timeframe of the DSC experiment. This thermal behavior was most frequently observed for compounds with long N-alkyl and N-cyanoalkyl chain lengths, as well as for most dicyanamide salts.

Thermal Analysis. Melting transitions were observed mainly for short-chain N-cyanoalkyl-functionalized cations, and the trends for T_g were generally the same with changing N-cyanoalkyl chain lengths. Nonetheless, the effects of N-alkyl chain length on T_g in general often depended on the type of anion present, where halides often showed a greater decrease in glass transition temperature than nitrates when comparing N-methyl versus N-butyl analogs. The dicyanamide salts had uniformly lower T_g values than analogous halides and nitrates, and the N-methyl-substituted dicyanamide ILs exhibited lower T_g values than N-(2-cyanoethyl)-functionalized salts.

There appeared to be considerably different trends in the observed $T_{5\%onset}$ values obtained by TGA with respect to changes in the N-alkyl substituent, the N-cyanoalkyl chain length, and the class of anion present. Halide salts with short N-cyanoalkyl substituents were less stable than the N-butyl analogs. Although the difference between N-methyl and N-butyl analogs of nitrate salts did not differ significantly, there was a much lower stability in short N-cyanoalkyl-functionalized nitrates in comparison with longer chain analogs.

For the dicyanamide-based ILs, all N-methyl substituted salts seemed to be very thermally stable in comparison with halides and nitrates. However, an exception to this was **5**[DCA] which showed a $T_{5\%onset}$ much lower than the others in the series. Recognizing the similarity in thermal decomposition behavior of **5**[DCA] with other N-(2-cyanoethyl)-functionalized compounds (**16-20**[DCA]), it is concluded that the cyanoethyl functionality may have a profound influence on the thermal decomposition pathway observed in the TGA experiment for these compounds. Furthermore, the prevalence of carbonaceous char for all compounds seemed to follow the anion trend [X]$^-$ < [NO$_3$]$^-$ < [DCA]$^-$, where all shorter N-cyanoalkyl functionalized ILs for halides and nitrates exhibited a characteristic 2-step decomposition pattern. The exception to

this was for N-(2-cyanoethyl)-functionalized nitrate salts (**5**[NO$_3$] and **12**[NO$_3$]), which showed complete decomposition without any residual material remaining.

Summary. Finally, in the case of the dicyanamide salts, the most char production was clearly evident, where up to 80% of the original weight was found to remain up to nearly 500 $^{\circ}$C. As such, the N-cyanoalkyl-substituted imidazolium salts studied here suggest potential use as building blocks for porous mesoscale materials that can be further functionalized to provide a versatile scaffold for numerous applications (e.g., heterogeneous catalysis, chemical separations, etc.).

4.4 Reactivity of N-cyanoalkyl-substituted imidazolium halide salts by simple elution through an azide anion exchange resin

Drab, D. M.; Kelley, S. P.; Shamshina, J. L.; Smiglak, M.; Cojocaru, O. A.; Gurau, G.; Rogers, R. D. "Reactivity of *N*-cyanoalkyl-substituted imidazolium halide salts by simple elution through an azide anion exchange resin," *Sci. China Chem.* **2012**, *55*, 1683-1687.

Building on the Click chemistry-based multi-heterocyclic IL synthesis platform discussed in section 4.1, we studied an ion exchange approach for synthesizing azolium azides as reported by Hawkins and coworkers. We believed such azide-based ILs would be interesting precursors for zwitterionic products by 1,3-dipolar cycloaddition between two ions of a single salt. In addition to improved atom economy (all atoms in the starting materials would be part of the zwitterionic product), the preparation of azolium azides with azide anion exchange resin has several other advantages over other azide anion sources, two of these being the simple regeneration of the supported reagent and a good exchange conversion (typically < 20 ppm of residual precursor anion).[38]
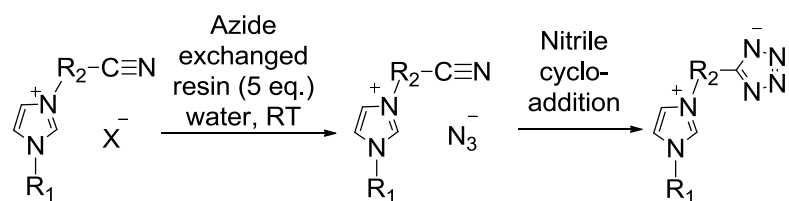
Scheme 4.4.1 Proposed synthesis of azide-based ILs as precursors for zwitterionic products

Structurally similar *N*-cyanoalkyl-functionalized imidazolium ionic liquids (ILs) were utilized for this investigation. Terminal nitrile-alkylene linkages included short linear (**2**[Cl] and **3**[Cl]), long linear (**1**[Br]), and branched (**4**[Br]) chains, as shown in Scheme 4.4.2. Under anion exchange conditions, it was found that the reaction outcome was greatly influenced by the structure of the starting imidazolium alkylnitrile (Scheme 4.4.2).
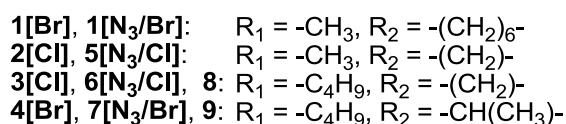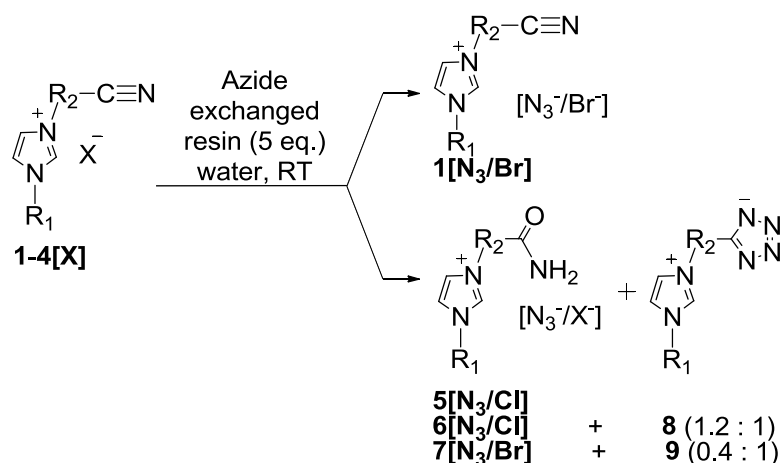
Scheme 4.4.2 Elution of *N*-cyanoalkyl-functionalized imidazolium halide salts (**1-4**[X]) on azide-exchanged resin columns resulted in cation **1** unchanged, cationic amide **5**, or a mixture of cationic amide with tetrazolate-functionalized zwitterion **6** + **8** or **7** + **9**.

Synthesis of Halide Precursors. Halide precursors **1-4**[X] were prepared as described in a previous study.[39] Amberlite IRA-400 strongly basic anion exchange resin (16-50 mesh, 8% styrene-divinylbenzene copolymer cross-linkage) was converted from the commercially available Cl⁻ form to the N_3^- form based on previously reported methods.[40] The desired anion exchange occurred in the case of **1**[Br], where the substrate contained an *n*-hexylene $(CH_2)_6$ linker between the terminal nitrile and imidazolium ring. However, under identical conditions, the unexpected formation of a mixture of tetrazole and hydrolysis products was observed for substrates with a single carbon atom between the nitrile and imidazolium ring, as is the case of **2**[Cl], **3**[Cl], and **4**[Br] (Scheme 4.4.2).

Use of "Click" Resin. Salts **1-4**[X] were introduced onto the N_3^--resin column (1 cm diameter; 8 cm length; prepared from 5 eq. of the resin) as *ca.* 5 mmol halide/15 mL water at a rate of 2 cm/min. After rinsing the column with an additional 2 bed volumes of water, the eluted fractions were combined and set to dry under air stream overnight, followed by additional drying under high vacuum for 24 h. The eluted products' structures were confirmed using NMR (both ^{1}H and ^{13}C) as well as FT-IR spectroscopy.

The precursor with the longest *N*-cyanoalkyl chain (-$(CH_2)_6$, **1**[Br]) did not react, and the anticipated azide-exchanged salt **1**[N_3] was isolated, albeit with some halide contamination. Appearance of a strong signal for the azide anion in the FT-IR (v_{max} = 2000-2005 cm^{-1}) suggested the formation of the desired salt. (The presence of azide groups in the FT-IR spectrum usually occurs at 2000-2100 cm^{-1}). Structural analysis *via* ^{1}H NMR indicated no change in the cation structure.

In contrast, halides with a single carbon linker (**2**[Cl], **3**[Cl], and **4**[Br]) reacted to form either pure amide (as in cation **5**) or a mixture of amide with tetrazole (as in (**6** + **8**) and (**7** + **9**) mixtures). The ^{1}H NMR spectra showed evidence for the formation of the amide group with a

15

doublet characteristic to the apparent separate signals for C(O)NH$_2$ due to restricted rotation of the amide group on the time-scale of the NMR experiment (*e.g.*, δ = 8.01 ppm, 7.52 ppm for 2H in **5**). The amide structure was confirmed by temperature gradient and deuterium exchange ^{1}H NMR experiments conducted on **5**.

The ^{13}C NMR spectra for the eluted products of **2**[Cl], **3**[Cl], and **4**[Br] also supported the formation of amide only (**5**) or an amide and tetrazole mixture (**6** + **8** and **7** + **9**), where cycloaddition was confirmed by the loss of the nitrile carbon signal (δ = 115-119 ppm) and the appearance of a new signal for the carbonyl C=O carbon (δ = 167 ppm). In the FT-IR spectrum, the presence of peaks characteristic for both the carbonyl (v_{max} = 1691 cm^{-1}) as well as the free azide anion (v_{max} = 2019 cm^{-1}) are in agreement with NMR data.

Unlike **2**[Cl], which forms only the amide cation **5**, **3**[Cl] and **4**[Br] formed mixtures of the amide cation and tetrazole zwitterion. Identification of the mixed products (**6** + **8** and **7** + **9**) was supported by the presence of both tetrazole carbon (δ = 156 ppm) and carbonyl carbon (δ = 167 ppm) peaks in the ^{13}C NMR spectrum. Furthermore, ^{1}H and ^{13}C NMR data indicate the presence of two distinct imidazolium-based products. The integration of ^{1}H NMR signals was used to estimate the ratio of amide to tetrazole product in each case (compare **5** (100% amide), **6** + **8** (1.2 to 1), and **7** + **9** (0.4:1)).

The reaction conditions were not optimized and the identity and ratios of the products greatly depended on structural variation of the starting materials. Thus, for the nitrile group in **1**[Br] that has the greatest separation from the imidazolium core, only the exchange of bromide anion for azide anion (**1**[N$_3$]) occurred, and no change in cation structure was observed. This may be explained in part by electronic factors, where the 6-carbon linkage weakens the electron-withdrawing effect of nitrogen in the imidazolium ring, since dipole induction rapidly diminishes with increasing distance.[41] Computational results also indicated that electron-withdrawing substituents activate the nitrile for both tetrazole formation as well as hydration,[42] where increasing the distance from the imidazolium cation renders the nitrile group unreactive.

By contrast, in substrates **2**[Cl], **3**[Cl], and **4**[Br], the nitrile group is separated from the imidazolium ring by a single carbon atom. Ratios of amide to tetrazole products in reactions of **3**[Cl] and **4**[Br] may depend on steric interactions between cyanoalkyl substituent and the imidazolium ring, where both substrates feature a short CH$_2$ spacer between the imidazolium ring and the CN group favorable towards formation of amide products in both cases. The presence of a branched CH(CH$_3$) spacer in **4**[Br] favors the formation of the more rigid and less sterically demanding tetrazole over the amide. The lower hydrolysis rate of **4**[Br] is also consistent with the electron-donating effect of the terminal CH$_3$-group in the branched (CH)CH$_3$ substituent, which contributes to a decrease in the electrophilicity of the nitrile carbon.

The structures of **2**[Cl] and **3**[Cl] are similar, yet each cation showed different reactivity in the formation of amide under the same elution conditions. Here, the difference in reactivities would appear to be related to the different lengths of the alkyl chains on imidazolium nitrogen N3. Aromatic alkyl substituents are more electron-donating with increasing chain length as a result of the alkyl inductive effect.[43] The longer alkyl side chain of **3**[Cl], thus, may donate electron density to reduce the reactivity of the nitrile carbon towards nucleophiles. This position is supported both by chemical theory[44] and experimental results, where longer reaction times and

higher temperatures are required for the hydrolysis of aromatic nitriles featuring longer alkyl substituents (*e.g.*, butyl *vs*. methyl).[45]

With possible coordination of the nitrile to the Lewis acidic cationic surface of the exchange resin polymer, cycloaddition of azide anion to nitriles results in the formed tetrazolate moieties. The reactivity of **4**[Br] to form the tetrazole product, **9**, over the hydration product, **7**, may occur due to the presence of the bromide anion as opposed to chloride anions in **2**[Cl] and **3**[Cl]. Bromide exchange for azide was expected to be complete, as the size and selectivity of azide is more similar to that of chloride, and both azide and chloride have lower affinity towards the resin than bromide. The prevalence of the tetrazolate product for **4**[Br] might also be a result of an electron-donating methyl substituent on the *α*-carbon.

Summary. Although the preparatory use of azide anion exchange resins has been reported for various synthetic applications,[46] this approach continues to be of high interest in discovering new and improved routes for the hydrolysis of nitriles. Typically, the use of high temperatures, metal catalysts or the persistence of sequential hydration to carboxylic acid products when reacting in aqueous media are technical challenges. Similarly, conventional methods to prepare tetrazoles from nitriles frequently use hazardous hydrazoic acid or require tedious separation of product from solvent, presenting challenges for scale-up considerations. The results reported here suggest that by proper selection of the reactive *N*-cyanoalkyl-functionalized imidazolium cations, the desired reactions can be accomplished by simple elution through an azide anion exchange resin under ambient conditions. A more systematic exploration of these preliminary trends between cation and anion structure and reactivity on azide anion exchange resin is currently underway.

4.5 Zinc-assisted synthesis of imidazolium-tetrazolate bi-heterocyclic zwitterions with variable alkyl bridge length

Drab, D. M.; Shamshina, J. L.; Smiglak, M.; Cojocaru, O. A.; Kelley, S. P.; Rogers, R. D. "Zinc-assisted synthesis of imidazolium-tetrazolate bi-heterocyclic zwitterions with variable alkyl bridge length," *Sci. China Chem.* **2012**, *55*, 1620-1626.

Our group has recently demonstrated a design platform to access multi-heterocyclic ionic liquids (MHILs) systematically by (i) synthesis of heterocycle-forming azoles, (ii) facile cyclization by Click methodology to form multi-heterocyclic structures,[47] and (iii) generation of MHILs via IL synthetic protocols.[48] Together with a 'dual-functional' approach to IL synthesis,[49,50] the MHIL platform provides new design options to target properties for high-performance applications, including potential alternatives to more traditional oligomeric energetic materials synthesis.[51]

Here we focus on two methodic changes for the synthesis of eight ZnX_2-complexed 1-(5-tetrazolidyl)-alkyl-3-alkylimidazolium structures (X = halide), including (i) variation of substituent on the nitrogen atom of the imidazolium core (methyl vs. butyl) and (ii) differences in alkyl linker chain length. Thus, from a series of N-methyl and N-butyl-functionalized imidazolium halide salts obtained in a previous study,[52] we selected our clickable starting materials. It was believed that the ionic nature of the N-cyanoalkyl-functionalized imidazolium salts would promote the Click synthesis of tetrazole rings under Sharpless conditions (e.g., $ZnBr_2$ catalyst in water under mild heating), where reactivity should not be restricted by alkyl substituent length (as is often the case with many neutral nitrile starting materials).[53] Furthermore, the ready formation of the Click products as water-insoluble ZnX_2 complexes should allow for easy product separation without the need for a more tedious, pH-sensitive workup protocol, often regarded as problematic for product recovery and purification.[54,55]

We have previously shown that Zn can be removed from the Click product by preparatory anion exchange resin technique to isolate either the cationic form of the ligand (as an NH-tetrazole-functionalized chloride salt) or as the tetrazolate-functionalized zwitterions. For this study, however, we report only the preparation of the ZnX_2-complexed Click products with variable bridge and N-alkyl substituent length that may easily serve as MHIL precursors.

Synthesis of Precursors. The precursors **1**-**8**[X] (Scheme 4.5.1) were easily obtained *via* alkylation reactions of *N*-methyl- or *N*-butylimidazole with commercially available haloalkylnitriles, where the details of the synthesis and characterization of these compounds has been previously reported. Reactions of **1**-**8**[X] with azide anion under Sharpless conditions resulted in the formation of target compounds, **9**-**16**.

Synthesis of Bridged Azoles. N-cyanoalkyl-N-alkylimidazoliuim halides (**1**-**8**[X]) were combined with sodium azide (1.1 equivalents) in a 100 mL round-bottom flask and dissolved in 50 mL of deionized water before adding zinc bromide (1.1 equivalents) and allowing the mixtures to stir at reflux for 24 h on a heated oil bath. During the reaction, the product formed as a white solid which separated from the aqueous solution, and further product precipitation occurred when allowing the reaction to cool to room temperature. To isolate the final product,

the solids were washed several times with water prior to filtration and drying in a furnace set to 60 °C for 24 h.

A subsequent kinetic experiment revealed that reflux is not necessary (vide infra), indicating that N-cyanoalkyl substituted imidazolium salts are very well-suited for Click synthesis of 5-tetrazoles – possibly due to the polar environment created by the ionic starting material.[56] The reaction proceeds smoothly in water with no need of additional co-solvent, where the resultant products (**9**-**16**) precipitate as solids, can be simply filtered from the reaction mixture, and dried with no other purification required.

|	
1-8[X]	**9-16**
1[Cl]*: R = -CH$_3$, n = 1	**9**: R = -CH$_3$, n = 1, 96%
2[Br]*: R = -CH$_3$, n = 2	**10**: R = -CH$_3$, n = 2, 38%
3[Cl]*: R = -CH$_3$, n = 3	**11**: R = -CH$_3$, n = 3, 46%
4[Cl]*: R = -CH$_3$, n = 4	**12**: R = -CH$_3$, n = 4, 74%
5[Cl]: R = -(CH$_2$)$_3$CH$_3$, n = 1	**13**: R = -(CH$_2$)$_3$CH$_3$, n = 1, 74%
6[Br]: R = -(CH$_2$)$_3$CH$_3$, n = 2	**14**: R = -(CH$_2$)$_3$CH$_3$, n = 2, 61%
7[Cl]: R = -(CH$_2$)$_3$CH$_3$, n = 3	**15**: R = -(CH$_2$)$_3$CH$_3$, n = 3, 70%
8[Cl]: R = -(CH$_2$)$_3$CH$_3$, n = 4	**16**: R = -(CH$_2$)$_3$CH$_3$, n = 4, 63%
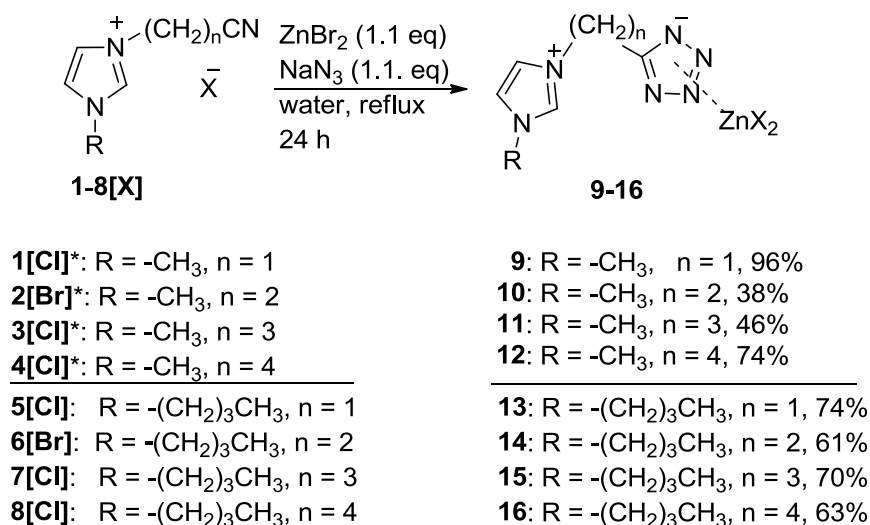
Scheme 4.5.1 Click reactions of *N*-cyanoalkyl-functionalized imidazolium halide salts (**1-4**[X], R = methyl; **5-8**[X], R = butyl) to zwitterionic products

Products **10** and **14** are presumed to be ZnBr$_2$ structures, as only bromide is introduced into the reaction sequence through the use of **2**[Br] and **6**[Br] as starting materials. Compounds obtained from the chloride salts **1**, **3-5**, **7**, **8**[Cl] are presumed to form mixed-halide coordination polymers, including products **9**, **11-13**, **15**, **16**. For each of them, the formula unit ZnBr(2-x)Cl(x) may describe the halide content for each structure, supported by the X-ray diffraction analysis of **9** which showed partial occupancy of the halides when refined as ZnBr$_{0.8}$Cl$_{1.2}$ (vide infra). Although a mixture of halides in the Zn-coordinated product could be avoided by including the same halide in **1-8**[X] as in the ZnX$_2$ salt, the work here explored the Click reaction using halide salts from our previously reported work, and ZnBr$_2$ was used for all Click reactions to remain consistent with the Click conditions reported in the literature.

Spectroscopy. The ^{1}H NMR and ^{13}C NMR spectra verified formation of **9-16**, where the disappearance of a signal for the -C≡N carbon (δ ~ 115-120 ppm) and appearance of a new signal for the C5 carbon of the tetrazole ring (δ ~ 155-160 ppm) was especially diagnostic. In addition, a significant shift of the α-carbon next to the carbon atom of the nitrile group (δ ~ 35 ppm) was noted when the cyano group was converted to a tetrazole ring (δ ~ 42-45 ppm) (Scheme 4.5.2). The above trends are most likely due to the change in hybridization of the nitrile *sp* carbon when converting to the C5 atom of the tetrazole unit (*sp*^{2}).
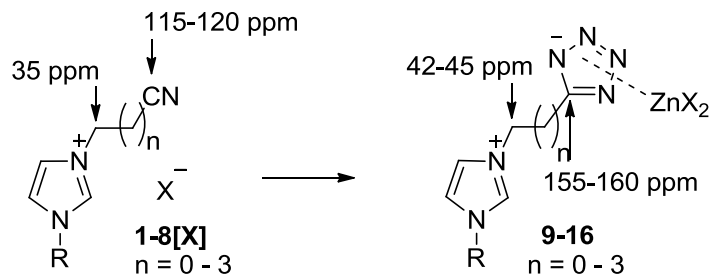
Scheme 4.5.2 Chemical shift (ppm) of diagnostic signals in the ^{13}C NMR spectra of **1-8**[X] compared with **9-16**.

A considerable change in chemical shifts was also observed in the proton NMR spectra for protons bound to the α-carbon next to the nitrile group when converting to tetrazole. The observed degree of change in chemical shift ($\Delta\delta$, in ppm) increases downfield when comparing compounds with short spacer lengths ($\Delta\delta$ (ppm) = -0.25, **9**, and -0,02, **13**) and long spacer lengths ($\Delta\delta$ (ppm) = +0.33, **12**, and +0.34, **16**). One interpretation of this trend is that for the shorter-spaced nitriles, the strong electron-withdrawing effect of the proximal imidazolium cation is countered by the delocalized electron density of the tetrazolate ring system. The downfield chemical shift of the protons on the α-carbon of the nitriles decreases with increasing separation from the imidazolium ring (*e.g.*, compare δ (ppm) = 5.82, **1**[Cl], 3.26, **2**[Br], 2.61, **3**[Cl], 2.54, **4**[Cl]). However, for Click products 9-16 the degree of downfield shift increased with spacer length when compared with analogous nitriles (*e.g.*, compare δ ($\Delta\delta$) (ppm) = 5.57 (-0.25), **9**, 3.44 (+0.18), **10**, 2.93 (+0.32), **11**, 2.87 (+0.33), **12**). One possible explanation for this observation is that, although the proximity of these protons to the imidazolium ring is directly related to the degree of downfield chemical shift due to deshielding from the imidazolium cation, additional deshielding may source from an inductive effect resulting from the better overlap of the C-H electrons with the sp^2 hybridized tetrazole electron system.
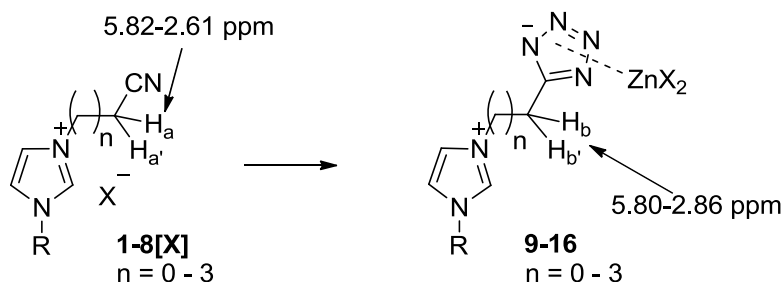
Scheme 4.5.2 Diagnostic signals in the ^{1}H NMR spectra of **1-8**[X] compared with **9-16**.

The appearance of a new absorption band (v = 1400-1420 cm^{-1}) indicated formation of a tetrazole ring, and the loss of the -C≡N stretching vibration band present in *N*-cyanoalkyl-functionalized starting materials (v = 2240 cm^{-1})[57] suggested that the nitrile groups of **1-8**[X] were transformed to the tetrazole moiety in the reaction.

Thermal Analysis. The Click products **9-16** were analyzed for phase transition temperatures by Differential Scanning Calorimetry (DSC) and for thermal stabilities by Thermograviometric Analysis (TGA). Glass transition and melting transition temperatures (T_g and T_m, respectively) were determined from the second heating cycle after initially heating the material from ambient temperature to an upper limit based upon the thermal stability of the compound as determined by

TGA. Melting transitions, T_m, were taken as the onset of a sharp, endothermic peak on heating, and T_g values were identified from the onset of small shifts in heat flow arising from the transition between amorphous glassy to liquid states when heating.

Thermal stabilities were assessed by TGA for all prepared compounds and taken as the onset of thermal decomposition for the first 5% weight loss ($T_{5\%onset}$). The $T_{5\%onset}$ values were considered more indicative of thermal stability than the onset of thermal decomposition (T_{onset}, included for comparison in parentheses in Table 1) which is more commonly reported in the literature.[58] Compounds were heated to 800 °C at a rate of 5 °C·min^{-1} with an isotherm of 30 min at 75 °C. Exceptions to this procedure were compounds **9** and **13**, which were heated to 600 °C, which was a sufficient temperature to observe their full decomposition.

The high temperature decomposition of **9**-**16** was characterized by a two-step weight loss pattern. This trend was also observed for many *N*-cyanoalkyl-functionalized salts in our previous work, where we suggested the formation of thermally stable carbonaceous materials following initial decomposition.[52] Support for this observation was reported by MacFarlane[59] and others,[60] where the *N*-CH$_2$CN groups may cyclize or polymerize upon heating to form thermally stable ring-containing or polymeric systems.

Summary. In this report we have described the synthesis and characterization of eight new 1-(5-tetrazolidyl)-alkyl-3-alkylimidazolium zwitterions, obtained through the Click reaction of *N*-cyanoalkyl-functionalized imidazolium halide salts with azide anion and zinc bromide. Our previous communication of a novel design platform for MHIL synthesis suggests the products are suitable precursors for new MHIL synthesis, where variable *N*-alkyl and alkyl linker chain lengths can direct the thermal stability and melting points when adjusted in bi-heterocyclic cations and dications. Work to optimize the reaction conditions suggests *N*-cyanoalkyl-substituted imidazolium salts are ideal for the Click synthesis of 5-tetrazoles, possibly due to the polar environment created by the ionic starting material. Thus, these results further extend the preliminary findings of MHIL synthetic platform to include new tetrazole-based multi-heterocycles, which may find application in a variety of fields (*e.g.*, energetic materials, coordination chemistry, pharmaceuticals, *etc.*).

4.6 **Synthesis, limitations, and thermal properties of energetically-substituted, protonated imidazolium picrate and nitrate salts and further comparison with their methylated analogs**

Smiglak, M.; Hines, C. C.; Reichert, W. M.; Vincek,A. S.; Katritzky, A. R.; Thrasher, J. S.; Sun, L. Y.; McCrary, P. D.; Beasley, P. A.; Kelley, S. P.; Rogers, R. D. "Synthesis, limitations, and thermal properties of energetically-substituted, protonated imidazolium picrate and nitrate salts and further comparison with their methylated analogs," *New J. Chem.* **2012**, *36*, 702-722.

The main research objective addressed during our study was to develop a better understanding of relationships between structural modifications and resulting thermal properties. Specific objectives included (i) learning the influence of the electron withdrawing groups, such as -NO$_2$ or -CN, on the properties of the alkylimidazole ring, especially on the nucleophilicity of the nitrogen in the heterocyclic core, (ii) comparison of the thermal properties of protonated derivatives of the imidazolium cation substituted with different functional groups on the carbon positions in the heterocyclic ring (-CH$_3$, -NO$_2$, -CN), and a variety of alkyl chains on the nitrogen position of the imidazolium ring, (iii) evaluation of the influence of the chosen counterions (picrate or nitrate) on the properties of the salts and their ability to form ILs, (iv) analysis of the influence of structural changes from the protonated to methylated imidazolium salts on the thermal properties, and (v) analysis of the potential energetic character of the salts (as evaluated by self heat rate maximum values) utilizing accelerating rate calorimetry (ARC).
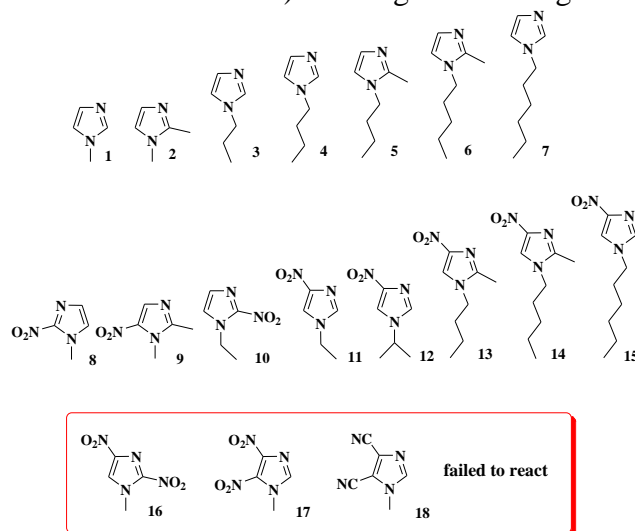
Scheme 4.6.1 Investigated imidazoles with functional groups appended to the heterocyclic core.

Synthesis of N-Alkylated-Substituted Imidazoles. Alkyl imidazoles were obtained from commercial sources (**1**, **2**, **4**), previously reported literature procedures (**8**-**11**, **16**-**18**),[61] or Method A or B below. Alkyl imidazoles **3**, **7**, and **13**-**15**) were prepared by the alkylation of corresponding imidazoles with alkyl bromides in acetonitrile in the presence of potassium carbonate under reflux (Method A). Method A provided low isolated yields (14–44%) for products **3** and **7** likely due to the low boiling point of propyl and *i*-propyl bromides. When the conditions were changed to potassium tert-butoxide in DMF at room temperature (Method B),

the isolated yields of **3** and **7** improved to 72–82%. Alkyl imidazoles (**5**, **6**, and **12**), were prepared by Method B.

Synthesis of Protonated Substituted Imidazolium Nitrate or Picrate Salts. The syntheses of a series of protonated 1-alkylimidazoles, containing combinations of nitro, cyano, or alkyl substituents were attempted (Scheme 4.6.2). The salts were prepared by neutralization reactions of the corresponding neutral azoles with nitric or picric acids in aqueous ethanol solutions. The protonated salts obtained successfully with nitrate and picrate anions include 15 cations: 1-methylimidazolium ([1-Me-3-H-Im]$^+$), 1,2-dimethylimidazolium ([1,2-diMe-3-H-Im]$^+$), 1-propylimidazolium ([1-Pr-3-H-Im]$^+$), 1-butylimidazolium ([1-Bu-3-H-Im]$^+$), 1-butyl-2-methylimidazolium ([1-Bu-2-Me-3-H-Im]$^+$), 1-pentyl-2-methylimidazolium ([1-Pent-2-Me-3-H-Im]$^+$), 1-hexylimidazolium ([1-Hex-3-H-Im]$^+$), 1-methyl-2-nitroimidazolium ([1-Me-2-NO$_2$-3-H-Im]$^+$), 1,2-dimethyl-5-nitroimidazolium ([1,2-diMe-5-NO$_2$-3-H-Im]$^+$), 1-ethyl-2-nitroimidazolium ([1-Et-2-NO$_2$-3-H-Im]$^+$), 1-ethyl-4-nitroimidazolium ([1-Et-4-NO$_2$-3-H-Im]$^+$), 1-isopropyl-4-nitroimidazolium ([1-*i*-Pr-4-NO$_2$-3-H-Im]$^+$), 1-butyl-2-methyl-4-nitroimidazolium ([1-Bu-2-Me-4-NO$_2$-3-H-Im]$^+$), 1-pentyl-2-methyl-4-nitroimidazolium ([1-Pent-2-Me-4-NO$_2$-3-H-Im]$^+$), and 1-hexyl-4-nitroimidazolium ([1-Hex-4-NO$_2$-3-H-Im]$^+$).

where   R$_1$ = Alk   HX = HNO$_3$, C$_6$H$_3$N$_3$O$_7$
Y$_2$ = Alk, NO$_2$
Y$_4$, Y$_5$ = NO$_2$, CN
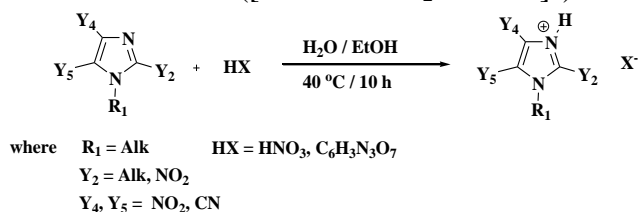
Scheme 4.6.2 General synthetic protocol for the formation of protonated substituted imidazolium nitrate and picrate salts.

ARC Calorimetry. Accelerating rate calorimetry (ARC) is a useful analytical technique for identification of self-heating runaway reactions and determination of information on the thermal stability of materials. Here, ARC was used to investigate the thermal decomposition of some of the synthesized salts in more detail. The decomposition temperature data for samples studied in an oxygen atmosphere in a titanium bomb are shown in Table 4.6.1. The analyzed salts show thermal stabilities on heating, indicated by the small residual increase in internal pressure until the thermal decomposition temperature is reached, at which point self-heating of the sample starts, resulting in an exothermic decomposition and evolution of gaseous products. The data in Table 4.6.1 describes the temperature value at which the self-heating exothermic reaction starts (T$_s$), the self-heating rate maximum (SHR$_{max}$) which describes the peak temperature change per mass unit during the sample's auto-decomposition, and pressure rate maximum (PR$_{max}$), which describes the peak pressure change per mass unit during the sample's auto-decomposition.
Seven ionic liquids: [1-Me-3-H-Im][NO$_3$] (**1b**), [1,2-diMe-3-H-Im][Pic] (**2a**), [1,2-diMe-3-H-Im][NO$_3$] (**2b**), [1-Bu-3-H-Im][NO$_3$] (**4b**), 1-butylimidazolium chloride ([1-Bu-3-H-Im][Cl]) (**4c**), [1-Bu-3-Me-Im][Pic] (**21a**), [1-Bu-3-Me-Im][NO$_3$] (**21b**), and 1-butyl-3-methylimidazolium chloride ([1-Bu-3-Me-Im][Cl]) (**21c**) were studied by ARC under an oxygen atmosphere. The T$_s$ and the SHR$_{max}$ during their exothermic decompositions were determined and the results show that both the cation and anion components in an ionic liquid play an important role regarding its energetic properties.

Table 4.6.1 Accelerating Rate Calorimetry (ARC) results for the selected protonated and alkylated imidazolium-based salts.

Compound	Ionic Liquid	T_s (°C)	SHR_{max} (Δ°C g^{-1}min^{-1})	PR_{max} (Δpsi g^{-1}min^{-1})
1b	[1-Me-3-H-Im][NO$_3$]	150 - 160	1523.58 at 254 °C	1289.74 at 264 °C
2a	[1,2-diMe-3-H-Im][Pic]	205 - 215	2650.48 at 271 °C	2514.28 at 262 °C
2b	[1,2-diMe-3-H-Im][NO$_3$]	130 -140	0.69 at 173 °C 0.53 at 272 °C	0.86 at 174 °C 2.22 at 278 °C
4b	[1-Bu-3-H-Im][NO$_3$]	145 - 155	487.80 at 225°C	1566.82 at 215 °C
4c	[1-Bu-3-H-Im][Cl]	215 - 225	0.90 at 269 °C	0.85 at 268 °C
21a	[1-Bu-3-Me-Im][Pic]	195 - 205	1502.27 at 278 °C	1253.18 at 266 °C
21b	[1-Bu-3-Me-Im][NO$_3$]	190 - 200	1.31 at 262 °C 0.54 at 280 °C	3.05 at 265 °C 4.74 at 283 °C
21c	[1-Bu-3-Me-Im][Cl]	190 - 200	1.39 at 257 °C 4.05 at 381 °C	2.00 at 258 °C 1.00 at 320 °C

From the available results for nitrate salts it was observed that alkylated imidazolium salts are much more stable than their protonated analogs. Moreover, based on the rates of the exothermic reactions among the four nitrate-based salts, [1-Me-3-H-Im][NO$_3$] (1b) is the most energetic, with a SHR$_{max}$ of 1523.58 °C g^{-1}min^{-1}; then [1-Bu-3-H-Im][NO$_3$] (4b) >> [1-Bu-3-Me-Im][NO$_3$] (21b) > [1,2-diMe-3-H-Im][NO$_3$] (2b) ordered from most to least energetic in terms of SHR$_{max}$.

Comparing the ARC results for [1,2-diMe-3-H-Im][NO$_3$] (2b) and [1,2-diMe-3-H-Im][Pic] (2a) (Table 4.6.1), it is interesting to note that the exotherm observed for [1,2-diMe-3-H-Im][Pic] (2a) started at a much higher temperature but progresses much more rapidly, as shown by the SHR$_{max}$ of 2650.48 °C·g^{-1}min^{-1}, making this salt the most energetic among the analyzed compounds. Also, the pressure curves show that [1,2-diMe-3-H-Im][Pic] (2a) is explosive when reaching its self-decomposition temperature, at which point the pressure rate maximum (PR$_{max}$) reached 2514.28 psi g^{-1}min^{-1}.

Among the series of protonated and methylated 1-butylimidazolium salts, [1-Bu-3-Me-Im][Pic] (21a) proved to be the most energetic with SHR$_{max}$ of 1502.27 °C·g^{-1}min^{-1}. In comparison, both [1-Bu-3-Me-Im][NO$_3$] (21b) and [1-Bu-3-Me-Im][Cl] (21c) were found to be much less energetic with SHR$_{max}$ reaching only 1.31 and 1.39 °C g^{-1} min^{-1}, respectively. However, the energetic character of the protonated 1-butylimidazolium nitrate salt (4b) is much higher than that of the alkylated analog (21b), reaching a SHR$_{max}$ value of 487.80 °C g^{-1}min^{-1}.

Summary. The focus of this work was on exploring the possibility of forming simple energetic ionic liquids via the straightforward protonation of neutral imidazole derivatives with nitric or picric acids. Moreover, the influence of substituent type (nitro-, cyano-, alkyl-substituents) and position on the properties of the resulting protonated imidazolium salts was investigated. This easy acid-base chemistry approach resulted in the formation of a large family of protonated imidazolium picrate and nitrate salts, however, not without limitations. It was found that functionalization of imidazoles with electron-withdrawing substituents, such as nitro or cyano, resulted in a reduction in nucleophilicity of the heterocycle. Mononitro-substituted protonated imidazolium salts could be isolated, but further ring substitution with electron-withdrawing groups resulted in the imidazoles failing to undergo protonation even with a strong acid such as HCl. The only products that were obtained were co-crystals of 1-Me-4,5-diCN-Im and 1-Me-2,4-diNO$_2$-Im with picric acid.

Comparing the simple protonated imidazolium nitrate and picrate salts with their methylated analogs it was found that the protonated ionic liquids did not differ substantially in their melting points from the methylated analogs. However, the thermal stabilities of protonated imidazolium salts were much lower than their alkylated derivatives. Nitrate salts with alkylated cations tended to be more thermally stable than the corresponding picrate salts, but with protonated cations, the picrate salts tended to be approximately 70-80 ^{o}C more stable than the nitrate salts.

The decomposition temperatures determined by accelerating rate calorimetry experiments under oxygen atmosphere roughly corresponded with those found by TGA. The ARC experiments revealed that the alkylated salts were much less explosive than the protonated analogs, and that among all the analyzed salts, the most energetic materials investigated were protonated [1-Me-3-H-Im][NO$_3$] (**1b**) and [1,2-diMe-3-H-Im][Pic] (**2a**) salts.

4.7 **Azolium azolates from reactions of neutral azoles with 1,3-diemethyl-imidazolium-2-carboxylate, 1,2,3-trimethyl-imidazolium hydrogen carbonate, and N,N dimethyl-pyrrolidinium hydrogen carbonate**

Combining the concepts developed during our previous studies: (i) the utilization of azolate-based anions in the synthesis of ILs, (ii) the use of the zwitterionic 1,3-dimethyl-imidazolium-2-carboxylate IL precursors for the clean synthesis of 1,3-dimethyl-imidazolium salts, and (iii) the development of new [HCO$_3$]$^-$ IL precursors ([1,2,3-triMe-Im]$^+$ and [*N,N*-diMe-Pyr]$^+$), it became possible to prepare a new family of azolate-based ILs in a fast and efficient fashion by reacting neutral azoles with the developed IL precursors. These routes would seem to provide an alternative for the formation of azolate salts, overcoming the previously experienced limitations related to ion exchange processes and allowing for much faster and more efficient routes to such compounds.

In the work we report here, we attempt to define the scope of the developed technique and its possible limitations in preparation of azolate-based IL salts. The syntheses of 18 new azolate-based salts (Figure 4.7.1), containing either 1,3-dimethyl-imidazolium ([1,3-diMe-Im-2-COO]), 1,2,3-trimethyl-imidazolium ([1,2,3-triMe-Im]$^+$), or *N,N*-dimethyl-pyrrolidinium ([*N,N*-diMe-Pyr]$^+$) cations is presented. The new salts include 12 examples of imidazolium azolates and 6 examples of pyrrolidinium azolate salts as a result of combinations of 3 cations and 6 anions. Even though the acidity of many of the neutral azoles utilized may seem to be too low for the reaction to be complete, these reactions can be driven toward completion by simple evacuation of CO_2 formed in the reaction. Thus, we gain access to a much larger group of new azolate based-salts that have been hard to obtain, due to problems with isolation of pure products from the ion metathesis reactions. The choice of small, symmetric cations for the preparation of the salts presented here was predicated by the need for high purity solid materials that were suitable for solid state analysis and thus confirmation of the applicability of the synthetic scheme, however, the methods are clearly applicable to a much wider range of substituted heterocycles.

Cations		Anions		

[1,3-diMe-Im]$^+$ (1)   [1,2,3-triMe-Im]$^+$ (2)   [4-NO$_2$-Im]$^-$ (a)   [2-Me-5-NO$_2$-Im]$^-$ (b)   [4,5-diNO$_2$-Im]$^-$ (c)

[*N,N*-diMe-Pyr]$^+$ (3)   [4-NO$_2$-1,2,3-Tri]$^-$ (d)   [3-NH$_2$-1,2,4-Tri]$^-$ (e)   [5-NH$_2$-Tetr]$^-$ (f)
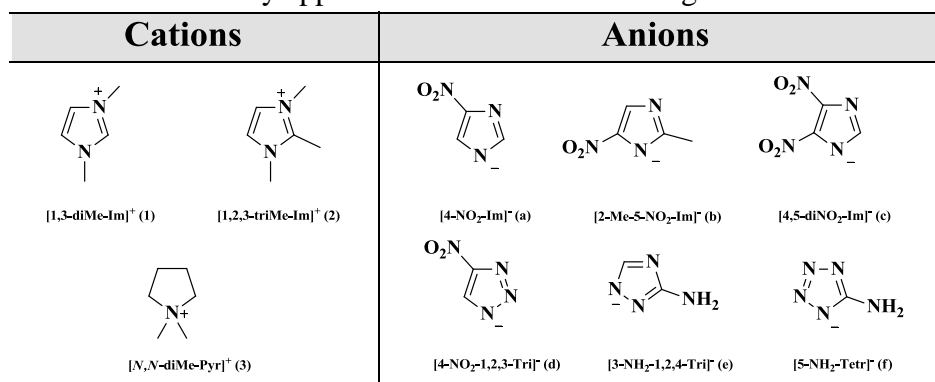
Figure 4.7.1 Cation and anion combinations explored and abbreviations used in this paper.

Synthesis. Eighteen azolate-based salts were synthesized via halide free, fast, and clean reactions of IL precursors [1,3-diMe-Im-2-COO], [1,2,3-triMe-Im][HCO$_3$], and [*N,N*-diMe-Pyr][HCO$_3$] with neutral azoles acting as weak acids in these systems. All of the salts were prepared in one step, simply by preparing standard solutions of all reagents in an EtOH/H$_2$O solvent system, and then mixing reactants in a 1:1 molar ratio (Figure 4.7.2). Most of the reaction mixtures with [4,5-diNO$_2$-Im]$^-$, [4-NO$_2$-1,2,3-Tri]$^-$, and [5-NH$_2$-Tetr]$^-$ evolved gas from the vial at the point of adding the reagents, confirming that the reaction was taking place in the systems instantaneously. Reactions involving [1,3-diMe-Im-2-COO], as reported earlier, required an addition of catalytic amounts of DMSO to be added to the system to enhance the reaction. All reactions were kept in open vials for an additional 48 h with constant stirring at 40 °C. After that time, the solvent was evaporated using a rotary evaporator at 90 °C, allowing for the recovery of the product. Any remaining DMSO was removed from the product by holding the product under an air stream for 12 h.

Successful conversion of the IL precursors to the desired products was monitored using ^{13}C NMR via analysis of the spectral region where the [HCO$_3$]$^-$ or carboxylate group of the zwitterion from the substrate would be expected. The absence of the relevant signal also served as an indicator of the completion of the reaction. None of the analyzed salts showed the presence

of a carboxylate signal at ~160 ppm, indicating no residual substrate. The ^{13}C NMR results provided evidence that all 18 new salts were formed in essentially quantitative yield.
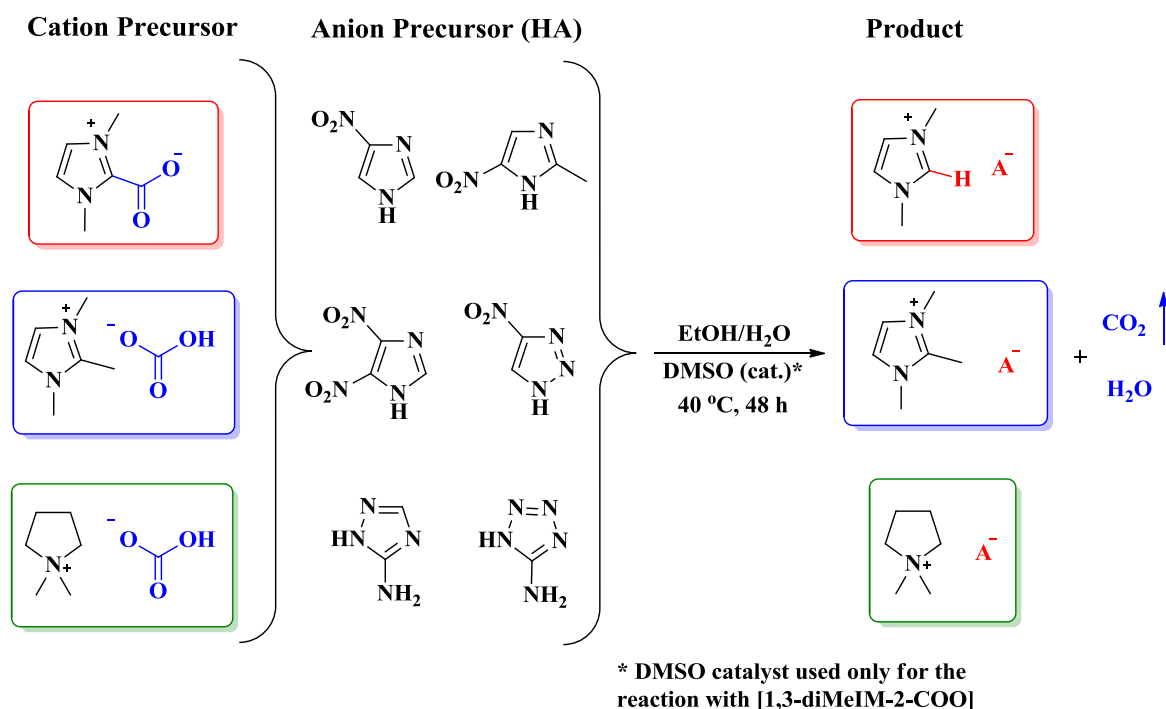
Figure 4.7.2 Reaction of [1,3-diMe-Im-2-COO], [1,2,3-triMe-Im][HCO$_3$], and [*N,N*-diMe-Pyr][HCO$_3$] with neutral azole acids.

Previously reported protocols for the halide- and metal free synthesis of organic salts *via* the reaction of either zwitterionic alkylimidazolium carboxylate, or alkylimidazolium and alkylpyrrolidinium hydrogen carbonates, were utilized in the syntheses of several azolate-based salts. Due to the low stability of the H$_2$CO$_3$ by-product, and its decomposition to CO$_2$ and H$_2$O in aqueous media, the purification steps using these protocols include only evaporation of the solvent.

Even though the synthesized model compounds were composed of symmetrical cations ([1,3-diMe-Im]$^+$, [1,2,3-triMe-Im]$^+$, and [*N,N*-diMe-Pyr]$^+$), which usually results in the formation of salts with relatively high melting points, six out of the 18 new salts exhibited melting points below 100 °C. We anticipate, based on our previous work investigating [1-Bu-3-Me-Im]$^+$ azolate-based salts, that the utilization of asymmetric azolium cations will further depress the melting points.

The thermal properties of the new salts are in satisfactory ranges, with $T_{5\%dec}$ typically above 170 °C. The observed thermal stabilities were also found to be in good correlation with those found for other azolate-based salts reported earlier.

Summary. The synthetic methods reported here for the formation of azolate-based salts can be easily transferred to more sophisticated IL systems (including energetic ILs) resulting in the fast and clean syntheses of a plethora of new azolium azolate salts. It is apparent that the cation and anion platforms needed for the formation of many new azolium azolate salts are readily available. Thus, a large library of new energetic salts can be formed free of inorganic impurities, while modification of the synthetic protocols for the use of longer alkyl chain dialkylcarbonates

27

will allow for the formation of new asymmetric cations that should exhibit the structural characteristics necessary for obtaining the low melting points needed for IL applications.

4.8 **Hypergolic Ionic Liquids to Mill, Suspend, and Ignite Boron Nanoparticles**

McCrary, P. D.; Beasley, P. A.; Cojocaru, O. A.; Schneider, S.; Hawkins, T. W.; Perez, J. P.; McMahon, B. W.; Pfeil, M.; Boatz, J. A.; Anderson, S. L.; Son, S. F.; Rogers, R. D. "Hypergolic Ionic Liquids to Mill, Suspend, and Ignite Boron Nanoparticles," *Chem. Commun.* **2012**, *48*, 4311-4313.

Energetic ionic liquids (EILs, salts which melt below 100 ^{o}C with potential as energetic materials) have been reported as hypergolic, indicating they spontaneously ignite on contact with a variety of oxidizers,[62,63,64] but many challenges still remain to their practical use such as low density[65] and relatively low heats of combustion[66] when compared to the current state of the art hypergols, such as hydrazine.[67] One approach that can be taken to improve EIL performance is to provide an additive which does not interfere with the desired IL traits such as low or negligible vapor pressure. Ionic liquids are already known as a solvent media to synthesize and stabilize nanoscale additives, such as Pt, Ir, and Pd;[68,69,70,71] however, we are interested in the ability of an IL to passivate the surface of nanoparticles while providing a stable suspension which could lead to higher energy density EILs.

Boron (B) is widely studied for its use as an energetic additive in both micro[72] and nano[73] sizes as a result of its high heat of combustion; however, because it is normally coated by a passivating oxide layer, it requires temperatures over 1500 °C to ignite.[74] Anderson *et al*. have demonstrated that air-stable and hydrocarbon-dispersible, nanoparticulate B can be prepared by milling macro B with a ligand to create ligand-protected B nanoparticles. For example, oleic acid was utilized as a ligand to create unoxidized B nanoparticles (60 nm in diameter) that are easily dispersible in petroleum based jet fuels.[75,76] Here, we report the use of the IL 1-methyl-4-amino-1,2,4-triazolium dicyanamide ([1-Me-4-NH$_2$-Tri][DCA]) as milling agent for B. [1-Me-4-NH$_2$-Tri][DCA] was chosen based both on the hypergolic nature of this IL and the likely amine-B surface interactions which we hypothesized would form.

Preparation of B Nanoparticles. Following the protocols developed by Anderson *et al.*, B with an average diameter of 2 μm was ball-milled using a tungsten carbide milling jar and 1/8" diameter spherical balls to create B nanoparticles (< 20 nm in diameter).[75,76] Boron (2 g) was added to the ball milling apparatus and dry milled, followed by additional milling with either no ligand, a combination of oleic acid and oleyl amine (1.5 mL, 1:1 v/v), or [1-Me-4-NH$_2$-Tri][DCA] (1.5 mL). Acetonitrile was then added for the final milling as a co-solvent to help reduce the viscosity and easily transfer the nanoparticles.

The resulting acetonitrile suspensions were stable to air and these samples were manipulated on the benchtop. The solvent was removed by rotoevaporation followed by heating and stirring under high vacuum. The samples were taken into a drybox where they were stored in an Ar atmosphere until used.

The suspendability and stability of the milled B particles were investigated by preparing mixtures with the IL 1-butyl-3-methylimidazolium dicyanamide ([1-Bu-3-Me-Im][DCA]).

This hypergolic IL was chosen for the initial studies in determining the appropriate loadings and handling conditions due to its easier preparation, characterization, and availability. [1-Bu-3-Me-Im][DCA] was freeze thawed to remove any dissolved gases by placing the vial in a $N_{2(l)}$ bath while under vacuum and subsequently allowed to warm, forcing out any trapped gases.

Synthesis of Nanoparticle Colloids. Compositions of 0.2 % to 0.7 % w/w B from each of the three milled samples were prepared by diluting the weighed B samples with neat [1-Bu-3-Me-Im][DCA] to prepare 1-2 mL samples. Initially a clear IL phase with aggregated B particles resting on the bottom was observed in each case. The vials were then removed from the drybox and vortex mixed and stirred, but without dispersion.
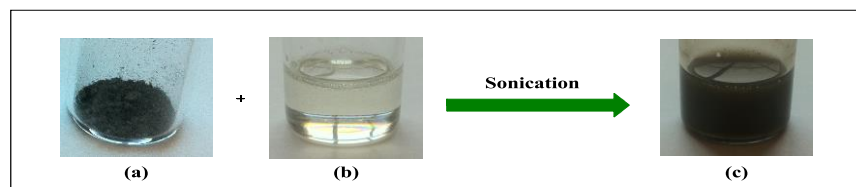

Figure 4.8.1 (a) [1-Me-4-NH$_2$-Tri][DCA]-milled B, (b) [1-Me-4-NH$_2$-Tri][DCA], and (c) 0.33% B

Each of the samples was ultimately dispersed by using a Branson 5510 bath sonicator. The vials were sonicated for consecutive 99 min cycles until no particles were visible, typically at least eight cycles. In each case black colloids (Figure 4.8.1) formed with very weak yellow-orange hues around the edges. These suspensions did settle out over time (see below), however, each sample (all milling conditions and loadings) was easily resuspended upon vortex mixing and sonication (many fewer cycles were required). All colloids exhibited the same stability whether freshly prepared or redispersed.

Interesting differences in the stabilities of the particles milled under different conditions were noted. Boron milled with no surfactant gave the least stable colloids with aggregation in less than 24 h. Boron particles milled with the surfactant mixture were slightly more stable, lasting 24 h, however, the compositions with B milled in [1-Me-4-NH$_2$-Tri][DCA] had the greatest stability with colloids lasting 48 h. In all cases, higher B loadings (0.5-0.7 %) were more prone to aggregation, but little difference in stability was noted for either the 0.2 % or the 0.33 % loadings.

Hypergolic Ignition Tests. Hypergolic drop tests were then conducted to determine the effects, if any, the B nanoparticles might have on ignition delay and other ignition characteristics. A droplet (10 µL) of the IL was added to a vial, *via* a Hamiltonian syringe, containing the oxidizer in large excess (500 µL of 98 % white fuming nitric acid (WFNA)) at 20 ºC to ensure complete ignition of the fuel. The ignition delay and flame duration times were determined using a Redlake MotionPro HS-4 high speed camera at 1000 frames per second. Each experiment was repeated for three ignitions and the values for ignition delay and ignition duration were averaged. The results are presented in Table 4.8.1.

The incorporation of 0.33 wt % B from any of the three preparations did not have any effect on the observed ignition delay of either IL tested (Table 4.8.1) within the accuracy of determination. However, as discussed below, differences in the number, intensity, and duration of the resulting flames were clearly different depending on which capping agent was utilized in the B milling step.

Neat [1-Bu-3-Me-Im][DCA] exhibited a single medium intensity flame as also reported in the literature.[77] Incorporation of the B milled with no ligand significantly reduced

hypergolic performance leading to smaller flames with observable residual mass deposited on the sides of the vial after ignition. Utilizing B particles milled in the oleic acid/olelyl amine surfactant mixture led to a complex flame behavior reproducibly exhibiting two flames which lengthened the overall time of combustion. The samples loaded with B milled in [1-Me-4-NH$_2$-Tri][DCA] gave the most complicated behavior with three flames.

Table 4.8.1 Hypergolic and Colloidal Stability properties of nanoparticle dispersions.

Compound	Colloidal Stability (h)	Ignition Delay[a] (ms)	Ignition Duration (ms)	Notes
Neat [1-Bu-3-Me-Im][DCA]	N/A	44(2)[b]	106(6)	One Flame Medium
0.33 % B no ligand	<24	44(3)	108(41)	One Flame Very weak
0.33 % B surfactant	24	43(3)	110(50)	Two Flames Medium
0.33 % B [1-Me-4-NH$_2$-Tri][DCA]	48	44(3)	130(31)	Three Flames Medium and High
Neat [1-Me-4-NH$_2$-Tri][DCA]	N/A	37(6)	77(18)	One Flame Medium
0.33 % B no ligand	<24	43(9)	52(12)	One/Two Flames Very weak
0.33 % B surfactant	24	45(11)	56(7)	One Flame Medium
0.33 % B [1-Me-4-NH$_2$-Tri][DCA]	48	45(14)	43(4)	One Flame Very Strong

It is clear from comparing the runs with neat [1-Bu-3-Me-Im][DCA] with those loaded with B nanoparticles that addition of the B nanoparticles did not enhance the reaction. There is also no evidence that the B ignited in these experiments. Additionally, such complicated behavior and multiple flames would provide extremely poor performance.

The hypergolic behavior of [1-Bu-3-Me-Im][DCA] can be contrasted to that of [1-Me-4-NH$_2$-Tri][DCA] where significant differences suggest a more robust hypergolic system. Incorporation of B nanoparticles milled with no ligand to [1-Me-4-NH$_2$-Tri][DCA] shortened the duration of the burn and led to very weak flames. Adding the B milled with the oleic acid/olelyl amine surfactant mixture also led to a shorter burn, but flame intensity observed was only slightly reduced.

Figure 4.8.2 Enhancement of ignition observed from [1-Me-4-NH$_2$-Tri][DCA] (left) to [1-Me-4-NH$_2$-Tri][DCA] with 0.33% B (right)

Adding B milled in [1-Me-4-NH$_2$-Tri][DCA] led to significant enhancements in performance (Fig. 4.8.2). When the 0.33 % B loaded [1-Me-4-NH$_2$-Tri][DCA] was dropped into WFNA, an extremely powerful and intense single flame appeared with a very short burn indicating a very quick and powerful ignition. *These drop tests led to the largest and most intense flames of any of the tested materials.* The extremely bright, white flames qualitatively indicated B ignition.

FT-IR data suggests at least one partial explanation for the differences in the hypergolicity after adding B to the two ILs. The data indicate that the hypergolic anion is interacting with the B surface in [1-Bu-3-Me-Im][DCA], but not in [1-Me-4-NH$_2$-Tri][DCA] with its coordinating cation.

Production of B nanoparticles by milling B in the presence of the hypergolic IL [1-Me-4-NH$_2$-Tri][DCA] leads to more stable dispersions of these nanoparticles in [1-Bu-3-Me-Im][DCA] and [1-Me-4-NH$_2$-Tri][DCA]. The presence of these nanoparticles does not change the hypergolic ignition delay for these ILs, however, when added to [1-Bu-3-Me-Im][DCA] there is little enhancement of the hypergolic burn and instead a complicated burn pattern emerges. By contrast, when B nanoparticles are milled in [1-Me-4-NH$_2$-Tri][DCA] and then dispersed in this IL, a single, shorter, much more intense burn is observed suggesting ignition of the B. These differences could be the result of the differing coordinative abilities of the two ILs to B, where, for example [1-Bu-3-Me-Im][DCA] can coordinate B via the anion, while [1-Me-4-NH$_2$-Tri][DCA] can coordinate B with the cation, the anion or both.

Summary. Taken as a whole, the results reported here suggest EILs can be designed to provide unique stabilizing environments for reactive nanoparticles and that the nanoparticles can provide unique enhancements of the EIL properties such as increased density or hypergolic performance. Future work from our Groups will focus on understanding the surface interactions of the ILs and nanoparticles in an effort to find suitable IL/nanoparticle combinations that will provide infinitely suspendable nanofluids with appropriate properties needed for new energetic materials.

4.9 **<u>Tuning azolium azolate ionic liquids to promote surface interactions with Titanium nanoparticles leading to increased passivation and colloidal stability</u>**

McCrary, P. D.; Beasley, P. A.; Kelley, S. P.; Schneider, S.; Hawkins, T. W.; Perez, J. P. L.; McMahon, B. W.; Pfeil, M.; Boatz, J. A.; Anderson, S. L.; Son, S. F.; Rogers, R. D. "Tuning azolium azolate ionic liquids to promote surface interactions with Titanium nanoparticles leading to increased passivation and colloidal stability," *Phys. Chem. Chem. Phys*. **2012**, *14*, 13194-13198.

Incorporation of the correctly chosen nanoparticle additives can lead to a variety of performance improvements, such as decreased ignition delay, decreased burn time, and higher density impulse.[78] ILs have already been found to be excellent solvents for nanoparticle synthesis and suspension as the ions provide a steric and electrostatic stabilizing force to prevent aggregation.[79-81] The use of non-functionalized ILs has led to some success in a variety of applications,[82,83] but the long-term stability is still an unknown factor with many of the ILs contemplated as energetic materials. We, for example,[84] demonstrated that boron nanoparticles can act as energetic additives in EILs based on the dicyanamide ([DCA]⁻) anion when correctly passivated through IL interactions along the surface of the nanoparticles. We found that if a non-coordinating cation was utilized, the surface interactions take place with the [DCA]⁻ anion leading to poor hypergolic ignition. This suggested that a methodology was needed to induce more favorable surface interactions with the non-trigger counter ion leaving the active ion free to ignite. These results suggested that if the EIL could be designed to include specific metal-surface coordinative interactions, one might be able to passivate and stabilize the nanoparticle dispersions, while greatly enhancing the energetic density.

Chemically designing the IL to specifically interact with the surface of the nanoparticle *via* coordination would allow one to alter the strength of such an interaction by control of the coordinating functionality. It has been shown that coordination can be utilized to increase the stability and catalytic activity of Rh and Pd nanoparticles in an IL by incorporating phosphine functional groups.[85,86] However, our challenge is greater than simply the stabilization of the nanoparticles. A properly chosen energetic composite system, must maintain the appropriate physical and chemical properties (*e.g*., high density, low viscosity, large liquid range, high thermal stability) and the unique chemical properties (*e.g*., hypergolicity, short ignition delay, improved energetic density), while simultaneously passivating and stabilizing the nanoparticle suspension.

Selection and Synthesis of AzAz ILs. In order to test our hypothesis that coordinative ability of a functional group of an IL ion could be used to tune nanoparticle stability, we chose to investigate a series of azolium azolate ILs that had been prepared as part of our EIL project.[87] Azolium azolate based EILs, by incorporation of aromatic nitrogen heterocycles in both cation and anion, have been previously reported to have many favorable energetic properties, such as high thermal stabilities, low melting points, and low viscosities. Here we choose the non-coordinating and commonly used cation, 1-butyl-3-methyl-imidazolium ([1-Bu-3-Me-Im]⁺) to allow focus on the potential coordinating interactions of each type of anion. The azolate anions studied, 4,5-dicyano-imidazolate ([4,5-DiCN-Im]⁻), 5-amino-tetrazolate ([5-NH₂-Tetr]⁻), 4-nitro-

imidazolate ([4-NO$_2$-Im]$^-$), and 2-methyl-4-nitro-imidazolate ([2-Me-4-NO$_2$-Im]$^-$), can interact with a metal surface through direct interaction *via* the –CN, –NH$_2$, and –NO$_2$ functional groups.

Each of the ILs was prepared using metathesis reactions with [1-Bu-3-Me-Im][Cl] and the corresponding *in situ* generated potassium azolate salt. Each IL has the ability to interact though the azolate nitrogen atoms, the π-systems, and a designed interaction through the incorporation of the functional groups on the azolate anion.

Titanium nanoparticles were chosen for this study, due to the high density (4.51 g/mL) and moderately high heat of combustion (20 kJ/g)[78] of titanium. Based on the high bond dissociation energy of a Ti-O bond (662 kJ/mol), the nitro functional group would be expected to have the highest coordinating ability with two equivalent oxygen atoms available for coordination per IL anion. A Ti-N bond would still provide adequate coordination (462 kJ/mol), which would suggest that the primary amine would provide the second greatest coordinating ability. The cyano functional group would be expected to show the least coordination based on the predicted bond enthalpy and lower nucleophilicity when compared to the primary amine functional group, however, in the dicyano-based anion studied chelation of two cyano groups is possible.[88] The predicted coordinating ability of the functional groups based on the bond dissociation energies is -NO$_2$ > -NH$_2$ > -CN, which corresponds to our experimental results.

Preparation of Colloids. Titanium nanoparticles (d$_{avg}$ = 100 nm) were obtained from Sigma-Aldrich (St. Louis, MO) and separated from the oil stabilizer by washing with freshly distilled *n*-hexane under an Ar atmosphere. The nanoparticles were dried by removal of the *n*-hexane at reduced pressure utilizing Schlenk line techniques and then weighed into vials under Ar in a VAC-Omni Labs (Hawthorne, CA) dry box as a black powder. To remove any remaining volatiles and entrapped gas, the ILs were frozen using a N$_{2(l)}$ bath and allowed to slowly thaw while under high vacuum (~1 x 10^{-4} torr). This process was repeated to ensure removal of gasses. Next, the predetermined amount of IL was added to the vials containing the Ti nanoparticles inside the drybox. Four concentrations of Ti in IL were investigated including molar ratios of 100:1, 150:1, 200:1, and 250:1 (IL:Ti), corresponding to Ti concentrations of 0.07 to 0.21 wt%.

Figure 4.9.1 [1-Bu-3-Me-Im][4,5-DiCN-Im] with 0.093 % Ti: (a) before sonication, (b) immediately following sonication, (c) 24 h (T$_s$), (d) 30 h, (e) 36 h (T$_f$).

The vials were capped, sealed, and removed from the dry box where it was initially observed that the nanoparticles had settled on the bottom of the vials. Vortex mixing and magnetic stirring were unable to disperse the Ti; however, sonication under ambient working conditions, approximately 50 $^{\circ}$C as the sonicator naturally provides thermal energy, for 24 h using a Branson 5510 bath sonicator in 99 minute cycles resulted in black colloids with a light green hue around the edge of the vial in each case (see Appendix B). NMR spectroscopy of the ILs after sonication did not reveal any degradation products and after sedimentation (discussed below), the ILs had not visibly darkened.

All combinations were monitored for colloidal stability and two timescales were recorded: when sedimentation was first observed (T$_s$) and once all of the Ti had settled out (T$_f$, Fig. 4.9.1). While higher concentrations of Ti were more prone, in general, to

sedimentation; the colloidal stability was also related to the coordinative ability of the functional group on the anion, with stability decreasing in the order [2-Me-4-NO$_2$-Im]$^-$ ~ [4-NO$_2$-Im]$^-$ > [5-NH$_2$-Tetr]$^-$ > [4,5-DiCN-Im]$^-$. The [1-Bu-3-Me-Im][2-Me-4-NO$_2$-Im] colloid (100:1) was stable for at least five days, compared to only 36 h for the 100:1 [1-Bu-3-Me-Im][4,5-DiCN-Im] colloid. Importantly, any settled particles were easily resuspended by a 3 to 5 min vortex mixing cycle and upon resuspension exhibited the same colloidal stability for all tested samples. This indicates that the sedimentation is reversible after the initial sonication step suggesting that an initial IL:Ti surface interaction is formed.

Sedimentation was not related to the viscosity or density of the neat ILs. As reported in Table 4.9.1, [1-Bu-3-Me-Im][5-NH$_2$-Tetr] was reported to have the highest viscosity of the four ILs prepared, but only the third highest dispersion stability. Higher densities seemed to correspond to higher stabilities, but this was not a direct trend. The data suggests a chemical stability mechanism is responsible for the increased dispersion stability and not differences in physical properties.

The increased stability of the colloids formed with ILs containing a nitro group, suggest that specific surface interactions with Ti(0) are responsible for the observed trends. To test this hypothesis, TiO$_2$ (rutile) particles (< 100 nm) were added to each of the four ILs originally studied; however, in these experiments colloids could not be formed. A white mixture was initially created after sonication with all four ILs, but rutile particles rapidly settled out on the order of minutes in all cases. This result suggests that the surface of the Ti(0) nanoparticles discussed above were not fully surface oxidized upon initial incorporation into the EILs.

Probing Surface Interactions. To determine whether the added functional groups on the azolate anion were chemically interacting with the Ti(0) particles, infrared (IR) spectra of the colloids were compared to neat IL samples. The least stable colloids containing [1-Bu-3-Me-Im][4,5-DiCN-Im] did not show any new or shifted bands and were essentially identical with or without Ti.
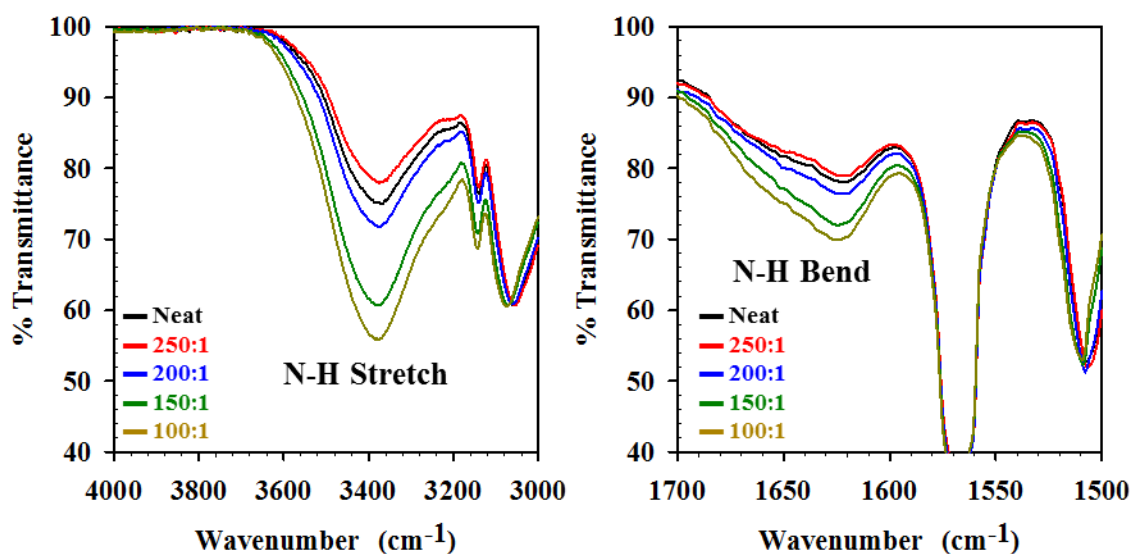

Figure 4.9.2 IR spectra of [1-Bu-3-Me-Im][5-NH$_2$-Tetr]/Ti(0) colloids: N-H stretch (left, 3370 cm^{-1}) and N-H bend (right, 1620 cm^{-1}).

Addition of Ti(0) nanoparticles to [1-Bu-3-Me-Im][5-NH$_2$-Tetr] resulted in enhanced and increased absorbance for the N-H stretching (~3370 cm^{-1}) and the N-H bending (~1620 cm^{-1}) modes (Fig. 4.9.2) compared to the neat IL. This increase in absorption does not appear to be proportional to nanoparticle concentration and may result from a surface enhancement effect. If this effect is responsible for the increase in absorption of the N-H stretch it is also consistent with the amine functional group donating, as the N-H bonds will be closest to the surface and thus more strongly affected by the surface enhancement.   The Ti surface should act as an electropositive reducing agent since the Ti surface would donate electron density to the protons attached to the amine as well as receiving net electron density from the Lewis basic amine functional group. The results presented in Fig. 4.9.2 indicate a potential Surface Enhanced IR absorption effect with no net shift of the N-H stretch and bend vibrational modes, suggesting that the surface of the Ti nanoparticle is at least partially unoxidized and coordinating with the amine functional group, which acts to further stabilize the [1-Bu-3-Me-Im][5-NH$_2$-Tetr] Ti dispersions.

In addition, the IR spectra indicate the appearance of a new peak at 1650 cm^{-1}, 90 cm^{-1} higher in energy than the –NO$_2$ symmetric stretch at 1560 cm^{-1}. In order to study this peak in more detail, a sample of the 100:1 colloid was concentrated by removing most of the neat IL once the Ti nanoparticles had sedimented to the bottom of the vial. The resulting concentrated sample was redispersed in the remaining IL and analyzed by IR, which indicated a larger relative stretch at 1650 cm^{-1}. This peak corresponds to that expected for a nitroso (R-N=O) functional group, which is a reduced form of a nitro group. With the relatively high oxophilicity of the Ti(0) surface, it is not unreasonable to suggest the formation of a new Ti-O bond through the nitro functional group that can act to stabilize the nanoparticles.
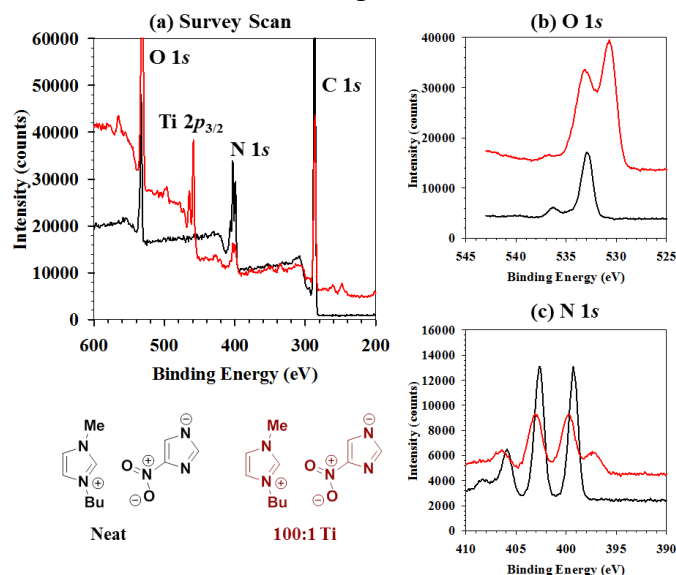
Figure 4.9.3 XPS spectra of [1-Bu-3-Me-Im][4-NO$_2$-Imid] neat and 100:1 with dispersed Ti(0): (a) survey scan, (b) High Resolution O 1s, (c) High Resolution N 1s

In order to further investigate the interactions suggested by IR, X-ray Photoelectron Spectroscopy (XPS) was utilized to study the surface of the nanoparticle systems *in situ*. The inherent non-volatility of the ILs we studied allowed us the opportunity to directly study the colloidal solutions under Ultra-High Vacuum (UHV) conditions.[89-91] Samples were applied as liquid droplets (either neat or as dispersions containing Ti nanoparticles) to Cu coated discs and brought under UHV (< 1 x 10^{-9} torr) to perform the XPS experiments. A more stable sample

with a coordinating IL, [1-Bu-3-Me-Im][4-NO$_2$-Im], and a less stable sample with the less coordinating, [1-Bu-3-Me-Im][4,5-DiCN-Im], were investigated.

The XPS spectra of [1-Bu-3-Me-Im][4,5-DiCN-Im] with and without Ti were identical and no Ti peak was observed. This suggests that in the time needed to prepare the samples for measurement (~2-3 h), the nanoparticles had sedimented and were no longer freely dispersed.

The more stable colloid of [1-Bu-3-Me-Im][4-NO$_2$-Im] loaded with Ti(0) at a molar ratio of 100:1, however, did provide some interesting results. As shown in Fig. 4.9.3a, a titanium peak is visible suggesting that the Ti nanoparticles are freely dispersed in the IL and able to access the very top of the droplet as XPS only probes the top 2-5 nm of the droplet. The Ti 2$p_{3/2}$ peaks indicate oxidation at the surface accessible to the XPS probe.

The O 1s spectrum (Fig. 4.9.3b) of the neat IL exhibits a single oxygen peak corresponding to the two equivalent oxygen atoms in the nitro functional group of [1-Bu-3-Me-Im][4-NO$_2$-Imid]. In the colloidal sample, a second O 1s peak at 531 eV, appears in the appropriate range for a titanium oxygen bond.[92] This may be indicative of the coordinated, reduced nitro oxygen atom.

Fig. 4.9.3c, focused on the N 1s spectra, also shows evidence of reduction through interaction with Ti where three distinct peaks are visible. The N atom at the highest binding energy corresponds to the nitrogen in the nitro group, which carries a formal positive charge. The peak at 403 eV can be attributed to the two equivalent nitrogen atoms in the cation, [1-butyl-3-methylimidazolium]$^+$. Two equivalent nitrogen atoms in the azolate anion can be assigned to lowest binding energy present in the neat spectrum, 399 eV. The N 1s peaks for the Ti dispersion match with those of the neat IL, which is consistent with our proposed mechanism that the oxygen atom of the nitro group is reduced, and ring nitrogen atoms are not involved. The lowest binding energy peak which only appears in the Ti dispersion is likely nitride impurity which was initially on the surface.

Summary. In total, the results presented here suggest that EILs can not only stabilize metallic nanoparticles through the steroelectronic effects of the individual ions, but that they can chemically interact with the surface of nanoparticles *via* specific ions as well. Based on the IR, XPS, and TGA data, we suggest stabilization of the Ti(0) particles *via* reaction with the nitro groups resulting in Ti-O bond formation. Ti(0) donates electronic density to the nitro functional group that allows for a reduced oxygen atom to bind to the newly oxidized Ti surface. This new interaction stabilizes the nanoparticle dispersion, allowing for easy resuspension and decreased sedimentation.

Azolium azolate ILs can be functionalized to control and increase the stability of suspensions of Ti(0) nanoparticles by adding specific groups to coordinate or interact with the surface metal *via* only one ion as determined here via IR, XPS, and TGA analysis of the loaded colloids. This approach also leads to surface passivation and safer/easier handing of these particles, while leaving the counterion free to, for example, ignite in a hypergolic reaction. This approach should be applicable to a wide variety of metal nanoparticles by specifically tuning the chemistry of the IL to the surface chemistry of the nanoparticles.

The ability to increase the stability of nanoparticles is crucial to the use of nanoparticles as energetic additives, as a catalyst, or in a variety of specialized applications. The 5-7 day stabilities observed here, however, must be further increased to allow for infinitely stable nanofluid systems for energetic materials and these efforts are currently under way in our laboratories.

4.10 Graphene and Graphene Oxide Can 'Lubricate' Ionic Liquids based on Specific Surface Interactions Leading to Improved Low Temperature Hypergolic Performance

McCrary, P. D.; Beasley, P. A.; Alaniz, S. A.; Griggs, C. S.; Frazier, R. M.; Rogers, R. D. "Graphene and Graphene Oxide Can 'Lubricate' Ionic Liquids based on Specific Surface Interactions Leading to Improved Low Temperature Hypergolic Performance," *Angew. Chem. Int. Ed.* **2012**, *51*, 9784-9787.

Graphene, a single layer of hexagonal, planar carbon atoms, has been proposed as a potential energetic additive due to its energetic reactivity and high surface area.[93] Dilute dispersions of nanoscale additives, including reduced graphene oxide (r-GO) sheets, have been previously utilized to catalytically increase burn rates.[94,95] Graphene can also be incorporated into ionic liquids (ILs, salts with melting points below 100 $^{\circ}$C) either through direct exfoliation of graphite to create pristine, or surface pure, graphene[96,97] or through the dispersion of single r-GO sheets *via* exfoliation of graphite oxide, which contains a degree of surface oxidation.[98] While sheets of pristine graphene and graphene oxide are discussed nearly interchangeably within the literature, the dramatically different surface morphologies and compositions can lead to extensive differences in bulk properties when utilized in dispersions. Here we demonstrate how the use of
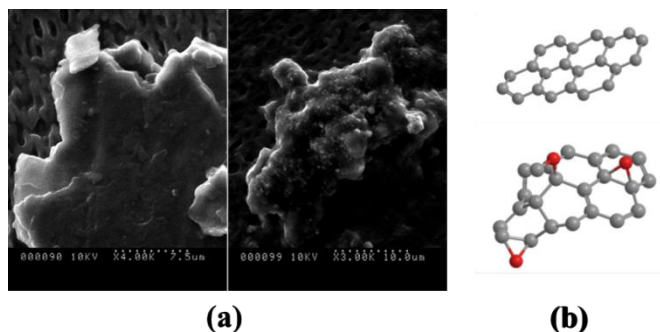
Figure 4.10.1 (a) SEM micrographs of partially aggregated pristine graphene sheets obtained from the [1-Me-4-NH$_2$-Tri][DCA] demonstrating a flat, sheet-like morphology (left) and dispersed r-GO obtained from [1-Me-4-NH$_2$-Tri][DCA] demonstrating a roughened surface (right); (b) Surface pristine graphene (top) and the projected disruption of the flat surface morphology observed with traditional graphene oxide chemical exfoliation (bottom)

graphene-based nanomaterials, with differing surface morphology and composition, can improve the low-temperature physical properties of ILs through the manipulation of intermolecular interactions between different IL molecular ions with specific types of graphene.

Energetic ionic liquids (EILs, ILs with potential as energetic materials) have been previously shown to be hypergolic (spontaneous ignition upon contact with an oxidizer)[99] with white fuming nitric acid (WFNA), inhibited red fuming nitric acid (IRFNA), or H$_2$O$_2$ by utilizing carefully selected hypergolic anions. As a result, these hypergolic ILs have been proposed as replacements for hydrazine,[100] which is toxic due to its dangerously high vapor pressure.[101] However, hypergolic ILs have only been screened for performance features under ambient conditions, which are not the typical temperatures associated with space or atmospheric flight. For example, ILs based on the dicyanamide ([DCA]$^-$) anion have been widely proposed as

potential replacements for hydrazine as they has been reported as hypergolic with WFNA while exhibiting low ignition delays and low viscosities under ambient conditions.[102] However, these values both exponentially rise with decreasing temperatures, which poses a major problem for the use of these compounds in practical systems. By controlling the low temperature viscosity of hypergolic ILs, these materials could be more effectively employed under realistic conditions.

Graphene sheets have been proposed as lubricating compounds, which in a dispersion act to reduce the system's internal friction[103] and could decrease the viscosity of these compounds. For application with hypergolic ILs, we would need to design the IL/graphene interactions to take place primarily with the cation to ensure that the hypergolic anion is not inhibited;[104] however, the different surfaces and morphologies present in pristine graphene (flat and unoxidized) and r-GO (crumpled and surfaced functionalized including a hydrogen bond acceptor) provide different options to IL cation design as demonstrated in Figure 4.10.1. To test this hypothesis we chose to compare (Table 4.10.1) a cation inherently non-coordinating and aromatic (1-butyl-3-methyl-imidazolium, [1-Bu-3-Me-Im]$^+$) with one which is non-coordinating and non-aromatic (N-butyl-N-methyl-pyrrolidinium, [N-Bu-N-Me-Pyr]$^+$), and one capable of hydrogen bond donation (1-methyl-4-amino-1,2,4-triazolium ([1-Me-4-NH$_2$-Tri]$^+$).

Graphene Colloid Preparation. Pristine graphene layers were exfoliated directly from graphite powder utilizing procedures developed by our group. Graphite powder was added directly to the neat hypergolic ILs to obtain a concentration of 0.03% (w/w), which initially deposited as a sediment at the bottom of the vial. The mixture was capped and placed in a Branson 5510 bath sonicator for 3 consecutive 99 min cycles to obtain a black colloid with a deep green hue. Reduced graphene oxide flakes were synthesized though the chemical reduction of exfoliated graphite oxide with hydrazine hydrate and obtained from Prof. Rod Ruoff's group.[105] r-GO dispersions were then prepared by the addition of r-GO flakes to the ILs to yield a concentration of 0.03 % (w/w) to directly compare to the pristine graphene dispersions. The resulting mixtures were dispersed after being capped and placed in a bath sonicator for 3 consecutive 99 min sonication cycles, which resulted in a black colloid with no visible aggregated solid along the bottom of the vial.

Graphene and r-GO dispersions in [N-Bu-N-Me-Pyr][DCA] were not stable and sedimentation was complete after less than 4 h. The lack of stability for this non-aromatic system supports earlier theoretical evidence that the [N-Bu-N-Me-Pyr]$^+$ cation would adopt an unfavorable conformation leading to a higher energy barrier when physically separating two graphene layers.[106] Conversely, colloids of pristine graphene sheets were equally stable utilizing either [1-Bu-3-Me-Im][DCA] and [1-Me-4-NH$_2$-Tri][DCA] without any noticeable sedimentation up to 48 h. Any of the particles which did sediment after 48 h were easily resuspended by repeating the original sonication cycle. Interestingly, r-GO dispersions in [1-Bu-3-Me-Im][DCA] (no observable sedimentation) and [1-Me-4-NH$_2$-Tri][DCA] (three week stability) are extremely stable with no observed sedimentation after extended periods of a few weeks. This might be expected as the oxidized surfaces could interfere with the reformation of the graphite intersheet structures.
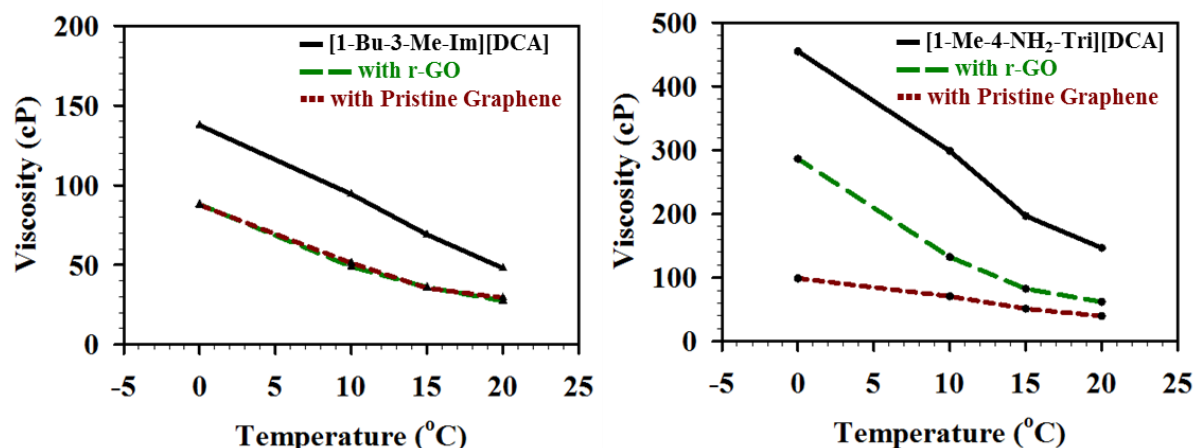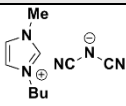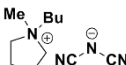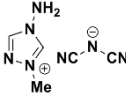
Figure 4.10.2 Viscosity vs. temperature for neat ILs and dispersions of lowering viscosities for pristine graphene vs. r-GO dispersions in graphene and r-GO.

Viscosity. A study of the effects on viscosity of the dispersion of the graphene and r-GO (Figure 4.10.2) reveal some interesting trends. The addition of graphene or r-GO to [1-Bu-3-Me-Im][DCA] results in a slight reduction of the viscosity of the dispersion at 20 $^{\circ}$C; however, at lower temperatures, graphene's ability to disrupt the interionic interactions becomes evident by large decreases in viscosity. There is not a major difference between the viscosities nor trends in lowering viscosities for pristine graphene vs. r-GO dispersions in [1-Bu-3-Me-Im][DCA] where only aromatic-aromatic interactions are expected with either type of graphene.

The third, IL [1-Me-4-NH$_2$-Tri][DCA] exhibits a much higher viscosity at room temperature than [1-Bu-3-Me-Im][DCA], presumably due to the additional hydrogen bond donating and accepting sites in the amine substituent. While both graphene and r-GO do act to reduce the viscosity in [1-Me-4-NH$_2$-Tri][DCA], pristine graphene led to viscosity reductions of up to 350 cP at 0 $^{\circ}$C compared to reductions of only 150 cP for r-GO dispersions. Interestingly, unlike the observations for [1-Bu-3-Me-Im][DCA], the dispersions of [1-Me-4-NH$_2$-Tri][DCA] varied greatly based on the chosen surface morphology of the graphene-based nanosheet, which might suggest a unique surface-IL interaction that causes the increase in viscosity seen in r-GO dispersions compared to those dispersions containing pristine graphene.

In contrast to pristine graphene, r-GO has surface functional groups, such as epoxides, alkoxides, and carbonyl derivatives,[107] that can be involved in more than aromatic-aromatic interactions with the [1-Me-4-NH$_2$-Tri]$^+$ cation; specifically hydrogen bond donation from the amine to the oxide on the surface. Non-covalent interactions between graphene oxide sheets and ILs have been previously shown to improve exfoliation of graphite oxide to graphene oxide,[108] however, these interactions produced increased viscosities compared with dispersions containing pristine graphene layers. Thus, dramatically different physical properties can be obtained through proper modification of the surface of the graphene-based nanomaterial.

Table 4.10.1 Hypergolic ILs utilized and evaluated for low temperature performance.

Ionic Liquids	Dispersion Loading (w/w)%	Stability	Lowest Hypergolic Temp.
[1-Bu-3-Me-Im][DCA]	Neat	N/A	0 ^{o}C
	0.03% Graphene	48 h	-10 ^{o}C
	0.03% r-GO	∞^a	0 ^{o}C
[N-Bu-N-Me-Pyr][DCA]	Neat	N/A	N/A^b
	0.03% Graphene	<4h	N/A^b
	0.03% r-GO	<4 h	N/A^b
[1-Me-4-NH$_2$-Tri][DCA]	Neat	N/A	-20 ^{o}C
	0.03% Graphene	48 h	-40 ^{o}C
	0.03% r-GO	3 weeks	-40 ^{o}C

^{a}On the timescale of publication (~6 months); ^{b}Hypergolicity not tested due to poor colloidal stability

Hypergolic Ignition Tests. To determine if the reduced viscosity did indeed lead to lower temperature hypergolic behavior, hypergolic drop tests were conducted on both the neat ILs, as well as the samples loaded with pristine graphene and r-GO at 23, 0, -10, -20, and -40 oC. The test apparatus we have used previously was slightly modified (see ESI). A droplet (10 μL) of the IL, with or without added graphene, was dropped into a vial containing 500 μL of 98% white fuming nitric acid (WFNA), which was precooled for 5 min in a dry ice/solvent mixture to achieve the desired temperature. The oxidizer was used in large excess to ensure the complete ignition of the entirety of the fuel, as well as proper control of the temperature of the reaction. Values for the ignition delay, defined as the time between contact with the surface and the first sign of ignition, were monitored using a Redlake MotionPro HS-4 high speed CCD camera at 1000 frames/s.

Neat [1-Bu-3-Me-Im][DCA] was ignitable upon contact with the oxidizer only until 0 ^{o}C (Table 4.10.1), where intermittent ignitions were observed with an ignition delay of around 300 ms. [1-Me-4-NH$_2$-Tri][DCA] remained hypergolic to -20 ^{o}C where an ignition delay of 153 m s was observed. The incorporation of pristine graphene or r-GO did result in reactions of the IL dispersions at lower temperatures (Table 4.10.1). r-GO in [1-Bu-3-Me-Im][DCA] did not lead to ignition at lower temperatures, however, significantly more smoke and visual evidence for a violent reaction was observed at -10 ^{o}C. Incorporating pristine graphene layers in [1-Bu-3-Me-Im][DCA], however, were consistently ignitable at -10 ^{o}C. Interestingly, the ignition temperature for [1-Me-4-NH$_2$-Tri][DCA] dispersions were decreased to -40 ^{o}C by addition of r-GO or pristine graphene.

Summary. Incorporation of graphene or graphene oxide into hypergolic ILs can depress viscosities leading to lower temperature hypergolic ignition, however, the type of graphene surface and the potential IL/graphene interactions can lead to dramatically different behavior. Dispersions of r-GO sheets led to lower viscosities than neat ILs at low temperatures, but its functionalized surface can form hydrogen bonds with the IL ions that can inhibit its viscosity reducing effect when paired with an IL capable of such hydrogen bonding. IL dispersions containing pristine graphene layers demonstrated improved low temperature ignition performance by sufficiently controlling the typical viscosity increases associated with lower temperatures. These dispersions in [1-Me-4-NH$_2$-Tri][DCA] exhibited large viscosity decreases (~350 cP) at 0 ^{o}C compared with the neat sample. Thus, proper consideration of the surface of

the nanomaterial additive and matching these surfaces with desired IL ion interactions can be a powerful tool towards control of bulk physical and ignition properties of hypergolic ILs.

V. Collaborations

Nano-IL Collaborative Team

Computational Design
Mark S. Gordon (Iowa State)
Edward J. Maginn (Notre Dame)
Jerry A. Boatz (AFRL)

Nanomaterial Design and Preparation
Scott L. Anderson (Utah)

Energetic Ionic Liquids
Robin D. Rogers (Alabama)
Stefan Schenider and Tommy W. Hawkins (AFRL)

Throughout our grant period, we have developed a strong collaboration in order to develop the chemistry of the interaction between the surface of specific nanomaterials and our designed ionic liquids. We have begun our exploration by developing a feedback loop between our computational collaborators (Prof. Gordon (ISU), Prof. Maginn (ND), and Dr. Boatz (AFRL)) and our experimental design (in collaboration with Prof. Anderson (Utah), Dr. Hawkins (AFRL), and Dr. Schneider (AFRL)), we will be able to fully understand the coordination chemistry, electrostatic stabilization, and reactivity along the surface of the nanoparticle at an atomic level, thereby giving us an unprecedented level of control over virtually any IL-nanoparticle system.

We intend to develop an understanding of which IL approaches will work for a given type of metal and for a given preparation method by utilizing the following strategies: (i) incorporation of single metals atoms directly into IL structures, (ii) incorporation of metal clusters, (iii) in situ synthetic methods, (iv) milling of nanoparticles, and (v) utilizing pre-prepared nanoparticles to investigate size vs. stability. Based on our established collaborations with Utah (milling), AFRL (EILs/EMs/computational), Notre Dame (computational), and Iowa State (computational), we will develop a feedback loops that will allow us to build our knowledge based on the strategy of "make, model, and measure." We will continue our exploration of the nanoparticle surface based on our newly formed collaboration.

Thus far, our collaboration has been quite successful and has led to the publication of 5 papers and the preparation of 6 presentations overall.

Collaborative Publications
McCrary, P. D.; Beasley, P. A.; Cojocaru, O. A.; Schneider, S.; Hawkins, T. W.; Perez, J. P.; McMahon, B. W.; Pfeil, M.; Boatz, J. A.; Anderson, S. L.; Son, S. F.; Rogers, R. D. "Hypergolic Ionic Liquids to Mill, Suspend, and Ignite Boron Nanoparticles," *Chem. Commun*. **2012**, *48*, 4311-4313.

McCrary, P. D.; Beasley, P. A.; Kelley, S. P.; Schneider, S.; Hawkins, T. W.; Perez, J. P. L.; McMahon, B. W.; Pfeil, M.; Boatz, J. A.; Anderson, S. L.; Son, S. F.; Rogers, R. D. "Tuning azolium azolate ionic liquids to promote surface interactions with Titanium nanoparticles leading to increased passivation and colloidal stability," *Phys. Chem. Chem. Phys*. **2012**, *14*, 13194-13198.

McMahon, B. W.; Perez, J. P. L.; Schneider, S.; Boatz, J.; Hawkins, T.; McCrary, P. D.; Beasley, P. A.; Rogers, R. D.; Anderson, S. L. "Dual ligand passivation and homogeneous media ball milling: novel approaches for both the synthesis and capping of air-stable aluminum nanoparticles," *In Preprints of Symposia - American Chemical Society, Division of Fuel Chemistry* **2012**, *57*, 965-967.

Perez, J. Paulo L.; McMahon, B. W.; Schnieder, S.; Boatz, J.; Hawkins, T.; McCrary, P. D.; Beasley, P. A.; Rogers, R. D.; Son, S.; Anderson, S. L. "Synthesis of air-stable, unoxidized, boron nanoparticles using ball milling technique," *In Preprints of Symposia - American Chemical Society, Division of Fuel Chemistry* **2012**, *57*, 955-956.

Perez, J. P. P.; McMahon, B. W.; Schneider, S.; Boatz, J. A.; Hawkins, T. W.; McCrary, P. D.; Beasley, P. A.; Rogers, R. D.; Anderson, S. L. "Exploring the structure of nitrogen-rich ionic liquids and their binding to the surface of oxide-free boron nanoparticles," *J. Phys. Chem. C* **2013**, *117*, 5693-5707.

VI. Personnel Supported

Prof. Robin D. Rogers (Principal Investigator)
Dr. Julia L. Shamshina (Research Scientist)
Parker D. McCrary (Graduate Student)
Preston A. Beasley (Graduate Student)
Spencer A. Alaniz (Graduate Student)
Luis A. Flores (Graduate Student)

VII. Publications

1. Drab, D. M.; Shamshina, J. L.; Smiglak, M.; Hines, C. C.; Cordes, D. B.; Rogers, R. D. "A general design platform for ionic liquid ions based on bridged multi-heterocycles with flexible symmetry and charge", *Chem. Commun.* **2010**, *46*, 3544-3546.
2. Shamshina, J. L.; Smiglak, M.; Drab, D. M.; Parker, T. G.; Dykes, Jr., H. W. H.; Di Salvo, R.; Reich, A. J.; Rogers, R. D. "Catalytic ignition of ionic liquids for propellant applications," *Chem. Commun.* **2010**, *46*, 8965-8967.
3. Smiglak, M.; Hines, C. C.; Rogers, R. D. "New hydrogen carbonate precursors for efficient and byproduct-free syntheses of ionic liquids based on 1,2,3-trimethylimidazolium and N,N-dimethylpyrrolidinium cores," *Green Chem.* **2010**, *12*, 491-501.
4. Smiglak, M.; Hines, C. C.; Wilson, T. B.; Singh, S.; Vincek, A. S.; Kirichenko, K.; Katritzky, A. R.; Rogers, R. D. "Ionic Liquids Based on Azolate Anions," *Chem. Eur. J.* **2010**, *16*, 1572-1584.
5. Drab, D. M.; Smiglak, M.; Shamshina, J. L.; Kelley, S. P.; Schneider, S.; Hawkins, T. W.; Rogers, R. D. "Synthesis of *N*-cyanoalkyl-functionalized imidazolium nitrate and dicyanamide ionic liquids with a comparison of their thermal properties for energetic applications," *New J. Chem.* **2011**, *35*, 1701-1717.
6. Pogodina, N. V.; Metwalli, E.; Müller-Buschbaum, P.; Wendler, K.; Lungwitz, R.; Spange, S.; Shamshina, J. L.; Rogers, R. D.; Friedrich, Ch. "Peculiar Behavior of Azolium Azolate Energetic Ionic Liquids," *J. Phys. Chem. Lett.* **2011**, *2*, 2571-2576.
7. Drab, D. M.; Kelley, S. P.; Shamshina, J. L.; Smiglak, M.; Cojocaru, O. A.; Gurau, G.; Rogers, R. D. "Reactivity of *N*-cyanoalkyl-substituted imidazolium halide salts by simple elution through an azide anion exchange resin," *Sci. China Chem.* **2012**, *55*, 1683-1687.
8. Drab, D. M.; Shamshina, J. L.; Smiglak, M.; Cojocaru, O. A.; Kelley, S. P.; Rogers, R. D. "Zinc-assisted synthesis of imidazolium-tetrazolate bi-heterocyclic zwitterions with variable alkyl bridge length," *Sci. China Chem.* **2012**, *55*, 1620-1626.
9. McMahon, B. W.; Perez, J. P. L.; Schneider, S.; Boatz, J.; Hawkins, T.; McCrary, P. D.; Beasley, P. A.; Rogers, R. D.; Anderson, S. L. "Dual ligand passivation and homogeneous media ball milling: novel approaches for both the synthesis and capping of air-stable aluminum nanoparticles," In *Preprints of Symposia - American Chemical Society, Division of Fuel Chemistry* **2012**, *57*, 965-967.
10. McCrary, P. D.; Beasley, P. A.; Cojocaru, O. A.; Schneider, S.; Hawkins, T. W.; Perez, J. P.; McMahon, B. W.; Pfeil, M.; Boatz, J. A.; Anderson, S. L.; Son, S. F.; Rogers, R. D. "Hypergolic Ionic Liquids to Mill, Suspend, and Ignite Boron Nanoparticles," *Chem. Commun.* **2012**, *48*, 4311-4313.
11. McCrary, P. D.; Beasley, P. A.; Kelley, S. P.; Schneider, S.; Hawkins, T. W.; Perez, J. P. L.; McMahon, B. W.; Pfeil, M.; Boatz, J. A.; Anderson, S. L.; Son, S. F.; Rogers, R. D. "Tuning azolium azolate ionic liquids to promote surface interactions with Titanium nanoparticles

leading to increased passivation and colloidal stability," *Phys. Chem. Chem. Phys*. **2012**, *14*, 13194-13198.

12. Perez, J. Paulo L.; McMahon, B. W.; Schnieder, S.; Boatz, J.; Hawkins, T.; McCrary, P. D.; Beasley, P. A.; Rogers, R. D.; Son, S.; Anderson, S. L. "Synthesis of air-stable, unoxidized, boron nanoparticles using ball milling technique," In *Preprints of Symposia - American Chemical Society, Division of Fuel Chemistry* **2012**, *57*, 955-956.

13. Smiglak, M.; Hines, C. C.; Reichert, W. M.; Vincek, A. S.; Katritzky, A. R.; Thrasher, J. S.; Sun, L. Y.; McCrary, P. D.; Beasley, P. A.; Kelley, S. P.; Rogers, R. D. "Synthesis, limitations, and thermal properties of energetically-substituted, protonated imidazolium picrate and nitrate salts and further comparison with their methylated analogs," *New J. Chem.* **2012**, *36*, 702-722.

14. McCrary, P. D.; Beasley, P. A.; Alaniz, S. A.; Griggs, C. S.; Frazier, R. M.; Rogers, R. D. "Graphene and Graphene Oxide Can 'Lubricate' Ionic Liquids based on Specific Surface Interactions Leading to Improved Low Temperature Hypergolic Performance," *Angew. Chem. Int. Ed.* **2012**, *51*, 9784-9787.

15. Perez, J. P. P.; McMahon, B. W.; Schneider, S.; Boatz, J. A.; Hawkins, T. W.; McCrary, P. D.; Beasley, P. A.; Rogers, R. D.; Anderson, S. L. "Exploring the structure of nitrogen-rich ionic liquids and their binding to the surface of oxide-free boron nanoparticles," *J. Phys. Chem. C* **2013**, *117*, 5693-5707.

16. Smiglak, M.; Hines, C. C.; Reichert, W. M.; Shamshina, J. L.; Beasley, P. A.; McCrary, P. D.; Kelley, S. P.; Rogers, R. D. "Azolium azolates from reactions of neutral azoles with 1,3-diemethyl-imidazolium-2-carboxylate, 1,2,3-trimethyl-imidazolium hydrogen carbonate, and N,N dimethyl-pyrrolidinium hydrogen carbonate," *New J. Chem.* **2013**, *37*, 1461-1469.

VIII. Presentations

1. Rogers, R. D. "Developing Ionic Liquid Know-How for the Design of Modular Functionality, Versatile Platforms, and New Synthetic Methodologies for Energetic Materials, Presented by R. D. Rogers before the AFOSR Review for Organic Materials Chemistry and Molecular Design and Synthesis (2010), National Harbor, MD, Abstract.

2. Rogers, R. D.; Smiglak, M.; Shamshina, J. "Azolium azolate ionic liquids from reactions of neutral azoles with 1,3-diemthylimidazolium-2-carboxylate, 1,2,3-trimethylimidazolium hydrogen carbonate, and *N,N*-dimethylpyrrolidinium hydrogen carbonate," Presented by R. D. Rogers before the 2010 International Chemical Congress of Pacific Basin Societies, Pacifichem 2010 (2010), Honolulu, HI, Abstract ENVI 237. Invited Presentation.

3. Rogers, R. D. "Developing Ionic Liquid Know-How for the Design of Modular Functionality, Versatile Platforms, and New Synthetic Methodologies for Energetic Materials," Presented by R. D. Rogers before the Air Force Office of Scientific Research Molecular Dynamics Contractors Meeting (May 15-17, 2011), Pasadena, CA, Abstract.

4. McCrary, P. D.; Beasley, P. A.; Hawkins, T. W.; Schneider, S.; Perez, J. P.; McMahon, B. W.; Anderson, S. L.; Son, S.; Rogers, R. D. "Loading Metal Nanoparticles in Energetic Ionic Liquids," Presented by P.D. McCrary before the AFOSR Molecular Dynamics Conference (2011), Pasadena, CA, Poster.

5. Shamshina, J.; Smiglak, M.; Drab, D. M.; Rogers, R. D. "Energetic Ionic Liquids," Presented by J. Shamshina before the 241st ACS National Meeting (2011), Anaheim, CA, Abstract I&EC 107.

6. McCrary, P. D.; Beasley, P. A.; Hawkins, T. W.; Schneider, S.; Perez, J. P.; McMahon, B. W.; Anderson, S. L.; Son, S.; Rogers, R. D. "Loading Metal Nanoparticles in Energetic Ionic Liquids", Presented by P. D. McCrary before the 4th Congress on Ionic Liquids, COIL-4 (June 15-18, 2011), Washington, D. C., Abstract 379.

7. Beasley, P. A.; McCrary, P. D.; Rogers, R. D. "New Generation of Energetic Materials based on Novel Asymmetric Multi-heterocyclic Architectures", Presented by P. A. Beasley before the 4th Congress on Ionic Liquids, COIL-4 (June 15-18, 2011), Washington, DC, Abstract 461.

8. McCrary, P. D.; Beasley, P. A.; Cojocaru, O. A.; Hawkins, T. W.; Schneider, S.; Perez, J. P.; McMahon, B. W.; Anderson, S. L.; Son, S.; Rogers, R. D., "Nanoparticles in Hypergolic and Energetic Ionic Liquids," Presented by P. D. McCrary before the 243rd ACS National Meeting (March 25-29, 2012), San Diego, CA, Abstract I&EC 3. Invited Speaker.

9. Drake, G. W.; McCrary, P. D.; Beasley P. A.; Rogers, R. D. "Evaluating Energetic Ionic Liquids as Hypergolic Fuels" Presented by P. D. McCrary and Preston A. Beasley before the 243rd ACS National Meeting (March 25-29, 2012), San Diego, CA, Abstract I&EC 7. Invited Speaker.

10. Beasley, P. A.; Cojocaru, O. A.; McCrary, P. D.; Rogers, R. D. "Energetic Ionic Liquid 'Liquid Clathrates,'" Presented by P.A. Beasley before the 243rd ACS National Meeting (March 25-29, 2012), San Diego, CA, Abstract I&EC 8. Invited Speaker.

11. McCrary, P. D.; Beasley, P. A.; Cojocaru, O. A.; Schneider, S.; Hawkins, T. W.; Perez, J. P.; McMahon, B. W.; Pfeil, M.; Boatz, J. A.; Anderson, S. L.; Son, S. F.; Rogers, R. D. "Controlling the Properties of Energetic Ionic Liquids (EILs) by Stabilizing Reactive Nanomaterials," Presented by P. D. McCrary before the AFOSR Contractors Meeting (2012), Arlington, VA. Poster.

12. McMahon, B. W.; Perez, J. P. L.; Anderson, S. L.; Schneider, S.; Boatz, J.; Hawkins, T.; McCrary, P. D.; Beasley P. A.; Rogers, R. D. "Dual ligand passivation and homogenous media ball milling: Novel approaches for both the synthesis and capping of air-stable aluminum nanoparticles," Presented by B. W. McMahon before the 243rd ACS National Meeting (March 25-29, 2012), San Diego, CA, Abstract FUEL 367.

13. Perez, J. P. L.; McMahon, B. W.; Anderson, S. L.; Schneider, S.; Boatz, J.; Hawkins, T.; McCrary, P. D.; Beasley P. A.; Rogers, R. D. "Synthesis of air-stable, unoxidized, boron nanoparticles using ball milling technique," Presented by J. P. L. Perez before the 243rd ACS National Meeting (March 25-29, 2012), San Diego, CA, Abstract FUEL 369.

14. P. A. Beasley, P. D. McCrary, O. A. Cojocaru, T. W. Hawkins, S. Schneider, and R. D. Rogers, "Energetic Ionic Liquid "Liquid Clathrates,"" Presented by P. A. Beasley before the AFOSR Contractors Meeting (2012), Arlington, VA. Poster.

15. McCrary, P. D.; Beasley, P. A.; Rogers, R. D. "Ionic Liquids as 'Practical' Energetic Materials," Presented by P. D. McCrary before the 3rd Asian-Pacific Conference on Ionic Liquids and Green Processes, APCIL'12 (Sept.17-19, 2012), Beijing, China, Abstract E-08.

16. McCrary, P. D.; Alaniz, S. A.; Rogers, R. D. "Controlling the Properties of Energetic Ionic Liquids through the Incorporation of Reactive Nanomaterials," Presented by P. D. McCrary before the 245th ACS National Meeting (April 7-11, 2013), New Orleans, LA, Abstract I&EC 116. Oral.

17. McCrary, P. D.; Alaniz, S. A.; Rogers, R. D. "Controlling the Properties of Energetic Ionic Liquids through the Incorporation of Reactive Nanomaterials," Presented by P. D. McCrary

before the 5th Congress on Ionic Liquids, COIL-5 (April 21-25, 2013), Algarve, Portugal, Abstract PFO36/PS291. Poster with Oral.

18. Rogers, R. D.; McCrary, P. D. "The Development of Advanced Liquid Composite Materials by Controlling Stabilization of Nanoparticles in Ionic Liquids," Presented by R. D. Rogers before the 2013 Materials Research Society's Spring Meeting & Exhibit (April 1 5, 2013) San Francisco, CA.

19. Rogers, R. D. "Developing Ionic Liquid Know-How for the Design of Modular Functionality, Versatile Platforms, and New Synthetic Methodologies for Energetic Materials," Presented by R. D. Rogers before the Air Force Office of Scientific Research Molecular Dynamics Synthesis Review (December 2-3, 2012), Pasadena, CA, Abstract.

20. McCrary, P. D.; Flores, L. A.; Chatel, G.; Rogers, R. D. "Evaluating Ionic Liquids as Hypergolic Fuels: From Reactive Nanomaterials to Trigger Additives," Presented by P. D. McCrary before the Energetic Ionic Liquid Mini-Symposium (May 21-22, 2013), Air Force Research Laboratory, Edwards Air Force Base, CA, No Abstract.

21. McCrary, P. D.; Rogers, R. D. "Controlling the Properties of Energetic Ionic Liquids through the Incorporation of Reactive Nanomaterials," Presented by P. D. McCrary before the American Chemical Society Summer School on Green Chemistry and Sustainable Energy (July 22-29, 2013), Colorado School of Mines, Golden, CO, No Abstract.

22. Flores, L. A.; McCrary, P. D.; Chatel, G.; Cojocaru, O. A.; Rogers, R. D. "Molecular Characteristics and Interactions Leading to Liquid Clathrate Behavior," Presented by L. A. Flores before the Energetic Ionic Liquid Mini-Symposium (May 21-22, 2013), Air Force Research Laboratory, Edwards Air Force Base, CA, No Abstract.

IX. Dissertations

1. David M. Drab, Ph.D., "A Versatile Design Platform for Multi-Heterocyclic Ionic Liquid Synthesis," The University of Alabama, 2011, 174 pages.
http://library.ua.edu/vwebv/holdingsInfo?bibId=3054591

2. Preston A. Beasley, M.S., "Understanding the Effects of Molecular Additions in Energetic Ionic Liquids," The University of Alabama, 2013, 50 pages.

Appendix A – Synthesis of ILs

A1. **A General Design Platform for Ionic Liquid Ions Based on Bridged Multi-Heterocycles With Flexible Symmetry and Charge**

Synthetic Protocols for the formation of Reported Major products:

Preparation of 1-cyanomethyl-3-methylimidazolium chloride precursor salt (1): Compound **1** was prepared by a solvent-free adaptation of a previously reported method. Yields and reaction times are unoptimized. The following serves as general procedure. In a 50 mL round bottom flask with magnetic stirbar, chloroacetonitrile (2.867 g, 37.9 mmol) was slowly added to 1-methylimidazole (2.87 g, 35 mmol). The mixture was stirred at room temperature overnight, and the resulting white solid precipitate washed with ethyl acetate (4 x 10 mL) and dried by rotovap then high vacuum at room temperature for 24 h. White solid, water soluble, 90% yield, mp (DSC) T_m = 178.7 ^{o}C, onset for 5% decomposition $T_{5\%onset}$ = 221.1 ^{o}C; ^{1}H NMR (500 MHz, DMSO-d_6) δ ppm 9.56 (s, 1H), 8.00 (t, J = 1.73 Hz, 1H), 7.87 (t, J = 1.64 Hz, 1H), 5.82 (s, 2H), 3.92 (s, 3H); ^{13}C (125 MHz, DMSO-d_6) δ ppm 138.292, 124.800, 123.026, 115.342, 37.207, 36.641. FT-IR (ν_{max}): 3392 (w), 3032 (s), 2977 (s), 2906 (s), 1575 (s), 1565 (s), 1439 (m), 1337 (m), 1254 (s), 1168 (s), 915 (m).

Preparation of 1-(5-tetrazolidyl)methyl-3-methylimidazolium•(ZnBrCl) and recrystallization as catena-poly[(bromochlorozinc)-μ-[1-(5-tetrazolato)methyl-3-methylimidazolium]-N^1:N^4] coordination polymer (2): Compound **2** was prepared by modifying the methods of Sharpless and coworkers from the halide salt 1-cyanomethyl-3-methylimidazolium chloride (**1**). Yields and reaction times are unoptimized. The following serves as a general procedure. Subsequent monitoring of the reaction by way of ^{1}H-NMR spectroscopy resulted in ~ 85% conversion of **1** to product **2** under room temperature conditions with all other factors the same.

   1-cyanomethyl-3-methylimidazolium chloride (**1**) (2.81 g, 17.2 mmol) was combined with NaN$_3$ (1.30 g, 20 mmol) in a 100 mL round-bottom flask with 50 mL water and stirred to dissolve with a magnetic stir bar. Zinc bromide was added (4.49 g, 20 mmol), and the mixture stirred to reflux overnight. The resultant white solid was rinsed with water and filtered. The final product was dried at 60 ^{o}C for 24 h in an oven. White powder, 80% yield, glass transition temperature (DSC) T_m = at decomposition temperature; onset for 5% decomposition, $T_{5\%onset}$ = 306.9 ^{o}C; ^{1}H NMR (360 MHz, DMSO-d_6) δ ppm 9.18 (s, 1H), 7.75 (t, J = 1.72 Hz, 1H), 7.68 (t, J = 1.74 Hz, 1H), 5.57 (s, 2H); 3.87 (3H, s); ^{13}C NMR (125 MHz, DMSO-d_6) δ ppm 154.171, 138.060, 124.442, 123.563, 42.915, 36.557. FT-IR (ν_{max}): 3498 (w), 3103 (s), 3078 (s), 2076 (s), 16128 (w), 1572 (s), 1446 (s), 1433 (s), 1421 (s), 1340 (m), 1171 (s), 1072 (m), 839 (s), 816 (s), 776 (s), 692 (s). **2** was crystallized for X-ray diffraction analysis by dissolution in a minimum amount of concentrated HNO$_3$, evaporating the resulting mixture to near dryness, washing the residual with dry acetone, and then slow evaporation in air.

Isolation and recrystallization of 1-(5-1H-tetrazolyl)methyl-3-methylimidazolium chloride as zinc-free salt (3): Compound **3** was obtained from the Zn-coordination polymer (**2**) via a preparatory adaptation of an anion exchange resin technique reported to remove trace Zn selectively from water and industrial waste samples. Yields and reaction times are unoptimized.

Conditioning of anion exchange resin: To 15.167 g of BioRad AG 1-X8 strongly basic anion exchange resin (100-200 mesh), 40 mL D.I. water was added and the resin stirred in a 125 mL flask to a slurry for 20 min. The slurry was then introduced into a glass column (~ 0.5 cm ID, 40 cm length; prewashed with 9 N HCl and rinsed several times with D.I. water) with a sand and glass wool plug. 9 N HCl was then eluted through the column (2 x 30 mL) and discarded upon neutralization.

Sample preparation for anion exchange: The Zn-coordination polymer **2** was added to a 50 mL Erlenmeyer flask (0.508 g, 1.473 mmol) and 15 mL of 9 N HCl was added and stirred to dissolve the solid material. The solution was sonicated briefly to break up residual solids suspended in the acidic solution, and an additional 10 mL 9 N HCl was added to completely dissolve the material.

*Zn separation from **2** by anion exchange resin:* 10 mL collection vials were numbered and arranged to collect eluted fractions from the column, and **2** dissolved in minimal 9 N HCl was introduced by 3 mL increments to the top of the resin bed and eluted at a rate of ~1 drop/sec (controlled by positive pressure introduced to top of column). When sample introduction was complete, 9 N HCl was eluted for complete removal of the salt **3**. After this step, the column was eluted with 0.005 M HCl followed by eluting the column with enough water until elution had tested negative for chloride by silver nitrate spot test (~1:1 v/v ratio of eluted fraction to 0.1 M AgNO$_3$). In all, 24 vials were collected from the exchange resin, where each vial contained approximated 5-10 mL of eluted material.

Qualitative analysis of Zn removal by pH measurement and K$_2$[Hg[CNS)$_4$] spot test: Determination of Zn in eluted fractions was estimated by two methods. First, the approximate pH of the elution in each collected vial was obtained by pH indicator paper (Vials 1-19, pH < 1; Vial 20, pH ~ 3-5; Vials 21-24, pH ~ 5). As the [ZnCl$_4$]$^{2-}$ anion is present at high chloride concentrations, the zinc should remain supported on the resin and it may be assumed that the earlier elution volumes were relatively Zn-free. Next, a solution of K$_2$[Hg(CNS)$_4$] (prepared the previous day by established methods, 2.7% HgCl$_2$ and 3.9% in D.I. water) was used to test each of the eluted fractions for Zn by spot test (1:1 ratio of 0.5 mL each, sample to test solution; concentration limit = 1/10,000). A white precipitate indicating the presence of Zn formed quickly (less than 1 min) for elution vials #14-22, where 14-16 only had a slight precipitate. To ensure the quality of the samples, only vials 2-5 and 7-11 were included for sample collection. Vials #1 and #6 seemed to visually contain column impurity (yellow coloring) and were stored separately. Vials 12 and 13, although not obviously precipitating, were kept separate as well to increase the window between the eluted sample and Zn-containing eluted solution.

Isolation of 1-(5-1H-tetrazolyl)methyl-3-methylimidazolium chloride (**3**): Each of the eluted fractions of **3** was heated (~60 °C, 24 h) to remove water and excess HCl, and the residual solids were triturated with dry ethanol. From evaporating the reserved ethanol solution, the product was obtained as a white solid. White solid, 71% yield, mp (DSC) T_m = 155.5 °C (melts during early onset of decomposition); onset for 5% decomposition, $T_{5\% onset}$ = 213.1 °C, ^{1}H-NMR (500 MHz, DMSO-d_6) δ ppm 9.35 (s, 1H), 7.86 (t, J = 1.65 Hz, 1H), 7.77 (t, J = 1.61 Hz, 1H), 5.89 (s, 2H), 3.89 (s, 3H); ^{13}C-NMR (125 MHz, DMSO-d_6) δ ppm 153.375, 137.561, 123.841, 122.956, 42.292, 36.914. FT-IR (ν_{max}): 3107 (m), 3001 (s), 2468 (w), 2395 (s), 1801 (m), 1668 (w), 1584 (m), 1552 (s), 1424 (w), 1178 (m), 1084 (s), 1027 (s), 1015 (s); 790 (s), 785 (s), 740 (s).

Separately, a crystal was obtained from 1:1 MeOH/CH₃CN by slow diffusion of diethyl ether and submitted for single crystal X-ray diffraction analysis.

Isolation and recrystallization of 1-(5-tetrazolidyl)methyl-3-methylimidazolium zwitterion (4): Compound **4** was obtained from the 1-(5-1*H*-tetrazolyl)methyl-3-methylimidazolium chloride salt (**3**) via neutralization reaction using hydroxide-exchanged anion exchange resin as solid-supported base. Yields and reaction times are not optimized.

Conditioning of anion exchange resin (OH⁻): Approximately 5 g of BioRad AG 1-X8 strongly basic anion exchange resin in chloride form was eluted with ~20 bed volumes (~1 L) of 1 N NaOH and each eluted volume was tested for Cl⁻ anion by using the silver nitrate test. The column was then washed with 2 bed volumes of D.I. water, filtered, and rinsed dry with ethanol before storing under high vacuum for 48 h.

Neutralization of 3 by OH form of anion exchange resin: The required volume of dry resin needed to convert **3** to the zwitterion **4** (eq. 1) was added to a 125 mL Erlenmeyer flask, washed three times with 25 mL of D.I. water and decanted to remove fines from ruptured resin beads, and then **3** (0.240 g, 1.20 mmol) was added to the flask as a solution in 25 mL of water.

$$\text{Dry Resin required (g)}$$
$$= \left(\text{mmol Cl}^- \text{ salt}\right) \times \left(\frac{1 \text{ g dry resin}}{(2.6 \text{ meq exchange capacity})}\right) \qquad \textbf{[EQ. 1]}$$
$$= (1.2 \text{ mmol}) \times \left(\frac{1 \text{ g}}{2.6 \text{ meq}}\right) = 0.46 \text{ g dry resin needed}$$
$$= 2.30 \text{ g dry resin } (5 \times \text{excess})$$

The mixture was gently stirred by rotating the flask for 20 min prior to spot checking the solution for Cl⁻ anion by silver nitrate test (0.1 M AgNO₃), the resin was filtered and washed with 3 x 10 mL D.I. water, and the resulting aqueous filtrates combined and evaporated to dryness at room temperature in an open beaker.

Isolation of 1-(5-tetrazolidyl)methyl-3-methylimidazolium (4): Neutralized fractions were combined and allowed to evaporate at room temperature to remove water. Additional recrystallization of isolated **4** from slow evaporation from hot methanol resulted in the final product. A crystal from this batch was submitted for single crystal X-ray diffraction analysis. White solid, 75% yield, mp (DSC) T_m = 124.8 °C ; onset for 5% decomposition, $T_{5\% \text{onset}}$ = 241.0 °C, ¹H-NMR (500 MHz, DMSO-d_6) δ ppm 9.15 (s, 1H), 7.72 (t, J = 1.50 Hz, 1H), 7.65 (t, J = 1.51 Hz, 1H), 5.52 (s, 2H), 3.84 (s, 3H); ¹³C-NMR (125 MHz, DMSO-d_6) δ ppm 155.584, 136.458, 123.226, 122.650, 44.619, 35.614. FT-IR (ν_{max}): 3146 (m), 3094 (s), 3074 (s), 1575 (m), 1560 (m), 1402 (w), 1331 (s), 1193 (w), 1150 (s), 1122 (m), 1080 (w), 862 (s), 815 (s), 780 (s), 751 (s), 698 (s).

Preparation of 1-(2-cyanoethyl)-1,2,4-triazole (6): Compound **6** was prepared from the 1,2,4-triazole, **5**. Yields and reaction times are unoptimized. The following serves as a general procedure. A sample of 1,2,4-triazole (1.724 g, 25 mmol) was dissolved in toluene (10 mL) and placed into a 50 mL round bottom flask to which a Teflon stirbar was added. Acrylonitrile (1.3562 g, 25 mmol) was added to the flask dropwise as a solution in toluene (2 mL) followed by addition of triethylamine (0.5 mL) directly to the reaction mixture. The reaction mixture was

fitted with a condenser and heated to reflux. The reaction mixture was then refluxed for an additional 30 h. *Caution: Acrylonitrile is a very hazardous irritant and permeator for skin and eyes, so protective clothing and a properly ventilated workspace should be utilized when handling this material. Prolonged exposure should be avoided, as there are possible carcinogenic/tetratogenic/mutagenic effects as well as well as toxicity related to target organs including blood, liver, central nervous system and kidneys. Additionally, explosive mixtures can be formed when vapors are allowed to mix with air, so accumulation of evaporated material is to be avoided. Please refer to Material Safety Data Sheet (MSDS) for further precautionary details (CAS # 107-13-1).*

At the end of the reaction time, **6** separated from the toluene as a second amber liquid phase and was isolated by decanting the toluene from the mixture and washing the residue with additional toluene. Residual solvent was then removed by rotary evaporation. White solid, 93.3% yield, mp (DSC) $T_m = 31.4$ ^{o}C ; onset for 5% decomposition, $T_{5\%\,onset} = $ 120.4 ^{o}C, ^{1}H NMR (360 MHz, DMSO-d_6) δ ppm 8.62 (s, 1H), 8.07 (s, 1H), 4.51 (d, J = 6.38 Hz, 2H), 3.13 (t, J = 6.38 Hz, 2H); ^{13}C NMR (90 MHz, DMSO-d_6) δ ppm 152.411, 144.958, 118.691, 44.737, 18.864. FT-IR (ν_{max}): 3406 (br m), 3120 (m), 2253 (m), 1508 (s), 1450 (m), 1418 (m), 1274 (s) 1206 (m), 1135 (s), 1040 (m), 1022 (m), 1003 (s), 919 (m), 872 (m), 679 (s).

Preparation of 5-(2-(1,2,4-triazol-1-yl)ethyl)tetrazolate as sodium coordination polymer (7)*:*
Compound **7** was prepared from 1-(2-cyanoethyl)-1,2,4-triazole (**6**). Yields and reaction times are not optimized. The following serves as a general procedure. In an Ace Glass high-pressure glass vial with a Teflon screw-cap, 1-(2-cyanoethyl)-1,2,4-triazole (1.195 g, 9.8 mmol) was combined with sodium azide (0.6437 g, 9.8 mmol) in glacial acetic acid (0.6 mL, 10 mmol). A Teflon magnetic stir bar was added, the vial sealed, and the mixture stirred on an oil bath at 60-70 ^{o}C for 24 h. At the end of the reaction period, the vial was set on a rotary evaporator at 70-80 ^{o}C for 4 h to remove residual acetic acid followed by dissolving the white solids with dry ethanol. Single crystals were obtained from slow evaporation of ethanol from the crude reaction mixture, and the final product, **6**, was obtained from removal of residual solvent by high vacuum. White solid, 48.5% yield, mp (DSC) T_m = decomposition temperature; onset for 5% decomposition, $T_{5\%\,onset} = $ 313.7 ^{o}C, ^{1}H NMR (360 MHz, DMSO-d_6) δ ppm 8.42 (s, 1H), 7.92 (s, 1H), 4.47 (t, J = 7.62 Hz, 2H), 3.15 (t, J = 7.59 Hz, 2H); ^{13}C NMR (90 MHz, DMSO-d_6) δ ppm 157.889, 151.547, 144.329, 48.809, 26.953. FT-IR (ν_{max}): 3322 (s), 3219 (s), 3144 (s), 1687 (m), 1571 (s), 1516 (s), 1468 (m), 1435 (m), 1380 (s), 1277 (s), 1205 (s), 1139 (s), 1104 (w), 1043 (w), 1014 (s), 970 (w), 923 (w), 858 (m), 673 (m).

Preparation of 1-(2-(5-tetrazolidyl)ethyl)-3-(5-1H-tetrazolyl)methylimidazolium zwitterion (10)*:* Azolium zwitterion, **10**, was achieved by reacting **9** (3.037 g, 20 mmol) with sodium azide (2.880 g, 44 mmol) in 10 mL of glacial acetic acid in a heated oil bath (60-70 ^{o}C) for 48 h. The mixture resulted in a suspended white solid in amber liquid, and the solid product was washed several times with dry ethanol. Final drying at high vacuum resulted in the final product. White solid, 78% yield, mp (DSC) T_m = 49.4 ^{o}C; onset of 5% decomposition, $T_{5\%\,onset}$ = 237.5 ^{o}C, ^{1}H NMR (500 MHz, DMSO- d_6) δ ppm 9.27 (s, 1H), 7.75 (dd, J = 10.47 Hz, 2H), 5.55 (s, 2H), 4.64 (t, J = 6.95 Hz, 2H), 3.50 (t, J = 6.97 Hz, 2H); ^{13}C (500 MHz, DMSO- d_6) δ ppm: 155.953, 154.151, 137.013, 123.361, 122.885, 46.868, 45.196, 24.732. FTIR (ν_{max}): 3143 (m), 3113 (m), 3043 (m), 2344 (br m), 1945 (br m), 1567 (s), 1459 (m), 1434 (m), 1234 (m), 1211 (m), 1170 (s), 1099 (s), 1045 (m), 950 (m), 872 (m), 860 (m), 802 (s), 761 (s), 744 (s), 690 (s), 665 (s).

Preparation of 1-(2-(5-1H-tetrazolyl)ethyl)-3-(5-1H-tetrazolyl)methylimidazolium bis(trifluoromethanesulfonyl)amide (11): The synthesis of **11** was carried out in the hood by reacting 123 mg (0.5 mmol) of zwitterion **10** and 140 mg (0.5 mmol) of hydrogen bis(trifluoromethanesulfonyl)amide (HNTf$_2$) in 10 mL of 1:1 methanol:water at RT for about 72 h in a 20 mL borosilicate glass vial. The mixture was kept at ambient conditions in order to allow the volatile solvent to evaporate and then water was removed by air stream. The product **11** was kept under high vacuum to afford a clear, viscous oil. Colorless oil, 80% yield, glass transition temperature (DSC) T_g/T_m = 10.5 ^{o}C, 50.8 ^{o}C; onset for 5% decomposition, $T_{5\%\,onset}$ = 245.6 ^{o}C, ^{1}H NMR (500 MHz, DMSO- d$_6$) δ ppm 9.35 (s, 1H), 7.87 (dt, J = 24.61 Hz, 2H), 5.91 (s, 2H), 4.71 (t, J = 6.81 Hz, 2H), 3.54 (t, J = 6.82 Hz, 2H); ^{13}C NMR (500 MHz, DMSO- d_6) δ ppm: 138.05, 123.83, 123.40, 121.40, 121.23, 118.67, 467.84, 43.07, 24,37. FTIR (ν_{max}): 3531 (w), 3245 (w), 3153 (m), 3090 (m), 1562 (s), 1442 (m), 1345 (s), 1183 (s), 1134 (s), 1054 (s), 791 (m), 741 (s).

Preparation of 1,3-dimethylimidazolium 1-(2-(5-tetrazolidyl)ethyl)-3-(5-tetrazolidyl)methyl-imidazolium (12): The synthesis of **12** was carried out in the hood by reacting 123 mg (0.5 mmol) of zwitterion **10** and 70 mg (0.5 mmol) of 1,3-dimethylimidazolium-2-carboxylate in 10 mL of a 1:1 solution of methanol:water (and 2 drops of DMSO) at RT for about 72 h in a 20 mL borosilicate glass vial. The mixture was kept at ambient conditions in order to allow the volatile solvent to evaporate and then water was removed by air stream. The compound was kept under high vacuum to afford a clear, viscous oil. Colorless oil, 78% yield. The NMR spectrum revealed the presence of 33% 1,3-dimethylimidazolium-2-carboxylate, which was removed by slow dissolution in hot acetone (6 x 2 mL). Yield of **12** after purification, 52%, glass transition temperature (DSC) T_g/T_m = -24.4 ^{o}C, 44.9 ^{o}C; onset of 5% decomposition, $T_{5\%\,onset}$ = 224.4 ^{o}C, ^{1}H NMR (500 MHz, DMSO- d_6) δ ppm 9.21 (d, J = 78.05 Hz, 2H), 7.69 (dt, J = 15.80, 15.54, 1.47 Hz, 4H), 5.51 (s, 2H), 4.52 (t, J = 7.23 Hz, 2H), 3.84 (s, 1H), 3.21 (t, J = 7.24 Hz, 2H); ^{13}C NMR (500 MHz, DMSO- d_6) δ ppm: 157.28, 156.11, 137.54, 136.70, 123.93, 122.93, 122.90, 48.66, 45.18, 36.15, 26.93. FTIR (ν_{max}): 3372 (w), 3149 (w), 3096 (m), 2956 (w), 2858 (w) 2602 (w), 2338 (w), 1727 (w), 1701 (w), 1656 (m), 1567 (s), 1516 (w), 1439 (m), 1397 (m), 1326 (m), 1229 (m), 1170 (s), 1111 (w), 1083 (w), 1051 (w), 1019 (w), 990 (w), 836 (w), 742 (s), 693 (w), 662 (w).

A2. <u>Catalytic Ignition of Ionic Liquids for Propellant Applications</u>

Hydroxyethylhydrazinium nitrate, [HO(CH$_2$)$_2$NHNH$_3$][NO$_3$] ([HEH][NO$_3$]). A preweighed 50 mL round bottom flask equipped with a condenser, a teflon stirbar, and a cooling bath was charged with 2-hydroxyethylhydrazine (15 mmol, 1.140 g). Aqueous nitric acid (15.8 M, 15 mmol, 0.95 mL) was added dropwise by means of an addition funnel. Excess heat evolved upon addition was removed via an ice bath. The clear homogenous solution was stirred at ambient temperature overnight (*ca.* 12 h). At the end of this time, the stirbar was removed and the solvent removed by air stream for 12 h, resulting in a colorless, viscous oil. The flask and the viscous product were transferred to a vacuum line and kept under vacuum for another 10 h. The resulting material was additionally dried in a 50 ^{o}C furnace, resulting in a viscous, clear oil. Yield: 97.6 %. ^{1}H NMR (360 MHz, DMSO-d_6) δ ppm 6.82 (s, 4H), 3.60 (t, J = 5.29 Hz, 2H), 2.98 (t, J = 5.33 Hz, 2H); ^{13}C (360 MHz, DMSO-d_6) δ ppm 56.641, 52.641; IR: 3320 (w), 3052

(w), 2891 (w), 1610 (w), 1297 (s), 1154 (m), 1067 (m), 1040 (m), 926 (m), 823 (m). Water content, ca. 8.1 %. Density, 1.423 g/mL.

Hydroxyethylhydrazinium dinitrate, [HO(CH₂)₂NH₂NH₃][NO₃] ([HEH][NO₃]₂). The above procedure was used to prepare [HEH][NO3]2 with the only difference in the amount of nitric acid, added (15.8M, 15 mmol, 1.9 mL). Yield: 98.1 %. ^{1}H NMR (360 MHz, DMSO-d_6) δ ppm 7.06 (s, 5H), 3.61 (t, J = 5.37 Hz, 3H), 2.98 (t, J = 5.40 Hz, 3H); ^{13}C (360 MHz, DMSO-d_6) δ ppm 56.641, 52.641. IR: 2884 (w), 264₁ (w), ₁613 (w), 1556 (w), 1395 (m), 1280 (s), 1065 (m), 1023 (m), 970 (m), 821 (m). Water content 4.2 %.

A3. <u>Synthesis of N-cyanoalkyl-functionalized imidazolium nitrate and dicyanamide ionic liquids with a comparison of their thermal properties for energetic applications</u>

***N*-cyanoalkyl-functionalized imidazolium halides (2a-q):**

General procedure to prepare 2a and 2g: Compounds **2a** and **2g** were each prepared by a solvent-free adaptation of a previous method.[1] Yields and reaction times were not optimized, and the following serves as a general procedure. In a 50 mL round bottom flask with a magnetic stirbar, chloroacetonitrile (10 % molar excess) was slowly added to 1-alkylimidazole (**1a** and **1b**, respectively). The mixture was stirred at room temperature overnight, and the resulting product was washed with ethyl acetate (4 x 5 mL) and dried by rotary evaporation prior to final removal of residual solvent by high vacuum at room temperature for 24 h.

1-cyanomethyl-3-methylimidazolium chloride (2a): Compound **2a** was prepared from **1a** (2.87 g, 35 mmol). White solid, water soluble, 90% yield, mp (DSC) T_m = 178.7 ^{o}C, $T_{5\%onset}$ = 221.1 ^{o}C; ^{1}H NMR (500 MHz, DMSO-d_6) **δ** ppm 9.56 (s, 1H), 8.00 (t, 1H), 7.87 (t, 1H), 5.82 (s, 2H), 3.92 (s, 3H); ^{13}C (125 MHz, DMSO-d_6) **δ** ppm 138.292, 124.800, 123.026, 115.342, 37.207, 36.641. FT-IR (v_{max} in cm^{-1}): 3392 (w), 3032 (s), 2977 (s), 2906 (s), 1575 (s), 1565 (s), 1439 (m), 1337 (m), 1254 (s), 1168 (s), 915 (m).

1-butyl-3-cyanomethylimidazolium chloride (2g): Compound **2g** was prepared from **1b** (2.612 g, 20 mmol). Amber liquid, 57% yield, mp (DSC) T_m = -7.13, $T_{5\%onset}$ = 200.9 ^{o}C; ^{1}H NMR (500 MHz, DMSO-d_6) **δ** ppm 9.70 (s, 1H), 8.04 (d, 1H), 7.99 (d, 1H), 5.83 (s, 2H), 4.27 (t, 2H), 1.75 (pent, 2H), 1.23 (hex, 2H), 0.88 (T, 3H); ^{13}C NMR (125 MHz, DMSO-d_6) **δ** ppm 137.2, 123.0, 122.6, 114.7, 48.79, 36.66, 31.10, 18.61, 13.14; FT-IR (v_{max} in cm^{-1}): 3370 (b), 3135 (w), 3064 (m), 2960 (s) 2934 (s), 2874 (m), 1638 (w), 1558 (s), 1463 (m), 1420 (w), 1337 (w), 1251 (w), 1209 (w), 1163 (s), 1115 (w), 1030 (m), 926 (w), 872 (w), 755 (s), 708 (w), 662 (w).

General procedure to prepare 2c-j: Compounds 2c-j were obtained under solvent-free conditions as with **2a** and **2b**, but with the addition of heat during the reaction time. Yields and reaction times were not optimized, and the following serves as a general procedure. To a 20 mL Ace Glass high temperature vial fitted with a Teflon screw-cap, the appropriate haloalkylnitrile (10 % molar excess) is added to 1-alkylimidazole (**1a** or **1b**). Upon fastening the screw-cap on the vial, the mixture is stored in a furnace set to 70 ^{o}C for 48 h. As exceptions to this procedure, compound **2c** was inadvertently left for 20 days in the furnace at 70 ^{o}C, and compound **2h** was

---

[1]   Herrmann, W. A.; Goossen, L. J.; Spiegler, M. *Organometallics* **1998**, *17*, 2162.

obtained by ᵃlkylation of prepared 1-(2-cyanoethyl)imidazole[109] with 1-bromobutane under the same solvent-free conditions in the furnace. After the reaction time was finished, each mixture was washed with ethyl acetate (4 x 5 mL) prior to drying first by rotary evaporation followed by removal of residual solvent by high vacuum over 24 hours at room temperature.

1-(1-cyanoethyl)-3-methylimidazolium bromide (2c): Compound **2c** was prepared from **1a** (0.615 g, 7.4 mmol). Yellow powder, 85% yield, mp (DSC) T_m = 138.0 °C, $T_{5\%\,onset}$ = 220.1 °C; ^{1}H NMR (500 MHz, DMSO-d_6) δ ppm 9.53 (s, 1H), 8.12 (s, 1H), 7.79 (s, 1H), 6.17 (q, 1H), 3.90 (s, 3H), 1.90 (d, 3H); ^{13}C NMR (125 MHz, DMSO-d_6) δ ppm 137.5, 125.1, 121.4, 117.5, 45.74, 36.70, 19.54; FT-IR (ν_{max} in cm^{-1}): 3172 (w), 3150 (w), 3170 (w), 3043 (s), 3012 (s), 2882 (m), 2847 (w), 2618 (w), 2556 (w), 2249 (w), 1776 (w), 1735 (w), 1654 (w), 1580 (m), 1552 (s), 1448 (m), 1419 (m), 1381 (w), 1324 (w), 1302 (m), 1260 (w), 1182 (s), 1168 (s), 1100 (s), 1020 (m), 989 (w), 892 (w), 863 (s), 843 (m), 768 (s), 717 (m), 674 (w).

1-butyl-3-(1-cyanoethyl)imidazolium bromide (2d): Compound **2d** was prepared from **1b** (2.755 g, 22 mmol). Amber liquid, 87% yield, glass transition (DSC) T_g = -7.64 °C, $T_{5\%\,onset}$ = 224.7 °C; ^{1}H NMR (500 MHz, DMSO-d_6) δ ppm 9.71 (s, 1H), 8.19 (s, 1H), 8.04 (s, 1H), 6.27 (q, 1H), 4.24 (t, 2H), 1.90 (d, 3H), 1.79 (pent, 2H), 1.27 (sext, 2H), 0.88 (t, 3H); ^{13}C NMR (125 MHz, DMSO-d_6) δ ppm 136.4, 123.3, 121.0, 117.0, 48.91, 46.22, 31.04, 18.69, 13.22; FT-IR (ν_{max} in cm^{-1}): 3126 (w), 3046 (s), 2959 (s), 2934 (s), 2873 (m), 2251 (w), 1691 (w), 1569 (m), 1551 (m), 1458 (m), 1381 (w), 1337 (w), 1315 (w), 1260 (w), 1210 (w), 1165 (s), 1115 (w), 1088 (w), 1021 (w), 983 (w), 948 (w), 842 (w), 752 (m).

1-(2-cyanoethyl)-3-methylimidazolium bromide (2e): Compound **2e** was prepared from **1a** (4.621 g, 38 mmol). Yellow solid, 86% yield, mp (DSC) T_m = 149.3 °C, $T_{5\%\,onset}$ = 222.3 °C; ^{1}H NMR (500 MHz, DMSO-d_6) δ ppm 9.31 (s, 1H), 7.88 (s, 1H), 7.80 (s, 1H), 4.53 (t, 2H), 3.90 (s, 3H), 3.25 (t, 2H); ^{13}C NMR (125 MHz, DMSO-d_6) δ ppm 137.5, 124.4, 122.8, 118.2, 44.91, 36.46, 19.21; FT-IR (ν_{max} in cm^{-1}): 3139 (w), 3082 (s), 3042 (s), 2958 (w), 2845 (w), 2250 (w), 1780 (w), 1761 (w), 1727 (w), 1676 (w), 1575 (m), 1559 (w), 1448 (w), 1426 (w), 1401 (w), 1359 (w), 1341 (w), 1280 (w), 1199 (w), 1160 (s), 1092 (w), 1022 (w), 892 (w), 864 (s), 789 (s), 741 (s), 652 (m).

1-butyl-3-(2-cyanoethyl)imidazolium bromide (2f): Compound **2f** was prepared from by alkylation of 1-(2-cyanoethyl)imidazolium, **1c** (1.521 g, 12 mmol; prepared by literature method)[109] with 1-bromobutane (2.125 g, 15 mmol). Yellow solid, 86% yield, mp (DSC) T_m = 91.6 °C, $T_{5\%\,onset}$ = 241.9 °C; ^{1}H NMR (500 MHz, DMSO-d_6) δ ppm 9.43 (s, 1H), 7.92 (d, 1H), 7.91 (d, 1H), 4.53 (t, 2H), 4.23 (t, 2H), 3.28 (t, 2H), 1.78 (pent, 2H), 1.24 (hex, 2H), 0.89 (t, 3H); ^{13}C NMR (125 MHz, DMSO-d_6) δ ppm136.4, 122.6, 122.3, 117.5, 48.57, 44.31, 31.10, 18.54, 18.53, 13.08; FT-IR (ν_{max} in cm^{-1}): 3378 (b), 3134 (w), 3055 (m), 2960 (m), 2935 (m), 2875 (w), 1707 (m), 1640 (w), 1557 (s), 1463 (w), 1421 (w), 1362 (m), 1223 (w), 1160 (s), 1115 (w), 1020 (w), 925 (w), 871 (w), 754 (s), 708 (w).

1-(3-cyanopropyl)-3-methylimidazolium chloride (2g): Compound **2g** was prepared from **1a** (3.610, 44 mmol). Yellow solid, 92% yield, mp (DSC) T_m = 96.3 °C, $T_{5\%\,onset}$ = 247.4 °C; ^{1}H NMR (500 MHz, DMSO-d_6) δ ppm 9.42 (s, 1H), 7.87 (t, 1H), 7.78 (t, 1H), 4.28 (t, 2H), 3.86 (s, 3H), 2.61 (t, 2H), 2.14 (pent, 2H); ^{13}C NMR (125 MHz, DMSO-d_6) δ ppm 136.9, 123.5, 122.2,

119.5, 47.43, 35.62, 25.16, 13.37; FT-IR (ν_{max} in cm^{-1}): 3435 (s), 3371 (s), 3244 (w), 3126 (w), 3109 (w), 3063 (m), 2971 (w), 2938 (w), 2915 (w), 2839 (w), 2244 (m), 2186 (w), 2111 (w), 1731 (w), 1655 (w), 1619 (m), 1574 (s), 1562 (s), 1453 (m), 1425 (m), 1391 (w), 1344 (w), 1334 (w), 1325 (w), 1266 (w), 1160 (s), 1092 (s), 1017 (m), 867 (s), 850 (w), 774 (s), 723 (w), 665 (m).

1-butyl-3-(3-cyanopropyl)imidazolium chloride (2h): Compound **2h** was prepared from **1b** (4.969 g, 40 mmol). Amber liquid, 45% yield, mp (DSC) T_g = -31.2 °C, $T_{5\% onset}$ = 260.0 °C; ^{1}H NMR (500 MHz, DMSO-d_6) δ ppm 9.44 (s, 1H), 7.87 (s, 1H), 7.85 (s, 1H), 4.28 (t, 2H), 4.17 (t, 2H), 2.61 (t, 2H), 2.15 (pent, 2H), 1.78 (pent, 2H), 1.28 (sext, 2H), 0.90 (t, 3H); ^{13}C NMR (125 MHz, DMSO-d_6) δ ppm 136.3, 122.4, 122.3, 119.5, 48.48, 47.60, 31.13, 25.02, 18.66, 13.42, 13.16; FT-IR (ν_{max} in cm^{-1}): 3372 (b), 3134 (w), 3049 (m), 2959 (m), 2935 (m), 2873 (w), 2245 (s), 1639 (w), 1561 (s), 1370 (w), 1335 (w), 1163 (s), 1115 (w), 1054 (w), 1021 (w), 949 (w), 852 (m), 753 (m).

1-(4-cyanobutyl)-3-methylimidazolium chloride (2i): Compound **2i** was prepared from **1a** (1.232 g, 15 mmol). Amber liquid, 95% yield, mp (DSC) T_g = -23.0 °C, $T_{5\% onset}$ = 239.5 °C; ^{1}H NMR (500 MHz, DMSO-d_6) δ ppm 9.39 (s, 1H), 7.84 (s, 1H), 7.77 (s, 1H), 4.25 (t, 2H), 3.86 (s, 3H), 2.58 (t, 2H), 1.89 (tt, 2H), 1.53 (sext, 2H); ^{13}C NMR (125 MHz, DMSO-d_6) δ ppm 136.7, 123.5, 122.1, 120.2, 47.67, 35.62, 28.38, 21.39, 15.56; FT-IR (ν_{max} in cm^{-1}): 3371 (b), 3143 (w), 3058 (m), 2951 (m), 2869 (w), 2242 (w), 1637 (w), 1571 (s), 1457 (m), 1426 (m), 1384 (w), 1335 (w), 1293 (w), 1163 (s), 1091 (w), 1020 (w), 842 (m), 759 (s), 697 (w).

1-butyl-3-(4-cyanobutyl)imidazolium chloride (2j): Compound **2j** was prepared from **1b** (1.870 g, 15 mmol). Amber liquid, 97% yield, glass transition T_g = -38.5 °C, $T_{5\% onset}$ = 310.6 °C; ^{1}H NMR (500 MHz, DMSO-d_6) δ ppm 9.62 (s, 1H), 7.91 (d, 1H), 7.90 (d, 1H), 4.27 (t, 2H), 4.20 (t, 2H), 2.59 (t, 2H), 1.89 (pent, 2H), 1.78 (pent, 2H), 1.53 (pent, 2H), 1.24 (sext, 2H), 0.89 (t, 3H); ^{13}C NMR (125 MHz, DMSO-d_6) δ ppm 136.2, 122.4, 122.3, 120.2, 48.70, 31.12, 28.30, 21.42, 18.63, 15.54, 13.11; FT-IR (ν_{max} in cm^{-1}): 3372 (b), 3131 (w), 3046 (m), 2957 (s), 2934 (s), 2872 (m), 2242 (w), 1638 (w), 1561 (s), 1458 (s), 1370 (w), 1333 (w), 1259 (w), 1160 (s), 1116 (w), 1050 (w), 1022 (w), 949 (w), 879 (m), 753 (s).

N-cyanoalkyl-functionalized imidazolium nitrates (3a-j):

Preparation of nitrate-form of anion exchange resin: Strongly basic anion exchange resin (BioRad AG 1-X8, chloride form) was converted to nitrate form by successive washes of a loaded column (~ 8 cm^3 bed volume) with 1 N NaNO$_3$. Each eluted fraction was tested with 0.1 M AgNO$_3$ to visually indicate when the resin had been fully exchanged (e.g., no AgCl precipitate formed). Final conditioning of the (NO$_3^-$)-form resin-loaded column includes washing with 2 bed volumes of deionized water.

General procedure for the exchange of halides 2a-j for nitrate product isolation, **3a-j**: A solution of *N*-cyanoalkyl imidazolium halide salt (**2a-j**) was prepared based upon the calculated 'dry weight' capacity of the resin being used (2.6 meq/g dry resin). 3.2 to 6.2 mmol of halide salt was eluted with the NO$_3$-exchanger resin as prepared.

1-cyanomethyl-3-methylimidazolium nitrate (3a): White solid, 81 % yield, mp T_m = 109.4 ^{o}C, $T_{5\%onset}$ = 189.0 ^{o}C; ^{1}H NMR (500 MHz, DMSO-d_6) δ ppm 9.26 (s, 1H), 7.89 (t, 1H), 7.79 (t, 1H), 5.59 (s, 2H), 3.89 (s, 3H); ^{13}C NMR (125 MHz, DMSO-d_6) δ ppm 137.7, 124.3, 122.4, 114.6, 36.66, 36.02; FT-IR (ν_{max} in cm^{-1}): 3431 (b), 3154 (w), 3130 (w), 3088 (m), 3035 (m), 3011 (m), 2966 (w), 1789 (w), 1748 (w), 1662 (w) 1581 (m), 1561 (m), 1472 (w), 1457 (w), 1425 (m), 1413 (m), 1387 (m), 1328 (s), 1275 (s), 1166 (s), 11087 (w), 1090 (w), 1041 (w), 1020 (w), 953 (w), 921 (w), 900 (s), 827 (m), 783 (m), 775 (m), 749 (m), 725 (w) 708 (w), 673 (w).

1-butyl-3-cyanomethylimidazolium nitrate (3b): Amber liquid, 76 % yield, glass transition T_g = -43.3 ^{o}C, $T_{5\%onset}$ = 177.0 ^{o}C; ^{1}H NMR (500 MHz, DMSO-d_6) δ ppm 9.39 (s, 1H), 7.93 (t, 1H), 7.91 (t, 1H), 5.61 (s, 2H), 4.22 (t, 2H), 1.77 (pent, 2H), 1.26 (hext, 2H), 0.89 (t, 3H); ^{13}C NMR (125 MHz, DMSO-d_6) δ ppm 137.3, 123.1, 122.7, 114.6, 48.92, 36.77, 31.11, 18.66, 13.17; FT-IR (ν_{max} in cm^{-1}): 3142 (w), 3100 (w), 2963 (w), 2937 (w), 2875 (w), 2430 (w), 1789 (w), 1560 (w), 1325 (s), 1163 (s), 1115 (m), 1041 (w), 1033 (w), 1021 (w), 926 (w), 832 (s), 754 (m), 708 (w).

1-(1-cyanoethyl)-3-methylimidazolium nitrate (3c): Yellow solid, 95 % yield, glass transition/mp T_g = -43.3 ^{o}C, T_m = 53.3 ^{o}C; $T_{5\%onset}$ = 192.8 ^{o}C; ^{1}H NMR (500 MHz, DMSO-d_6) δ ppm 9.44 (s, 1H), 8.09 (s, 1H), 7.85 (s, 1H), 6.05 (q, 1H), 3.89 (s, 3H), 1.89 (d, 3H); ^{13}C NMR (125 MHz, DMSO-d_6) δ ppm 137.0, 124.5, 120.8, 116.9, 45.13, 36.00, 18.83; FT-IR (ν_{max} in cm^{-1}): 3149 (w), 3097 (w), 2951 (w), 1747 (w), 1631 (w), 1581 (m), 1557 (m), 1452 (w), 1330 (s), 1261 (w), 1170 (s), 1090 (m), 1041 (w), 1021 (w), 984 (w), 842 (w), 829 (m) 755 (m), 718 (w).

1-butyl-3-(1-cyanoethyl)imidazolium nitrate (3d): Yellow solid, 89 % yield, glass transition T_g = -50.9 ^{o}C, $T_{5\%onset}$ = 190.0 ^{o}C; ^{1}H NMR (500 MHz, DMSO-d_6) δ ppm 9.49 (s, 1H), 8.12 (t, 1H), 7.95 (t, 1H), 6.01 (q, 1H), 4.21 (t, 2H), 1.90 (d, 3H), 1.79 (pent, 2H), 1.28 (sext, 2H), 0.90 (t, 3H); ^{13}C NMR (125 MHz, DMSO-d_6) δ ppm 136.4, 123.3, 121.0, 116.9, 48.97, 42.24, 31.00, 18.77, 18.66, 13.13; FT-IR (ν_{max} in cm^{-1}): 3253 (s), 3156 (m), 3118 (m), 3083 (m), 2878 (w), 1754 (w), 1587 (m), 1550 (m), 1470 (s), 1335 (m), 1309 (m), 1280 (m), 1162 (w), 1007 (s), 933 (m), 855 (w), 828 (w), 754 (w), 715 (w), 666 (w).

1-(2-cyanoethyl)-3-methylimidazolium nitrate (3e): Yellow solid, 84 % yield, glass transition/mp T_g = -58.4 ^{o}C, T_m = 52.2 ^{o}C; $T_{5\%onset}$ = 184.0 ^{o}C; ^{1}H NMR (500 MHz, DMSO-d_6) δ ppm 9.28 (s, 1H), 7.82 (t, 1H), 7.76 (t, 1H), 3.89 (s, 3H), 3.21 (t, 2H); ^{13}C NMR (125 MHz, DMSO-d_6) δ ppm 137.0, 123.9, 122.2, 117.6, 44.30, 35.78, 18.47; FT-IR (ν_{max} in cm^{-1}): 3156 (w), 3126 (w), 3088 (m), 3040 (m), 2258 (m), 1746 (w), 1664 (w), 1579 (m), 1566 (m), 1450 (w), 1426 (w), 1363 (m), 1332 (s), 1301 (m), 1176 (s), 1084 (w), 1042 (w), 1029 (w), 1016 (w), 943 (w), 888 (m), 877 (m), 827 (m), 775 (s), 748 (m), 706 (w), 657 (m).

1-butyl-3-(2-cyanoethyl)imidazolium nitrate (3f): Yellow solid, 94 % yield, glass transition/mp T_g = -30.5 ^{o}C, T_m = 91.6 ^{o}C; $T_{5\%onset}$ = 191.7 ^{o}C; ^{1}H NMR (500 MHz, DMSO-d_6) δ ppm 9.34 (s, 1H), 7.88 (t, 1H), 7.86 (t, 1H), 4.51 (t, 2H), 4.22 (t, 2H), 3.23 (t, 2H), 1.77 (pent, 2H), 1.26 (sext, 2H), 0.88 (t, 3H); ^{13}C NMR (125 MHz, DMSO-d_6) δ ppm 136.5, 122.8, 122.4, 117.7, 48.68, 44.42, 31.22, 18.64, 18.53, 13.18; FT-IR (ν_{max} in cm^{-1}): 3140 (w), 3096 (w), 3038 (w), 2962 (w), 2935 (w), 2875 (w), 2252 (w), 1745 (w), 1631 (w), 1563 (m), 1459 (m), 1335 (s), 1163 (s), 1113 (w), 1041 (w), 1023 (w), 949 (w), 914 (w), 854 (w), 829 (w), 754 (w).

1-(3-cyanopropyl)-3-methylimidazolium nitrate (3g): Amber liquid, 76 % yield, glass transition T_g = -52.0 ^{o}C; $T_{5\%\,onset}$ = 280.8 ^{o}C; ^{1}H NMR (500 MHz, DMSO-d_6) δ ppm 9.18 (s, 1H), 7.80 (t, 1H), 7.73 (t, 1H), 4.24 (t, 2H), 3.84 (s, 3H), 2.58 (t, 2H), 2.13 (pent, 2H); ^{13}C NMR (125 MHz, DMSO-d_6) δ ppm 136.8, 123.6, 122.2, 119.5, 47.53, 35.62, 25.12, 13.33; FT-IR (v_{max} in cm^{-1}): 3151 (w), 3101 (m), 2960 (w), 2247 (w), 1745 (w), 1633 (w), 1576 (m), 1566 (m), 1451 (w), 1425 (w), 1327 (s), 1166 (s), 1084 (w), 1024 (w), 847 (w), 830 (m), 756 (m), 699 (w).

1-butyl-3-(3-cyanopropyl)imidazolium nitrate (3h): Amber liquid, 83 % yield, glass transition T_g = -59.0 ^{o}C; $T_{5\%\,onset}$ = 273.6 ^{o}C; ^{1}H NMR (500 MHz, DMSO-d_6) δ ppm 9.28 (s, 1H), 7.83 (s, 1H), 7.82 (s, 1H), 4.26 (t, 2H), 4.17 (t, 2H), 2.59 (t, 2H), 2.15 (pent, 2H), 1.78 (pent, 2H), 1.26 (sext, 2H), 0.90 (t, 3H); ^{13}C NMR (125 MHz, DMSO-d_6) δ ppm 136.3, 122.5, 122.3, 119.5, 48.54, 47.68, 31.14, 25.03, 18.66, 13.34, 13.13; FT-IR (v_{max} in cm^{-1}): 3140 (w), 3096 (w), 2961 (w), 2934 (w), 2875 (w), 2246 (w), 1744 (w), 1564 (m), 1459 (w), 1330 (s), 1162 (s), 1114 (w), 1084 (w), 1040 (w), 1026 (w), 949 (w), 852 (w), 830 (w), 753 (m), 708 (w).

1-(4-cyanobutyl)-3-methylimidazolium nitrate (3i): Amber liquid, 83 % yield, glass transition T_g = -55.8 ^{o}C; $T_{5\%\,onset}$ = 279.8 ^{o}C; ^{1}H NMR (500 MHz, DMSO-d_6) δ ppm 9.17 (s, 1H), 7.78 (t, 1H), 7.72 (t, 1H), 4.21 (t, 2H), 3.85 (s, 3H), 2.54 (t, 2H), 1.87 (dt, 2H), 1.54 (dt, 2H); ^{13}C NMR (125 MHz, DMSO-d_6) δ ppm 136.6, 123.6, 122.1, 120.2, 47.81, 35.61, 28.42, 21.45, 15.54; FT-IR (v_{max} in cm^{-1}): 3147 (w), 3100 (w), 2955 (w), 2244 (w), 1744 (w), 1574 (s), 1458 (w), 1426 (w), 1330 (s), 1216 (w), 1163 (w), 1084 (w), 1039 (w), 1024 (w), 854 (w), 830 (m), 754 (m), 698 (w).

1-butyl-3-(4-cyanobutyl)imidazolium nitrate (3j): Amber liquid, 79 % yield, glass transition T_g = -58.9 ^{o}C; $T_{5\%\,onset}$ = 276.2 ^{o}C; ^{1}H NMR (500 MHz, DMSO-d_6) δ ppm 9.25 (s, 1H), 7.82 (d, 1H), 7.81 (d, 1H), 4.21 (t, 2H), 4.17 (t, 2H), 2.56 (t, 2H), 1.88 (dt, 2H), 1.79 (dt, 2H), 1.54 (dt, 2H), 1.26 (dt, 2H), 0.90 (t, 3H); ^{13}C NMR (125 MHz, DMSO-d_6) δ ppm 136.0, 122.4, 122.3, 120.2, 48.51, 47.90, 31.12, 28.34, 21.48, 18.66, 15.54, 13.11; FT-IR (v_{max} in cm^{-1}): 3139 (w), 3093 (w), 2961 (w), 2934 (w), 2874 (w), 2244 (w), 1744 (w), 1564 (s), 1459 (m), 1330 (s), 1217 (w), 1160 (s), 1114 (w), 1084 (w), 1039 (w), 1026 (w), 949 (w), 857 (w), 830 (w), 753 (m), 707 (w).

*Typical synthesis of N-cyanoalkyl-N-alkylimidazolium halide salts (precursors, **2c-f**):*

A 20 mL Ace Glass high pressure vial with Teflon screwcap is charged with 1-methylimidazole (15 mmol), the appropriate haloalkylnitrile (15 mmol), and mixed with a stir bar in an oil bath at about 50-60 ^{o}C for 48 h. The products were washed several times with ethyl acetate to extract unreacted starting materials, and residual ethyl acetate was removed overnight on high vacuum.

*Alternative syntheses for precursors **2a-b**:*

Precursors **2a** and **2b** were synthesized by alternate means, due to the tendency towards thermal decomposition when heated in the case of **2a** and the predominance of β-elimination over N-substitution for **2b** under the conditions described above for **2c-f**.

To synthesize **2a**, 1-methylimidazole (50 mmol) and chloroacetonitrile (50 mmol) were combined in a 100 mL round-bottom flask and stirred together for 48 hours. The product **2a** was removed as a solid precipitate from solution that was subsequently washed with acetonitrile and dried under high vacuum to obtain the final product.

For the synthesis of **2b**, a 20 mL Ace Glass high pressure vial with a Teflon screwcap with 1-(2-cyanoethyl)imidazole (20 mmol) and methyl iodide (40 mmol) in ethyl acetate (20 mL) was mixed with a stir bar at room temperature for 48 hours. The formed yellow-orange solid was washed with diethyl ether prior to drying on high vacuum overnight to isolate the final product.

1-cyanomethyl-3-methylimidazolium chloride (2a): White solid, 86.3 % yield, mp (DSC) T_m = 178.7 $^{\circ}$C, $T_{5\%onset}$ = 221.1 $^{\circ}$C; ^{1}H NMR (500 MHz, DMSO-d_6) δ ppm = 9.56 (s, 1H), 8.00 (t, 1H), 7.87 (t, 1H), 5.82 (s, 2H), 3.92 (s, 3H); ^{13}C (125 MHz, DMSO-d_6) δ ppm = 138.292, 124.800, 123.026, 115.342, 37.207, 36.641. FT-IR (v_{max} in cm^{-1}): 3392 (w), 3032 (s), 2977 (s), 2906 (s), 1575 (s), 1565 (s), 1439 (m), 1337 (m), 1254 (s), 1168 (s), 915 (m).

1-(2-cyanoethyl)-3-methylimidazolium iodide (2b): A 20 mL Ace Glass high pressure vial with a Teflon screwcap with 1-(2-cyanoethyl)imidazole (20 mmol, 2.422 g) and methyl iodide (40 mmol, 5.702 g) in ethyl acetate (20 mL) was mixed with a stir bar at RT for 48 h. The formed yellow-orange solid was washed with diethyl ether (4X10 mL) prior to drying on high vacuum overnight. Yellow solid, 77.5 % yield, glass transition/mp (DSC) T_g = -24.8 $^{\circ}$C, T_m = 88.7 $^{\circ}$C, $T_{5\%onset}$ = 220.3 $^{\circ}$C; ^{1}H NMR (500 MHz, DMSO-d_6) δ ppm = 9.22 (s, 1H), 7.84 (s, 1H), 7.73 (s, 1H), 4.52 (t, 2H), 3.90 (s, 3H), 3.23 (s, 2H); ^{13}C (125 MHz, DMSO-d_6) δ ppm = 137.1, 124.1, 122.4, 117.8, 44.5, 36.2, 18.9. FT-IR (v_{max} in cm^{-1}): 3149 (w), 3121 (w), 3078 (m), 3011 (s), 2941 (w), 2912 (w), 2869 (w), 2848 (w), 2248 (w), 1726 (w), 1626 (w), 1608 (w), 1582 (m), 1560 (m), 1440 (w), 1418 (w), 1375 (w), 1343 (w), 1294 (w), 1232 (w), 1173 (s), 1109 (w), 1090 (w), 1045 (w), 1022 (w), 991 (w), 911 (w), 874 (w), 863 (w), 824 (w), 751 (s), 704 (m).

1-(3-cyanopropyl)-3-methylimidazolium bromide (2c): Amber liquid, 79.9 % yield, glass transition (DSC) T_g = -33.8 $^{\circ}$C, $T_{5\%onset}$ = 257.7 $^{\circ}$C; ^{1}H NMR (500 MHz, DMSO-d_6) δ ppm = 9.27 (s, 1H), 7.84 (s, 1H), 7.76 (s, 1H), 4.27 (t, 2H), 3.86 (s, 3H), 2.61 (t, 2H), 2.14 (pent, 2H); ^{13}C (125 MHz, DMSO-d_6) δ ppm = 137.4, 124.2, 122.7, 120.1, 48.0, 36.3, 25.8, 14.0; FT-IR (v_{max} in cm^{-1}): 3408 (b), 3148 (w), 3083 (m), 2956 (w), 2247 (w), 1627 (w), 1574 (m), 1564 (m), 1451 (w), 1425 (w), 1340 (w), 1262 (w), 1231 (w), 1164 (s), 1090 (w), 1022 (w), 845 (m), 755 (m), 697 (w).

1-(4-cyanobutyl)-3-methylimidazolium chloride (2d): Amber liquid, 95.3 % yield, glass transition/mp (DSC) T_g = -24.3 $^{\circ}$C, T_m = 45.6 $^{\circ}$C, $T_{5\%onset}$ = 224.0 $^{\circ}$C; ^{1}H NMR (500 MHz, DMSO-d_6) δ ppm = 9.24 (s, 1H), 7.82 (t, 1H), 7.75 (t, 1H), 4.24 (t, 2H), 3.86 (s, 3H), 2.57 (t, 2H), 1.87 (pent, 2H), 1.53 (pent, 2H); ^{13}C (125 MHz, DMSO-d_6) δ ppm = 137.1, 124.1, 122.7, 120.9, 48.3, 36.3, 29.0, 22.0, 16.2; FT-IR (v_{max} in cm^{-1}): 3372 (b), 3143 (w), 3058 (m), 2952 (w), 2869 (w), 2242 (w), 1637 (w), 1571 (s), 1458 (m), 1427 (w), 1385 (w), 1335 (w), 1293 (w), 1161 (s), 1091 (w), 1020 (w), 843 (w), 760 (m), 697 (w).

1-(5-cyanopentyl)-3-methylimidazolium bromide (2e): Amber liquid, 94.5 % yield, glass transition (DSC) T_g = -34.2 $^{\circ}$C, $T_{5\%onset}$ = 250.0 $^{\circ}$C; ^{1}H NMR (500 MHz, DMSO-d_6) δ ppm = 9.31 (s, 1H), 7.85 (s, 1H), 7.77 (s, 1H), 4.21 (t, 2H), 3.87 (s, 3H), 2.52 (t, 2H), 1.83 (pent, 2H),

1.59 (pent, 2H), 1.33 (pent, 2H); ^{13}C (125 MHz, DMSO-d_6) δ ppm = 136.8, 123.8, 122.5, 120.8, 48.6, 36.0, 28.8, 24.7, 24.3, 16.3; FT-IR (ν_{max} in cm^{-1}): 3381 (b), 3141 (w), 3060 (m), 2936 (m), 2864 (w), 2242 (w), 1571 (s), 1459 (m), 1426 (m), 1362 (w), 1336 (w), 1167 (s), 1094 (w), 1029 (w), 835 (w), 755 (m), 697 (w).

1-(6-cyanohexyl)-3-methylimidazolium bromide (2f): Amber liquid, 92.5 % yield, glass transition/mp (DSC) Tg = -44.6 ^{o}C, T_m = 49.9 ^{o}C, $T_{5\%\,onset}$ = 247.0 ^{o}C; ^{1}H NMR (500 MHz, DMSO-d_6) δ ppm = 9.23 (s, 1H), 7.82 (s, 1H), 7.74 (s, 1H), 4.18 (t, 2H), 3.87 (s, 3H), 2.50 (t, 2H), 1.80 (pent, 2H), 1.55 (pent, 2H), 1.37 (pent, 2H), 1.27 (pent, 2H); ^{13}C (125 MHz, DMSO-d_6) δ ppm = 137.0, 124.1, 122.7, 121.1, 49.1, 36.2, 29.5, 27.8, 25.1, 24.9, 16.5; FT-IR (ν_{max} in cm^{-1}): 3417 (b), 3141 (w), 3059 (m), 2934 (m), 2861 (w), 2242 (w), 1731 (w), 1570 (s), 1459 (m), 1426 (m), 1365 (w), 1337 (w), 1297 (w), 1246 (w), 1164 (s), 1088 (w), 1046 (w), 1020 (w), 829 (m), 756 (m), 697 (w).

Typical synthesis of N-(2-cyanoethyl)-N-cyanoalkylimidazolium halide salts (precursors, 2h-k):

To a 20 mL Ace Glass high pressure vial with Teflon screwcap, the appropriate haloalkylnitrile (20 mmol) is combined with previously prepared 1-(2-cyanoethyl)imidazole (10-20 mmol) in ethyl acetate and stirred for 48 hours on an oil bath at 70-80 ^{o}C. The products separate as an amber liquid lower phase, where the upper solvent phase is decanted and the product is washed several times with ethyl acetate to remove residual starting material prior to drying on high vacuum for 48 hours.

Alternative synthesis for 2g:

To a 50 mL round bottom flask, chloroacetonitirle (22 mmol) is combined with prepared 1-(2-cyanoethyl)imdazole (20 mmol) and stirred for 24 hours at room temperature. The resulting mixture is washed several times with acetone to remove residual starting material and then dried on high vacuum for 48 hours to yield an amber liquid product.

1-cyanomethyl-3-(2-cyanoethyl)imidazolium chloride (2g): White solid, 87.0 % yield, mp (DSC) T_m = 49.2 ^{o}C, $T_{5\%\,onset}$ = 196.0 ^{o}C; ^{1}H NMR (500 MHz, DMSO-d_6) δ ppm = 7.82 (s, 1H), 4.51 (t, 2H), 3.14 (t, 2H), 2.74 (s, 2H); ^{13}C (125 MHz, DMSO-d_6) δ ppm = 146.0, 122.2, 118.3, 43.6, 18.6, 10.0; FT-IR (ν_{max} in cm^{-1}): 3327 (s), 3276 (s), 3167 (w), 3140 (w), 3126 (w), 3068 (m), 3036 (s), 2986 (m), 2954 (w), 2855 (w), 2254 (m), 1808 (w), 1693 (w), 1678 (w), 1651 (m), 1574 (w), 1561 (s), 1511 (w), 1449 (m), 1418 (m), 1404 (m), 1367 (w), 1349 (m), 1289 (m), 1238 (w), 1161 (s), 1113 (m), 1051 (w), 1020 (w), 1000 (w), 952 (w), 925 (m), 914 (m), 907 (m), 863 (s), 797 (s), 750 (m), 661 (s).

1-(2-cyanoethyl)-3-(3-cyanopropyl)imdazolium bromide (2h): Amber liquid, 91.3 % yield, glass transition/mp (DSC) T_g = -23.5^{o}C, T_m = 98.5 ^{o}C, $T_{5\%\,onset}$ = 196.4 ^{o}C; ^{1}H NMR (500 MHz, DMSO-d_6) δ ppm = 9.59 (s, 1H), 7.97 (s, 1H), 7.95 (s, 1H), 4.55 (t, 2H), 4.33 (t, 2H), 3.28 (t, 2H), 2.62 (t, 2H), 2.16 (pent, 2H); ^{13}C (125 MHz, DMSO-d_6) δ ppm = 137.5, 123.2, 123.1, 120.1, 118.2, 48.3, 44.9, 25.7, 19.1, 14.0; FT-IR (ν_{max} in cm^{-1}): 3370 (b), 3140 (w), 3058 (m), 2963 (w), 2906 (w), 2845 (w), 2248 (w), 1705 (w), 1638 (w), 1563 (s), 1450 (m), 1420 (m),

1358 (w), 1342 (w), 1229 (w), 1163 (s), 1109 (w), 1076 (w), 1050 (w), 1021 (w), 910 (w), 847 (w), 826 (w), 762 (s).

1-(2-cyanoethyl)-3-(4-cyanobutyl)imidazolium bromide (2i): Amber liquid, 61.1 % yield, glass transition/mp (DSC) T_g = -34.5 ^{o}C, T_m = 51.6 ^{o}C, $T_{5\%onset}$ = 189.7 ^{o}C; ^{1}H NMR (500 MHz, DMSO-d_6) δ ppm = 9.20 (s, 1H), 7.81 (s, 1H), 7.73 (s, 1H), 4.17 (t, 2H), 2.51 (t, 2H), 1.80 (pent, 2H), 1.55 (pent, 2H), 1.37 (pent, 2H), 1.27 (pent, 2H); ^{13}C (125 MHz, DMSO-d_6) δ ppm = 137.0, 124.1, 122.7, 121.1, 49.1, 36.2, 29.5, 27.8, 25.1, 16.5; FT-IR (ν_{max} in cm^{-1}): 3376 (b), 3137 (w), 3054 (m), 2958 (s), 2246 (w), 1639 (w), 1561 (s), 1455 (m), 1423 (m), 1363 (w), 1340 (w), 1236 (w), 1161 (s), 1052 (w), 1033 (w), 914 (w), 871 (w), 828 (w), 759 (s), 660 (w).

1-(2-cyanoethyl)-3-(5-cyanopentyl)imidazolium bromide (2j): Amber liquid, 97.4 % yield, glass transition (DSC) T_g = -39.7^{o}C, $T_{5\%onset}$ = 201.2 ^{o}C; ^{1}H NMR (500 MHz, DMSO-d_6) δ ppm = 9.39 (s, 1H), 7.91 (d, 2H), 4.53 (t, 2H), 4.25 (t, 2H), 3.26 (t, 2H), 2.51 (t, 2H), 1.84 (pent, 2H), 1.59 (pent, 2H), 1.34 (pent, 2H); ^{13}C (125 MHz, DMSO-d_6) δ ppm = 137.0, 123.3, 123.0, 121.0, 118.2, 49.1, 45.0, 28.9, 24.5, 19.2, 16.5; FT-IR (ν_{max} in cm^{-1}): 3401 (s), 3140 (w), 3078 (m), 2940 (m), 2867 (w), 2246 (w), 1628 (m), 1561 (s), 1509 (w), 1458 (m), 1421 (m), 1363 (w), 1340 (w), 1290 (w), 1234 (w), 1158 (s), 1108 (w), 1083 (w), 1051 (w), 1033 (w), 915 (w), 826 (m), 754 (m), 660 (w).

1-(2-cyanoethyl)-3-(6-cyanohexyl)imidazolium bromide (2k): Amber liquid, 86.4 % yield, glass transition/mp (DSC) T_g = -38.9 ^{o}C, T_m = 59.4 ^{o}C, $T_{5\%onset}$ = 178.9 ^{o}C; ^{1}H NMR (500 MHz, DMSO-d_6) δ ppm = 9.36 (s, 1H), 7.89 (d, 2H), 4.52 (t, 2H), 4.23 (t, 2H), 3.25 (t, 2H), 2.51 (t, 2H), 1.81 (pent, 2H), 1.54 (pent, 2H), 1.35 (pent, 2H), 1.26 (pent, 2H); ^{13}C (125 MHz, DMSO-d_6) δ ppm = 137.0, 123.3, 123.0, 121.1, 118.2, 49.4, 44.9, 29.4, 27.8, 25.0, 24.9, 19.2, 16.5; FT-IR (ν_{max} in cm^{-1}): 3409 (b), 3135 (w), 3058 (m), 2838 (s), 2863 (m), 2244 (w), 1628 (w), 1561 (s), 1455 (s), 1422 (m), 1358 (w), 1340 (w), 1234 (w), 1161 (s), 1107 (w), 1052 (w), 1033 (w), 914 (w), 824 (w), 757 (s), 659 (w).

Typical exchange of halide precursor **2a-k** for resulting dicyanamide salts (**3a-k**):

To a tared 100 mL round bottom flask, halide precursor salt **2a-k** (2.8 to 18.7 mmol, depending on precursor availability) is dissolved in 40 mL DI water. A Teflon stirbar is added, and then previously prepared silver dicyanamide (1.2 equivalents) is added and the suspension is stirred in darkness for more than 1 hour at 40-50 ^{o}C. The resulting yellowish/white solids are filtered and washed several times with water. The aqueous filtrate is reduced in volume by evaporation in an air stream prior to final drying on high vacuum for 48 hours at 60 ^{o}C.

To determine the residual halide content for each of the dicyanamide salts obtained, 3(a-k) (~0.5 g each) was dissolved in a solution of K_2CrO_4 (1.5 g, 25 mM in D.I. water) and then titrated with 17 mM $AgNO_3$ solution until the persistence of a red precipitated indicative of Ag_2CrO_4 formation was observed as the end-point and Ag^+ titrated at endpoint taken as equivalent to the amount of halide present in the solution. The ratio of mass of halide per mass of sample analyzed is made to calculate the concentration of halide residing in the isolated sample in parts per million (ppm).

1-cyanomethyl-3-methylimidazolium dicyanamide (3a): White solid, 87.1 % yield, glass transition/mp (DSC) T_g = -58.9 ^{o}C, T_m = 67.0 ^{o}C, $T_{5\%onset}$ = 186.6 ^{o}C; ^{1}H NMR (500 MHz, DMSO-d_6) δ ppm = 9.24 (s, 1H), 7.88 (t, 1H), 7.78 (t, 1H), 5.58 (s, 2H), 3.98 (s, 3H); ^{13}C (125 MHz, DMSO-d_6) δ ppm = 137.6, 124.2, 122.5, 119.0, 114.6, 36.7, 36.0; FT-IR (ν_{max} in cm^{-1}): 3681 (m), 3493 (w), 3149 (m), 3088 (m), 2953 (s), 2867 (w), 2230 (s), 2195 (m), 2125 (s), 1712 (w), 1612 (w), 1577 (w), 1558 (m) 1419 (w), 1410 (w), 1305 (s), 1218 (w), 1170 (s), 1111 (w), 1055 (m), 1033 (m), 933 (w), 906 (w), 857 (m), 745 (s); Impact sensitivity: > 200 kg·cm^{-1}.

1-(2-cyanoethyl)-3-methylimidazolium dicyanamide (3b): Amber liquid, 74.5 % yield, glass transition/mp (DSC) T_g = -66.7 ^{o}C, T_m = 11.9 ^{o}C, $T_{5\%onset}$ = 158.4 ^{o}C; ^{1}H NMR (500 MHz, DMSO-d_6) δ ppm = 9.11 (s, 1H), 7.80 (t, 1H), 7.48 (t, 1H), 4.50 (t, 2H), 3.89 (s, 3H) 3.19 (s, 2H); ^{13}C (125 MHz, DMSO-d_6) δ ppm = 136.9, 123.9, 122.2, 119.0, 117.6, 43.3, 35.8, 18.5; FT-IR (ν_{max} in cm^{-1}): 3681 (m), 3494 (w), 3150 (w), 3108 (m), 2967 (m), 2865 (w), 2229 (s), 2192 (m), 2119 (s), 1577 (m), 1562 (m) 1455 (w), 1420 (w), 1306 (s), 1165 (s), 1108 (w), 1053 (m), 1033 (m), 904 (w), 844 (m), 750 (m); Impact sensitivity: 172 kg·cm^{-1}.

1-(3-cyanopropyl)-3-methylimidazolium dicyanamide (3c): Amber liquid, 92.7 % yield, glass transition (DSC) T_g = -77.5 ^{o}C, $T_{5\%onset}$ = 243.2 ^{o}C; ^{1}H NMR (500 MHz, DMSO-d_6) δ ppm = 9.11 (s, 1H), 7.76 (s, 1H), 7.70 (s, 1H), 4.23 (t, 2H), 3.84 (s, 3H), 2.57 (t, 2H), 2.13 (m, 2H); ^{13}C (125 MHz, DMSO-d_6) δ ppm = 136.7, 123.6, 122.2, 119.5, 47.6, 35.7, 25.1, 13.4; FT-IR (ν_{max} in cm^{-1}): 3681 (m), 3428 (m), 3152 (w), 3108 (w), 3010 (w), 2966 (m), 2866 (w), 2233 (s), 2196 (m), 2125 (s), 1632 (w), 1575 (m), 1565 (m) 1454 (w), 1425 (w), 1309 (s), 1166 (s), 1054 (m), 1033 (m), 1015 (w), 905 (w), 843 (w), 751 (m); Impact sensitivity: 170 kg·cm^{-1}.

1-(4-cyanobutyl)-3-methylimidazolium dicyanamide (3d): Amber liquid, 82.6 % yield, glass transition (DSC) T_g = -73.9 ^{o}C, $T_{5\%onset}$ = 238.2 ^{o}C; ^{1}H NMR (500 MHz, DMSO-d_6) δ ppm = 9.10 (s, 1H), 7.76 (t, 1H), 7.71 (t, 1H), 4.20 (t, 2H), 3.85 (s, 3H), 2.55 (q, 2H), 1.87 (m, 2H), 1.55 (m, 2H); ^{13}C (125 MHz, DMSO-d_6) δ ppm = 136.5, 123.6, 122.1, 120.2, 119.0, 47.8, 35.7, 28.4, 21.4, 15.6; FT-IR (ν_{max} in cm^{-1}): 3681 (m), 3489 (w), 3149 (w), 3104 (w), 3011 (w), 2950 (m), 2867 (w), 2227 (s), 2192 (m), 2125 (s), 1623 (w), 1574 (m), 1456 (w), 1425 (w), 1305 (s), 1163 (s), 1055 (m), 1033 (w), 1017 (w), 903 (w), 842 (w), 749 (m); Impact sensitivity: 170 kg·cm^{-1}.

1-(5-cyanopentyl)-3-methylimidazolium dicyanamide (3e): Amber liquid, 84.3 % yield, glass transition (DSC) T_g = -75.7 ^{o}C, $T_{5\%onset}$ = 260.3 ^{o}C; ^{1}H NMR (500 MHz, DMSO-d_6) δ ppm = 9.11 (s, 1H), 7.77 (t, 1H), 7.71 (t, 1H), 4.18 (t, 2H), 3.86 (s, 3H), 2.51 (t, 2H), 1.82 (m, 2H), 1.60 (m, 2H), 1.34 (m, 2H); ^{13}C (125 MHz, DMSO-d_6) δ ppm = 136.4, 123.5, 122.1, 120.4, 119.0, 48.3, 35.6, 28.4, 24.4, 23.9, 15.8; FT-IR (ν_{max} in cm^{-1}): 3681 (w), 3491 (w), 3149 (w), 3104 (w), 3011 (w), 2941 (m), 2866 (w), 2227 (s), 2192 (m), 2125 (s), 1624 (w), 1574 (m), 1460 (w), 1425 (w), 1304 (s), 1168 (s), 1055 (m), 1033 (w), 1017 (w), 903 (w), 841 (w), 751 (m) Impact sensitivity: 170 kg·cm^{-1}.

1-(6-cyanohexyl)-3-methylimidazolium dicyanamide (3f): Amber liquid, 86.8 % yield, glass transition/mp (DSC) T_g = -77.2 ^{o}C, $T_{5\%onset}$ = 263.1 ^{o}C; ^{1}H NMR (500 MHz, DMSO-d_6) δ ppm = 9.10 (s, 1H), 7.76 (s, 1H), 7.69 (s, 1H), 4.16 (t, 2H), 3.85 (s, 3H), 2.48 (t, 2H), 1.80 (m, 2H), 1.56 (m, 2H), 1.40 (m, 2H), 1.34 (m, 2H); ^{13}C (125 MHz, DMSO-d_6) δ ppm = 136.4, 123.5, 122.1, 120.5, 190.0, 48.6, 35.6, 29.0, 27.3, 24.6, 24.4, 15.9; FT-IR (ν_{max} in cm^{-1}): 3667 (w), 3490 (w),

3149 (w), 3104 (w), 2938 (m), 2865 (w), 2230 (s), 2194 (m), 2125 (s), 1625 (w), 1573 (m), 1460 (w), 1425 (w), 1308 (s), 1167 (s), 1055 (m), 1033 (w), 903 (w), 842 (w), 753 (m); Impact sensitivity: 170 kg·cm^{-1}.

1-cyanomethyl-3-(2-cyanoethyl)imidazolium dicyanamide (3g): Amber liquid, 88.3 % yield, glass transition/mp (DSC) T_g = -27.6 ^{o}C, T_m = 60.0 ^{o}C, $T_{5\% onset}$ = 144.8 ^{o}C; ^{1}H NMR (500 MHz, DMSO-d_6) δ ppm = 9.38 (s, 1H), 7.96 (t, 1H), 7.91 (t, 1H), 5.63 (s, 2H), 4.56 (t, 2H), 3.21 (s, 2H) ^{13}C (125 MHz, DMSO-d_6) δ ppm = 138.3, 123.7, 123.6, 119.6, 118.1, 115.1, 45.3, 37.6, 19.0; FT-IR (ν_{max} in cm^{-1}): 3427 (w), 3145 (w), 3114 (w), 3015 (w), 2981 (w), 2233 (s), 2195 (m), 2125 (s), 1692 (w), 1623 (w), 1562 (m), 1457 (w), 1418 (w), 1310 (s), 1233 (w), 1164 (s), 1107 (w), 1080 (w), 1027 (w), 909 (w), 846 (w), 747 (m); Impact sensitivity: 176 kg·cm^{-1}.

1-(2-cyanoethyl)-3-(3-cyanopropyl)imidazolium dicyanamide (3h): Amber liquid, 91.8 % yield, glass transition/mp (DSC) T_g = -61.2 ^{o}C, $T_{5\% onset}$ = 161.8 ^{o}C; ^{1}H NMR (500 MHz, DMSO-d_6) δ ppm = 9.26 (s, 1H), 7.85 (t, 1H), 7.84 (t, 1H), 4.50 (t, 2H), 4.29 (t, 2H), 3.19 (t, 2H), 2.58 (t, 2H), 2.15 (m, 2H); ^{13}C (125 MHz, DMSO-d_6) δ ppm = 136.7, 122.7, 122.5, 119.4, 119.0, 117.6, 47.8, 44.4, 25.1, 18.5, 13.4; FT-IR (ν_{max} in cm^{-1}): 3491 (w), 3144 (w), 3108 (w), 3015 (w), 2967 (w), 2229 (s), 2193 (m), 2125 (s), 1624 (w), 1564 (m), 1504 (w), 1452 (w), 1420 (w), 1306 (s), 1233 (w), 1161 (s), 1108 (w), 1079 (w), 1047 (w), 1023 (w), 906 (w), 844 (w), 750 (m); Impact sensitivity: 176 kg·cm^{-1}.

1-(2-cyanoethyl)-3-(4-cyanobutyl)imidazolium dicyanamide (3i): Amber liquid, 90.8 % yield, glass transition/mp (DSC) T_g = -60.8 ^{o}C, $T_{5\% onset}$ = 167.5 ^{o}C; ^{1}H NMR (500 MHz, DMSO-d_6) δ ppm =9.25 (s, 1H), 7.84 (s, 2H), 4.50 (t, 2H), 4.26 (t, 2H), 3.20 (t, 2H), 2.55 (t, 2H), 1.89 (m, 2H), 1.55 (m, 2H); ^{13}C (125 MHz, DMSO-d_6) δ ppm =136.5, 122.7, 122.5, 120.2. 119.0, 117.6, 48.1, 44.4, 28.4, 21.4, 18.5, 15.6; FT-IR (ν_{max} in cm^{-1}): 3697 (w), 3665 (w), 3488 (w), 3144 (w), 2981 (m), 2939 (m), 2923 (m), 2866 (m), 2844 (m), 2233 (s), 2195 (m), 2125 (s), 1631 (w), 1563 (m), 1509 (w), 1455 (w), 1420 (w), 1310 (s), 1239 (w), 1159 (s), 1107 (w), 1055 (s), 1033 (s), 1016 (s), 908 (w), 827 (w), 748 (m); Impact sensitivity: 174 kg·cm^{-1}.

1-(2-cyanoethyl)-3-(5-cyanopentyl)imidazolium dicyanamide (3j): Amber liquid, 85.4 % yield, glass transition/mp (DSC) T_g = -65.6 ^{o}C, T_m = 53.3 ^{o}C, $T_{5\% onset}$ = 162.6 ^{o}C; ^{1}H NMR (500 MHz, DMSO-d_6) δ ppm = 9.26 (s, 1H), 7.85(s, 2H), 4.50 (t, 2H), 4.24 (t, 2H), 3.21 (t, 2H), 2.49 (t, 2H), 1.84 (m, 2H), 1.60 (m, 2H), 1.36 (m, 2H); ^{13}C (125 MHz, DMSO-d_6) δ ppm = 136.4, 122.7, 122.4, 120.4, 119.0, 117.6, 48.5, 28.4, 24.4, 23.9, 18.6, 15.9; FT-IR (ν_{max} in cm^{-1}): 3707 (w), 3681 (w), 3488 (w), 3144 (w), 2981 (m), 2967 (m), 2939 (m), 2866 (m), 2844 (m), 2229 (s), 2193 (m), 2125 (s), 1563 (m), 1509 (w), 1455 (w), 1420 (w), 1345 (m), 1308 (s), 1160 (s), 1055 (s), 1033 (s), 1016 (s), 906 (w), 826 (w), 749 (m); Impact sensitivity: 174 kg·cm^{-1}.

1-(2-cyanoethyl)-3-(6-cyanohexyl)imidazolium dicyanamide (3k): Amber liquid, 85.4 % yield, glass transition/mp (DSC) T_g = -66.7 ^{o}C, T_m = 57.7 ^{o}C, $T_{5\% onset}$ = 154.2 ^{o}C; ^{1}H NMR (500 MHz, DMSO-d_6) δ ppm = 9.25 (s, 1H), 7.85(q, 2H), 4.49 (t, 2H), 4.21 (t, 2H), 3.21 (t, 2H), 2.49 (t, 2H), 1.80 (m, 2H), 1.54 (m, 2H), 1.36 (m, 2H), 1.22 (m, 2H); ^{13}C (125 MHz, DMSO-d_6) δ ppm =136.4, 122.7, 122.4, 120.5, 119.0, 117.6, 48.8, 44.4, 28.9, 27.2, 24.5, 24.3, 18.6, 15.9; FT-IR (ν_{max} in cm^{-1}): 3697 (w), 3681 (w), 3489 (w), 3144 (w), 2966 (m), 2939 (m), 2866 (m), 2844

(m), 2231 (s), 2194 (m), 2125 (s), 1624 (w), 1563 (m), 1508 (w), 1455 (w), 1421 (w), 1308 (s), 1162 (s), 1055 (s), 1033 (s), 1017 (s), 906 (w), 825 (w), 752 (m); Impact sensitivity: 170 kg·cm^{-1}.

A4. <u>Reactivity of N-cyanoalkyl-substituted imidazolium halide salts by simple elution through an azide anion exchange resin</u>

General procedure for the elution of N-cyanoalkyl-functionalized imidazolium halides on azide exchanged resin: The synthesis and characterization of all *N*-cyanoalkyl functionalized imidazolium halides (**1[Br]**, **2[Cl]**, **3[Cl]**, and **4[Br]**) have been reported previously.[39] The 5 mmol halide/15 mL water solution of the halide samples (**1-4[X]**) were introduced onto the N$_3^-$-resin column with an elution rate of 2 cm/min. After eluting the halide solution from the column, the column was additionally rinsed with 20 mL water, and all eluted fractions were combined. Almost all water was removed first by blowing dry air through the solution. Then, the IL was kept under high vacuum overnight with a slight heating of 40 °C, to remove residual water. Isolation resulted in monocationic mixtures (**1[N$_3$/Br]** and **5[N$_3$/Cl]**) and the mixed amide and tetrazole products **6[N$_3$/Cl]** + **8** and **7[N$_3$/Br]** + **9**.

1-(6-cyanohexyl)-3-methylimidazolium azide/bromide (1[N$_3$/Br])
Mixed salt **1[N$_3$/Br]** was prepared from **1[Br]** (1.373 g, 5.1 mmol). Amber liquid; ^{1}H NMR (500 MHz, DMSO-d_6) δ ppm 9.14 (s, 1H), 7.78 (t, 1H), 7.71 (t, 1H), 4.16 (t, 2H), 3.85 (s, 3H), 2.49 (m, 3H), 1.52 (m, 2H), 1.38 (m, 2H), 1.28 (m, 2H), 1.23 (t, 2H); ^{13}C NMR (125 MHz, DMSO-d_6) δ ppm 136.5, 123.6, 122.2, 120.6, 48.6, 35.7, 29.0, 27.3, 24.6, 24.4, 16.0. FT-IR (v_{max} in cm^{-1}): 3707 (w), 3665 (w), 3376 (w), 3309 (w), 3145 (w), 2938 (s), 2864 (m), 2242 (w), 2000 (vs), 1644 (w), 1571 (m), 1456 (w), 1426 (w), 1332 (m), 1168 (s), 1055 (s), 1033 (s), 1015 (s), 840 (w), 756 (w), 736 (w).

1-(acetamido)methyl-3-methylimidazolium azide/chloride (5[N$_3$/Cl])
Mixed salt **5[N$_3$/Cl]** was prepared from **2[Cl]** (0.788 g, 5.0 mmol). Brown solid; ^{1}H NMR (500 MHz, DMSO-d_6) δ ppm 9.13 (s, 1H), 8.01 (s, 1H), 7.70 (s, 2H), 7.52 (s, 1H), 4.98 (s, 2H), 3.89 (s, 3H); ^{13}C NMR (125 MHz, DMSO-d_6) δ ppm 166.7, 137.7, 123.8, 122.9, 50.4, 35.7. FT-IR (v_{max} in cm^{-1}): 3442 (w), 3391 (w), 3314 (w), 3148 (s), 3109 (s), 3090 (s), 2985 (w), 2945 (w), 2019 (vs), 1692 (vs), 1626 (s), 1571 (s), 1470 (w), 1440 (w), 1396 (s), 1381 (w), 1352 (m), 1303 (s), 1208 (m), 1166 (s), 1092 (w), 1033 (w), 974 (w), 850 (s), 775 (w), 757 (w), 672 (w).

1-(acetamido)methyl-3-butylimidazolium azide/chloride and 1-(5-tetrazolidyl)-methyl-3-butylimidazolium (6[N$_3$/Cl] + 8, 1.2:1 mixture)
The mixture (**6[N$_3$/Cl]** + **8**) was prepared from **3[Cl]** (1.231 g, 6.0 mmol). Amber liquid (70%); ^{1}H NMR (500 MHz, DMSO-d_6) δ ppm 9.27 (s, 1H), 9.17 (s, 1H), 7.98 (s, 1H), 7.85 (d, 2H), 7.71 (d, 2H), 7.54 (s, 1H), 5.53 (s, 2H), 4.96 (s, 2H), 4.21 (t, 2H), 4.18 (t, 2H), 1.76 (m, 2H), 1.73 (m, 2H), 1.26 (m, 2H), 1.21 (m, 2H), 0.91 (t, 3H), 0.88 (t, 3H); ^{13}C NMR (125 MHz, DMSO-d_6) δ ppm 166.7, 155.7, 137.3, 136.1, 124.0, 122.9, 122.2, 121.7, 50.5, 48.6, 48.5, 44.8, 31.4, 31.3, 18.8, 18.7, 13.2. FT-IR (v_{max} in cm^{-1}): 3330 (w), 3148 (w), 3099 (w), 2965 (w), 2925 (w) 2204 (w), 2009 (vs), 1694 (s), 1671 (w), 1565 (m), 1466 (w), 1403 (w), 1310 (w), 1165 (m), 1143 (w), 1036 (w), 861 (w), 753 (m).

1-(acetamido)methyl-3-butylimidazolium azide/bromide and 1-(5-tetrazolidyl)methyl-3-butylimidazolium (7[N₃/Br] + 9, 0.4:1 mixture)

The mixture **7[N$_3$/Br]** + **9** was prepared from **4[Br]** (1.678 g, 6.5 mmol). Amber liquid (83%); ^{1}H NMR (500 MHz, DMSO-d_6) δ ppm 9.36 (s, 1H), 9.34 (s, 1H), 8.13 (s, 1H), 7.97 (s, 2H), 7.78 (s, 2H), 7.59 (s, 1H), 5.94 (m, 1H), 5.17 (m, 1H) 7.54 (s, 1H), 4.22 (t, 2H), 4.18 (t, 2H), 1.80 (d, 3H), 1.76 (d, 3H), 1.73 (m, 2H), 1.71 (m, 2H), 1.28 (m, 2H), 1.20 (m, 2H), 0.92 (t, 3H), 0.89 (t, 3H); FT-IR (v_{max} in cm^{-1}): 3330 (w), 3148 (w), 3099 (w), 2965 (w), 2925 (w) 2204 (w), 2009 (vs), 1694 (s), 1671 (w), 1565 (m), 1466 (w), 1403 (w), 1310 (w), 1165 (m), 1143 (w), 1036 (w), 861 (w), 753 (m).

A5. <u>Zinc-assisted synthesis of imidazolium-tetrazolate bi-heterocyclic zwitterions with variable alkyl bridge length</u>

General procedure for synthesis of zinc halide-complexed 1-(5-tetrazolidyl)alkyl-3-alkylimidazolium zwitterions, 9-16: N-cyanoalkyl-N-alkylimidazolium halide (**1-8[X]**) (0.77 to 10.6 mmol) was combined with sodium azide (1.1 equivalents) in a 100 mL round-bottom flask with 50 mL water and stirred to dissolve with a magnetic stir bar. Zinc bromide was added (1.1 equivalent), and the mixture was stirred to reflux overnight. The resultant white, solid was washed several times with water and filtered. The final product was dried at 60 °C for 24 h in the furnace, and reported yields are based upon the formula weight of the product calculated with ZnBr$_{0.8}$Cl$_{1.2}$ (**9**), ZnBr$_2$ (**10** and **14**), or ZnBrCl (**11-13**, **15**, **16**).

1-(5-tetrazolidyl)methyl-3-methylimidazolium·(ZnBr$_{0.8}$Cl$_{1.2}$) (9)

Compound **9** was prepared from **1[Cl]** (1.662 g, 10 mmol). White powder, (96%), ^{1}H NMR (360 MHz, DMSO-d_6) δ ppm 9.18 (s, 1H), 7.75 (t, J = 1.72 Hz, 1H), 7.68 (t, J = 1.74 Hz, 1H), 5.57 (s, 2H); 3.87 (3H, s); ^{13}C NMR (125 MHz, DMSO-d_6) δ ppm 154.17, 138.06, 124.44, 123.56, 42.91, 36.55; FT-IR (v_{max}): 3498 (w), 3103 (s), 3078 (s), 2076 (s), 1618 (w), 1572 (s), 1446 (s), 1433 (s), 1421 (s), 1340 (m), 1171 (s), 1072 (m), 839 (s), 816 (s), 776 (s), 692 (s) cm^{-1}.

Optimization data collection for the conversion of 1-cyanomethyl-3-methylimidazolium chloride, 1[Cl], to zinc-coordination product, 9: **1[Cl]** (0.015 g, 0.010 mmol) was dissolved with 1.1 equivalents of both ZnBr$_2$ and NaN$_3$ in D$_2$O (1 mL). The progress of the reaction was monitored at the 500 MHz instrument frequency for ^{1}H NMR, where 85% conversion to **9** was observed at room temperature after about 2.5 h. The experiment was performed in a borosilicate glass NMR tube (5 mm diameter, thin wall, 7 inches length, Wilmad LabGlass, Vineland, NJ) where the progress of the reaction was checked periodically by ^{1}H NMR. A comparison of the signals for the CH_2 peaks of the α-carbon nearest the nitrile precursor (**1-8[X]**) and tetrazole product (**9-16**) served as the measurable to quantify the estimated conversion for the Click reaction.

1-(2-(5-tetrazolidyl)ethyl)-3-methylimidazolium·(ZnBr$_2$) (10)

Compound **10** was prepared from **2[Br]** (0.491 g, 2.5 mmol). White powder, (38%), ^{1}H NMR (360 MHz, DMSO-d_6) δ ppm 9.08 (s, 1H), 7.65 (td, J = 4.48, 1.80 Hz, 2H), 4.58 (t, J = 6.91 Hz, 2H), 3.84 (s, 3H), 3.45 (t, J = 6.92 Hz, 2H); ^{13}C NMR (125 MHz, DMSO-d_6) δ ppm 157.95, 137.41, 124.11, 122.95, 48.10, 36.42, 26.20; FT-IR (v_{max}): 3569 (m), 3103 (m), 3098

(m), 2146 (m), 2066 (s), 1575 (m), 1560 (m), 1487 (m), 1421 (s), 1335 (m), 1161 (s), 1082 (m), 854 (s), 761 (s), 705 (m) cm^{-1}.

1-(3-(5-tetrazolidyl)propyl)-3-methylimidazolium·(ZnBr$_{2-x}$Cl$_x$) (11)

Compound **11** was prepared from **3[Cl]** (1.963 g, 10.6 mmol). White powder, (46%), ^{1}H NMR (500 MHz, DMSO-d_6) δ ppm 9.10 (s, 1H), 7.70 (d, J = 25.61 Hz, 2H), 4.21 (t, J = 6.40 Hz, 2H), 3.85 (s, 3H), 3.00-2.86 (m, 2H), 2.18 (t, 2H); ^{13}C NMR (125 MHz, DMSO-d_6) δ ppm 160.32, 137.08, 124.08, 122.73, 48.82, 36.31, 29.01, 21.32; FT-IR (ν_{max}): 3518 (w), 3104 (m), 3083 (m), 2066 (s), 1570 (s), 1560 (s), 1489 (s), 1439 (s), 1428 (s), 1156 (s), 1064 (m), 837 (s), 748 (s), 698 (m) cm^{-1}.

1-(4-(5-tetrazolidyl)butyl)-3-methylimidazolium·(ZnBr$_{2-x}$Cl$_x$) (12)

Compound **12** was prepared from **4[Cl]** (0.815 g, 4.1 mmol). Yellowish solid, (74%), ^{1}H NMR (500 MHz, DMSO-d_6) δ ppm 9.07 (s, 1H), 7.68 (d, J = 24.35 Hz, 2H), 4.14 (t, J = 6.96 Hz, 2H), 3.83 (s, 1H), 2.87 (t, J = 6.82 Hz, 3H), 1.79-1.75 (m, 2H), 1.58 (q, 2H); ^{13}C NMR (125 MHz, DMSO-d_6) δ ppm 161.37, 137.00, 124.18, 122.77, 49.11, 36.44, 29.62, 25.68, 23.76; FT-IR (ν_{max}): 3514 (w), 3104 (w), 2946 (w), 2061 (s), 1570 (s), 1486 (m), 1426 (s), 1337 (m), 1161 (s), 1074 (m), 1019 (w), 829 (m), 743 (s) cm^{-1}.

1-(5-tetrazolidyl)methyl-3-butylimidazolium·(ZnBr$_{2-x}$Cl$_x$) (13)

Compound **13** was prepared from **5[Cl]** (1.000 g, 3.8 mmol). White powder, (74%), ^{1}H NMR (500 MHz, DMSO-d_6) δ ppm 9.26 (s, 1H), 7.78 (d, J = 29.47 Hz, 2H), 5.80 (s, 2H), 4.20 (t, J = 7.07 Hz, 2H), 1.83-1.72 (m, 2H), 1.26 (m, J = 14.38, 7.08 Hz, 2H), 0.90 (t, J = 7.29 Hz, 3H); ^{13}C NMR (125 MHz, DMSO-d_6) δ ppm 156.27, 136.96, 123.33, 122.95, 49.19, 44.00, 31.78, 19.26, 13.74; FT-IR (ν_{max}): 3098 (s), 2946 (m), 2865 (w), 2075 (m), 1565 (s), 1441 (s), 1335 (m), 1161 (s), 1138 (m), 1075 (m), 822 (s), 746 (s), 710 (s), 672 (s) cm^{-1}.

1-(2-(5-tetrazolidyl)ethyl)-3-butylimidazolium·(ZnBr$_2$) (14)

Compound **14** was prepared from **6[Br]** (0.198 g, 0.77 mmol). White powder, (61%), ^{1}H NMR (500 MHz, DMSO-d_6) δ ppm 9.18 (s, 1H), 7.77 (s, 1H), 7.75 (s, 1H), 4.60 (t, J = 6.71 Hz, 2H), 4.13 (t, J = 7.02 Hz, 2H), 3.51 (t, J = 6.59 Hz, 2H), 1.70 (m, J = 7.14 Hz, 2H), 1.18 (m, J = 7.55 Hz, 2H), 0.85 (t, J = 7.36 Hz, 3H); ^{13}C NMR (125 MHz, DMSO-d_6) δ ppm 153.52, 136.76, 122.72, 48.82, 46.48, 31.48, 24.09, 18.84, 13.41; FT-IR (ν_{max}): 3572 (w), 3402 (w), 3140 (w), 3106 (w), 2962 (w), 2962 (w), 2934 (w), 2873 (w), 2161 (m), 2061 (s), 1561 (m), 1491 (w), 1439 (s), 1338 (m), 1288 (w), 1240 (w), 1158 (s), 1108 (w), 1070 (w), 1027 (w), 953 (w), 922 (w), 826 (m), 747 (m) cm^{-1}.

1-(3-(5-tetrazolidyl)propyl)-3-butylimidazolium·(ZnBr$_{2-x}$Cl$_x$) (15)

Compound **15** was prepared from **7[Cl]** (1.020 g, 4.5 mmol). White powder, (70%), ^{1}H NMR (500 MHz, DMSO-d_6) δ ppm 9.14 (s, 1H), 9.14 (s, 1H), 7.73 (s, 1H), 4.16 (t, J = 6.89 Hz, 2H), 4.11 (t, J = 7.23 Hz, 2H), 2.86 (t, J = 7.35 Hz, 2H), 2.20-2.11 (m, 2H), 1.78-1.69 (m, 2H), 1.22 (dd, J = 14.99, 7.45 Hz, 2H), 0.85 (t, J = 7.37 Hz, 3H); ^{13}C NMR (125 MHz, DMSO-d_6) δ ppm 160.33, 136.50, 122.94, 122.91, 49.18, 48.92, 31.67, 28.97, 21.40, 19.34, 13.80; FT-IR (ν_{max}): 3493 (w), 3108 (w), 2942 (w), 2061 (s), 1565 (s), 1426 (s), 1337 (m), 1161 (s), 1074 (m), 1021 (s), 834 (m), 743 (s) cm^{-1}.

1-(4-(5-tetrazolidyl)butyl)-3-butylimidazolium·(ZnBr$_{2-x}$Cl$_x$) (16)

Compound **16** was prepared from **8[Cl]** (1.039 g, 4.3 mmol). Dark yellow waxy solid, (63%), ^{1}H NMR (500 MHz, DMSO-d_6) δ ppm (9.19 (s, 1H), 7.77 (d, J = 10.07 Hz, 2H), 4.32-3.89 (m, 4H), 2.92 (t, J = 7.34 Hz, 2H), 1.79 (dd, J = 14.80, 7.23 Hz, 4H), 1.64-1.55 (m, 2H), 1.26 (dd, J = 14.94, 7.44 Hz, 2H), 0.90 (t, J = 7.34 Hz, 3H); ^{13}C NMR (125 MHz, DMSO-d_6) δ ppm 161.03, 136.34, 122.93, 122.89, 49.15, 49.11, 31.68, 29.46, 25.54, 23.82, 19.31, 13.75; FT-IR (v_{max}): 3503 (w), 3099 (w), 2956 (w), 2066 (s), 1560 (s), 1489 (m), 1429 (s), 1158 (s), 1075 (m), 1019 (w), 829 (m), 743 (s) cm^{-1}.

A6. Synthesis, limitations, and thermal properties of energetically-substituted, protonated imidazolium picrate and nitrate salts and further comparison with their methylated analogs

Procedure for Alkylimidazoles (*Method A*) (3, 7, 13-15)

A mixture of appropriate imidazole (10 mmol), alkyl bromide (12 mmol), potassium carbonate (3.32 g, 24 mmol), and tetrabutylammonium bromide (0.032 g, 0.1 mmol) in acetonitrile (50 mL) was stirred vigorously under reflux for 2 h. After cooling to room temperature, the precipitate was filtered off and washed with acetonitrile. The filtrate was evaporated, and the crude products were purified via column chromatography using ethyl acetate/hexane.

Procedure for Alkylimidazoles (*Method B*) (3, 5-7, 12)

The appropriate imidazole (50 mmol) was dissolved in DMF (10 mL). Potassium *tert*-butoxide (6.7 g, 60 mmol) was added at 0–5 °C followed by the addition of appropriate alkyl bromide (72 mmol). The reaction mixture was stirred at room temperature overnight. Water (20 mL) was added to the mixture. The solution was extracted with ethyl acetate (3 × 40 mL). The extract was washed with brine and dried over anhydrous magnesium sulfate. The solvent was evaporated under reduced pressure (bath 60–70 °C) to remove DMF and the residue was purified via column chromatography using ethyl acetate/hexane to give the desired *N*-alkylimidazoles.

1-Propylimidazole (1-Pr-Im, 3).[110] Oil, 60% yield, ^{1}H NMR (300 MHz, [D$_1$] CHCl$_3$) δ, 0.91 (t, J = 7.4 Hz, 3H), 1.85-1.73 (m, 2H), 3.89 (t, J = 7.1 Hz, 2H), 6.90 (s, 1H), 7.04 (s, 1H), 7.45 (s, 1H), ^{13}C NMR (75 MHz, [D$_1$] CHCl$_3$) δ 10.8, 24.1, 48.3, 118.5, 129.0, 136.8.

1-Butyl-2-methylimidazole (1-Bu-2-Me-Im, 5).[111] Oil (87%^{b}); ^{1}H NMR (300 MHz, [D$_1$] CHCl$_3$) δ 0.94 (t, J = 7.3 Hz, 3H), 1.33 (m, 2H), 1.72–1.67 (m, 2H), 2.36 (s, 3H), 3.81 (t, J = 7.2 Hz, 2H), 6.80 (d, J = 1.0 Hz, 1H), 6.88 (d, J = 1.0 Hz, 1H); ^{13}C NMR (75 MHz, [D$_1$] CHCl$_3$) δ 12.8, 13.3, 19.5, 32.5, 45.5, 118.8, 126.7, 144.0. Anal. Calcd for C$_8$H$_{14}$N$_2$: C, 69.52; H, 10.21; N, 20.27. Found: C, 68.91; H, 10.62; N, 20.02.

1-Pentyl-2-methylimidazole (1-Pent-2-Me-Im, 6). Oil, 92%^{b} yield, ^{1}H NMR (300 MHz, [D$_1$] CHCl$_3$) δ 0.90 (t, J = 7.0 Hz, 3H), 1.37–1.26 (m, 4H), 1.75–1.65 (m, 2H), 2.35 (s, 3H), 3.79 (t, J = 7.1 Hz, 2H), 6.79 (d, J = 1.2 Hz, 1H), 6.88 (d, J = 1.2 Hz, 1H), ^{13}C NMR (75 MHz, [D$_1$] CHCl$_3$) δ, 12.6, 13.5, 21.8, 28.2, 30.0, 45.6, 118.6, 126.5, 143.8. Anal. Calcd for C$_9$H$_{16}$N$_2$: C, 71.01; H, 10.59; N, 18.40. Found: C, 70.25; H, 11.09; N, 17.96.

1-Hexylimidazole (1-Hex-Im, **7**). Oil, 44%[a] and 72%[b] yield, ^{1}H NMR (300 MHz, [D$_1$] CHCl$_3$) δ, 0.88 (t, J = 7.6 Hz, 3H) 1.33-1.26 (m, 6H), 1.75 (p, J = 14.4 Hz, J = 7.0 Hz, 2H), 3.91 (t, J = 7.1 Hz, 2H), 6.90 (t, J = 1.2 Hz, 1H), 7.04 (t, J = 1.0 Hz, 1H), 7.45 (s, 1H); ^{13}C NMR (75 MHz, [D$_1$] CHCl$_3$) δ 13.6, 22.1, 25.8, 30.7, 30.8, 46.6, 118.4, 128.9, 136.7. Anal. Calcd for C$_9$H$_{16}$N$_2$: C, 71.01; H, 10.59; N, 18.40. Found: C, 69.96; H, 10.98; N, 18.39.

1-Isopropyl-4-nitroimidazole (1-i-Pr-4-NO$_2$-Im, **12**). Plates from ethyl acetate/hexane 78%[b] yield, mp 50-53 °C; ^{1}H NMR (300 MHz, [D$_1$] CHCl$_3$) δ 1.59 (d, J = 6.7 Hz, 6H), 4.56-4.47 (m, 1H), 7.58 (d, J = 1.1 Hz, 1H), 7.91 (d, J = 1.3 Hz, 1 H), ^{13}C NMR (75 MHz, [D$_1$] CHCl$_3$) δ 23.3, 50.9, 117.3, 134.3, 147.9. Anal. Calcd for C$_6$H$_9$N$_3$O$_2$: C, 46.45; H, 5.85; N, 27.08. Found: C, 46.85; H, 5.82; N, 27.11.

1-Butyl-2-methyl-4-nitroimidazole (1-Bu-2-Me-4-NO$_2$-Im, **13**). Microcrystals from ethyl acetate/hexane, 84%[a] yield, mp 58-60 °C, ^{1}H NMR (300 MHz, [D$_1$] CHCl$_3$) δ 0.99 (t, J = 7.4 Hz, 3H), 1.46-1.33 (m, 2H), 1.84-1.74 (m, 2H), 2.44 (s, 3H), 3.94 (t, J = 7.3 Hz, 2H), 7.71 (s, 1H), ^{13}C NMR (75 MHz, [D$_1$] CHCl$_3$) δ 13.0, 13.4, 19.5, 32.1, 46.9, 119.5, 144.5, 146.2. Anal. Calcd for C$_8$H$_{13}$N$_3$O$_2$: C, 52.45; H, 7.15; N, 22.94. Found: C, 52.80; H, 7.33; N, 22.87.

1-Pentyl-2-methyl-4-nitroimidazole (1-Pent-2-Me-4-NO$_2$-Im, **14**). Microcrystals from ethyl acetate/hexane, 65%[a] yield, mp 35-37 °C, ^{1}H NMR (300 MHz, [D$_1$] CHCl$_3$) δ 0.93 (t, J = 6.7 Hz, 3H), 1.40-1.32 (m, 4H), 1.85-1.75 (m, 2H), 2.44 (s, 3H), 3.92 (t, J = 7.4 Hz, 2H), 7.70 (s, 1H), ^{13}C NMR (75 MHz, [D$_1$] CHCl$_3$) δ 13.1, 13.7, 22.1, 28.4, 29.9, 47.2, 119.5, 144.5, 146.3. Anal. Calcd for C$_9$H$_{15}$N$_3$O$_2$: C, 54.81; H, 7.67; N, 21.30. Found: C, 55.13; H, 7.90; N, 21.22.

1-Hexyl-4-nitroimidazole (1-Hex-4-NO$_2$-Im, **15**). Microcrystals from ethyl acetate/hexane, 62%[a] yield, mp 39-41 °C, ^{1}H NMR (300 MHz, [D$_1$] CHCl$_3$) δ 0.89 (t, J = 6.9 Hz, 3H), 1.36-1.28 (m, 6H), 1.90-1.80 (m, 2H), 4.04 (t, J = 7.1 Hz, 2H), 7.46 (d, J = 1.3 Hz, 1H), 7.79 (d, J = 1.4 Hz, 1H), ^{13}C NMR (75 MHz, [D$_1$] CHCl$_3$) δ 13.7, 22.2, 25.8, 30.5, 30.9, 48.3, 119.1, 135.9, 147.9. Anal. Calcd for C$_9$H$_{15}$N$_3$O$_2$: C, 54.81; H, 7.67; N, 21.30. Found: C, 55.13; H, 7.93; N, 21.10.

General Procedure for Preparation of Protonated Imidazolium Nitrate and Picrate Salts
A variety of acid-base paired, protonated imidazolium salts were prepared using a neutralization reaction procedure.[112] The appropriate imidazole (0.6 mmol) was dissolved in EtOH (3 mL) and a solution of the appropriate acid (0.6 mmol; 3% excess of nitric acid was used for the preparation of nitrates) was added dropwise to the imidazole solution with stirring at 40 °C. All of the neutralization reactions were exothermic. The solution was stirred for up to 10 h at 40 °C, after which the solvent was removed on a rotary evaporator, under reduced pressure, at 50 °C. Reaction progress was monitored using TLC chromatographic techniques, using chloroform and methanol as eluent, comparing the signatures of the obtained products with the TLC signature of the starting materials. Solid products were washed with cold EtOH to remove any unreacted substrates. Similarly, liquid samples were washed with dry acetone. Pure products were obtained in 82-99% yields after drying under vacuum at 40 °C for 10 h. The reactions with 1-methylimidazolium, 1,2-dimethylimidazolium, and 1-butylimidazolium salts were performed using the same procedure but on larger scale (50 mmol).

1-Methylimidazolium Picrate ([1-Me-3-H-Im][Pic]) (1a): Yellow solid, 98% yield; ^{1}H NMR (360 MHz, [D$_6$] DMSO) δ = 3.85 (s, 3H, N-CH$_3$), 7.61 (s, 1H, C5-H), 7.65 (s, 1H, C4-H), 8.58 (s, 2H, picrate), 8.94 (s, 1H, N-H); ^{13}C NMR (90 MHz, [D$_6$] DMSO) δ = 35.24 (N-CH$_3$), 120.14, 122.97 (C4/5), 124.13 (picrate), 125.14 (picrate), 135.87 (C2), 141.83 (picrate), 160.77 (picrate).

1,2-Dimethylimidazolium Picrate ([1,2-diMe-3-H-Im][Pic]) (2a): Yellow solid, 98% yield; ^{1}H NMR (360 MHz, [D$_6$] DMSO) δ = 2.54 (s, 3H, C2-CH$_3$), 3.72 (s, 3H, N-CH$_3$), 7.51 (s, 1H, C5-H), 7.56 (s, 1H, C4-H), 8.58 (s, 2H, picrate); ^{13}C NMR (90 MHz, [D$_6$] DMSO) δ = 10.22 (C2-CH$_3$), 33.84 (N-CH$_3$), 117.59, 122.95 (C4/5), 124.11 (picrate), 125.15 (picrate), 141.84 (picrate), 144.41 (C2), 160.77 (picrate).

1-Propylimidazolium Picrate ([1-Pr-3-H-Im][Pic]) (3a): Yellow solid, 95% yield; ^{1}H NMR (360 MHz, [D$_6$] DMSO) δ = 0.82 (t, 3H, -C̲H̲$_3$), 1.80 (m, 2H, -C̲H̲$_2$-CH$_3$), 4.12 (t, 3H, N-CH$_2$-), 7.59 (s, 1H, C5-H), 7.70 (s, 1H, C4-H), 8.59 (s, 2H, picrate), 8.93 (s, 1H, C2-H); ^{13}C NMR (90 MHz, [D$_6$] DMSO) δ = 10.20 (-C̲H̲$_3$), 22.73 (-C̲H̲$_2$-CH$_3$), 49.44 (N-C̲H̲$_2$-), 120.79, 121.36 (C4/C5), 123.85 (picrate), 124.91 (picrate), 135.22 (C2), 141.54 (picrate), 160.57 (picrate).

1-Butylimidazolium Picrate ([1-Bu-3-H-Im][Pic]) (4a): Yellow viscous liquid, 98% yield,; ^{1}H NMR (360 MHz, [D$_6$] DMSO) δ = 0.90 (t, 3H, -CH$_3$), 1.23 (sextet, 2H, -CH$_2$-), 1.76 (p, 2H, -CH$_2$-), 4.13 (t, 2H, N-CH$_2$-), 7.52 (s, 1H, C5-H), 7.65 (s, 1H, C4-H), 8.60 (s, 2H, picrate), 9.19 (s, 1H, C2-H); ^{13}C NMR (90 MHz, [D$_6$] DMSO) δ = 13.34 (-C̲H̲$_3$), 18.93 (-C̲H̲$_2$-CH$_3$), 31.02 (-C̲H̲$_2$-), 46.52 (N-C̲H̲$_2$-), 118.20, 121.85 (C4/C5), 124.15 (picrate), 125.11 (picrate), 141.55 (picrate), 144.52 (C2), 160.75 (picrate).

1-Butyl-2-methylimidazolium Picrate ([1-Bu-2-Me-3-H-Im][Pic]) (5a): Yellow solid, 98% yield; ^{1}H NMR (360 MHz, [D$_6$] DMSO) δ = 0.91 (t, 3H, -C̲H̲$_3$), 1.29 (m, 2H, -C̲H̲$_2$-CH$_3$), 1.71 (p, 2H, -C̲H̲$_2$-CH$_2$-), 2.58 (s, 3H, C2-C̲H̲$_3$), 4.07 (t, 3H, N-C̲H̲$_2$-), 7.56 (s, 1H, C5-H), 7.64 (s, 1H, C4-H), 8.59 (s, 2H, picrate); ^{13}C NMR (90 MHz, [D$_6$] DMSO) δ = 10.23 (-C̲H̲$_3$), 13.38 (C2-C̲H̲$_3$), 18.96 (-C̲H̲$_2$-CH$_3$), 31.01 (-C̲H̲$_2$-), 46.52 (N-C̲H̲$_2$-), 118.11, 121.81 (C4/C5), 124.09 (picrate), 125.07 (picrate), 141.47 (picrate), 144.06 (C2), 160.83 (picrate).

1-Pentyl-2-methylimidazolium Picrate ([1-Pent-2-Me-3-H-Im][Pic]) (6a): Yellow solid, 96% yield; ^{1}H NMR (360 MHz, [D$_6$] DMSO) δ = 0.87 (t, 3H, -C̲H̲$_3$), 1.30 (m, 4H, -C̲H̲$_2$-C̲H̲$_2$-), 1.73 (p, 2H, -C̲H̲$_2$-CH$_2$-), 2.56 (s, 3H, C2-C̲H̲$_3$), 4.05 (t, 3H, N-C̲H̲$_2$-), 7.54 (s, 1H, C5-H), 7.63 (s, 1H, C4-H), 8.59 (s, 2H, picrate); ^{13}C NMR (90 MHz, [D$_6$] DMSO) δ = 10.47 (-C̲H̲$_3$), 13.92 (C2-C̲H̲$_3$), 21.77 (-C̲H̲$_2$-CH$_3$), 27.95 (-C̲H̲$_2$-), 28.88 (-C̲H̲$_2$-), 46.84 (N-C̲H̲$_2$-), 118.39, 121.92 (C4/C5), 124.39 (picrate), 125.34 (picrate), 141.37 (picrate), 144.00 (C2), 160.80 (picrate).

1-Hexylimidazolium Picrate ([1-Hex-3-H-Im][Pic]) (7a): Yellow liquid, 97% yield; ^{1}H NMR (360 MHz, [D$_6$] DMSO) δ = 0.84 (t, 3H, -C̲H̲$_3$), 1.25 (m, 6H, -C̲H̲$_2$-C̲H̲$_2$-C̲H̲$_2$-), 1.77 (p, 2H, -C̲H̲$_2$-CH$_2$-), 4.13 (t, 3H, N-C̲H̲$_2$-), 7.55 (s, 1H, C5-H), 7.68 (s, 1H, C4-H), 8.50 (s, 2H, picrate), 8.86 (s, 1H, C2-H); ^{13}C NMR (90 MHz, [D$_6$] DMSO) δ = 13.74 (-C̲H̲$_3$), 21.81 (-C̲H̲$_2$-CH$_3$), 25.17 (-CH$_2$-), 29.48 (-C̲H̲$_2$-), 30.45 (-C̲H̲$_2$-), 47.98 (N-C̲H̲$_2$-), 120.30, 121.40 (C4/C5), 124.15 (picrate), 125.10 (picrate), 135.45 (C2), 141.76 (picrate), 159.84 (picrate).

1-Methyl-2-nitroimidazolium Picrate ([1-Me-2-NO$_2$-3-H-Im][Pic]) (8a): Yellow slowly crystallizing viscous liquid; ^{1}H NMR (360 MHz, [D$_6$] DMSO) δ = 3.99 (s, 3H, N-CH$_3$), 7.15 (s, 1H, C5-H), 7.64 (s, 1H, C4-H), 8.61 (s, 2H, picrate), 11.42 (b, N-H); ^{13}C NMR (90 MHz, [D$_6$] DMSO) δ = 37.05 (N-CH$_3$), 124.46 (picrate), 125.17 (picrate), 127.47, 128.48 (C4/5), 141.76 (picrate), 151.58 (C2), 160.52 (picrate).

1,2-Dimethyl-5-nitroimidazolium Picrate ([1,2-diMe-5-NO$_2$-3-H-Im][Pic]) (9a): Yellow thin crystals, 92% yield; ^{1}H NMR (360 MHz, [D$_6$] DMSO) δ = 2.49 (s, 3H, C2-CH$_3$), 3.85 (s, 3H, N-CH$_3$), 8.27 (s, 1H, C4-H), 8.59 (s, 2H, picrate); ^{13}C NMR (90 MHz, [D$_6$] DMSO) δ = 13.05(C2-CH$_3$), 33.50 (N-CH$_3$), 124.52 (picrate), 125.13 (picrate), 129.06 (C4), 141.76 (picrate), 143.62 (C2), 150.09 (C5), 160.85 (picrate).

1-Ethyl-2-nitroimidazolium Picrate ([1-Et-2-NO$_2$-3-H-Im][Pic]) (10a): Yellow viscous liquid, 86% yield; ^{1}H NMR (360 MHz, [D$_6$] DMSO) δ = 1.38 (t, 3H, -CH$_3$), 4.40 (q, 2H, N-CH$_2$-), 7.17 (d, 1H, C5-H), 7.70 (d, 1H, C4-H), 8.59 (s, 2H, picrate), ca. 9.2 (b, N-H); ^{13}C NMR (90 MHz, [D$_6$] DMSO) δ = 15.56 (-CH$_3$), 44.72 (N-CH$_2$-), 124.81 (picrate), 125.14 (picrate), 127.06, 128.86 (C4/5), 141.76 (picrate), 150.22 (C2), 160.41 (picrate).

1-Ethyl-4-nitroimidazolium Picrate ([1-Et-4-NO$_2$-3-H-Im][Pic]) (11a): Yellow viscous liquid, 83% yield; ^{1}H NMR (360 MHz, [D$_6$] DMSO) δ = 1.41 (t, 3H, -CH$_3$), 4.12 (q, 2H, N-CH$_3$), 7.91 (s, 1H, C5-H), 8.48 (s, 1H, C2-H), 8.61 (s, 2H, picrate), 9.35 (b, N-H); ^{13}C NMR (90 MHz, [D$_6$] DMSO) δ = 15.70 (CH$_2$-CH$_3$), 42.51 (N-CH$_2$), 121.20 (C5), 124.31 (picrate), 125.15 (picrate), 136.95 (C2), 141.78 (picrate), 146.89 (C4), 160.58 (picrate).

1-Isopropyl-4-nitroimidazolium Picrate ([1-i-Pr-4-NO$_2$-3-H-Im][Pic]) (12a): Yellow solid, 91% yield; ^{1}H NMR (360 MHz, [D$_6$] DMSO) δ = 1.44 (d, 6H, -CH$_3$), 4.53 (m, 1H, N-CH-), 7.95 (s, 1H, C5-H), 8.52 (s, 1H, C2-H), 8.59 (s, 2H, picrate); ^{13}C NMR (90 MHz, [D$_6$] DMSO) δ = 22.91 (-CH$_3$), 50.59 (N-CH-), 119.84 (C5), 124.52 (picrate), 125.27 (picrate), 135.95 (C4), 141.92 (picrate), 147.14 (C2), 160.69 (picrate).

1-Butyl-2-methyl-4-nitroimidazolium Picrate ([1-Bu-2-Me-4-NO$_2$-3-H-Im][Pic]) (13a): Yellow solid, 94% yield; ^{1}H NMR (360 MHz, [D$_6$] DMSO) δ = 0.89 (t, 3H, -CH$_3$), 1.26 (m, 2H, -CH$_2$-CH$_3$), 1.69 (p, 2H, -CH$_2$-), 2.35 (s, 3H, C2-CH$_3$), 3.97 (t, 2H, N-CH$_2$-), 8.32 (s, 1H, C5-H), 8.59 (s, 2H, picrate); ^{13}C NMR (90 MHz, [D$_6$] DMSO) δ = 12.48 (-CH$_3$), 13.32 (C2-CH$_3$), 18.99 (-CH$_2$-CH$_3$), 31.44 (-CH$_2$-), 46.10 (N-CH$_2$-), 121.97 (C5), 124.35 (picrate), 125.10 (picrate), 141.75 (picrate), 144.77 (C4), 145.18 (C2), 160.52 (picrate).

1-Pentyl-2-methyl-4-nitroimidazolium Picrate ([1-Pent-2-Me-4-NO$_2$-3-H-Im][Pic]) (14a): Yellow solid, 95% yield; ^{1}H NMR (360 MHz, [D$_6$] DMSO) δ = 0.86 (t, 3H, -CH$_3$), 1.29 (m, 4H, -CH$_2$-CH$_2$-), 1.71 (p, 2H, -CH$_2$-), 2.35 (s, 3H, C2-CH$_3$), 3.96 (t, 2H, N-CH$_2$-), 8.33 (s, 1H, C5-H), 8.59 (s, 2H, picrate); ^{13}C NMR (90 MHz, [D$_6$] DMSO) δ = 12.51 (-CH$_3$), 13.73 (C2-CH$_3$), 21.57 (-CH$_2$-CH$_3$), 27.67 (-CH$_2$-), 29.12 (-CH$_2$-), 46.32 (N-CH$_2$-), 122.01 (C5), 124.32 (picrate), 125.18 (picrate), 141.76 (picrate), 144.79 (C4), 145.19 (C2), 160.56 (picrate).

1-Hexyl-4-nitroimidazolium Picrate ([1-Hex-4-NO$_2$-3-H-Im][Pic]) (15a): Yellow viscous liquid, 94% yield; ^{1}H NMR (360 MHz, [D$_6$] DMSO) δ = 0.84 (t, 3H, -CH$_3$), 1.25 (m, 6H, -CH$_2$-

CH<u>2</u>-C<u>H2</u>-), 1.76 (p, 2H, -C<u>H2</u>-), 4.05 (t, 2H, N-C<u>H2</u>-), 7.88 (d, 1H, C5-H), 8.44 (s, 1H, C2-H), 8.59 (s, 2H, picrate); ^{13}C NMR (90 MHz, [D$_6$] DMSO) δ = 13.50 (-C<u>H3</u>), 21.51 (-C<u>H2</u>-CH$_3$), 24.93, 29.24, 30.22 (-C<u>H2</u>-), 47.75 (N-C<u>H3</u>-), 119.14 (C5), 124.87 (picrate), 125.18 (picrate), 135.18 (C2), 141.53 (picrate), 144.20 (C4), 160.49 (picrate).

1-Methyl-2,4-dinitroimidazolium Picrate ([1-Me-2,4-diNO₂-3-H-Im][Pic]) (16a): This reaction failed. Yellow co-crystals of 1-methyl-2,4-dinitroimidazole and picric acid were isolated, 1-Me-2,4-diNO2-IM•HPic.

1-Methyl-4,5-dinitroimidazolium Picrate ([1-Me-4,5-diNO₂-3-H-Im][Pic]) (17a): This reaction failed. No product was observed, only a mixture of the reactants.

1-Methyl-4,5-dicyanoimidazolium Picrate ([1-Me-4,5-diCN-3-H-Im][Pic]) (18a): This reaction failed. Yellow co-crystals of 1-methyl-4,5-dicyanoimidazole and picric acid were isolated, 1-Me-4,5-diCN-IM• 1.5 HPic.

1-Methylimidazolium Nitrate ([1-Me-3-H-Im][NO₃]) (1b): White solid, 99% yield; ^{1}H NMR (360 MHz, [D$_6$] DMSO) δ = 3.86 (s, 3H, N-CH$_3$), 7.66 (s, 1H, C5-H), 7.69 (s, 1H, C4-H), 9.05 (s, 1H, C2-H); ^{13}C NMR (90 MHz, [D$_6$] DMSO) δ = 35.40 (N-CH$_3$), 119.66, 123.09 (C4/5), 135.86 (C2).

1,2-Dimethylimidazolium Nitrate ([1,2-diMe-3-H-Im][NO₃]) (2b): White crystals, 99% yield; ^{1}H NMR (360 MHz, [D$_6$] DMSO) δ = 2.55 (s, 3H, C2-CH$_3$), 3.73 (s, 3H, N-CH$_3$), 7.52 (s, 1H, C5-H), 7.57 (s, 1H, C4-H); ^{13}C NMR (90 MHz, [D$_6$] DMSO) δ =10.10 (C2-CH$_3$), 33.83 (N-CH$_3$), 117.52, 122.91 (C4/5), 144.41 (C2).

1-Propylimidazolium Nitrate ([1-Pr-3-H-Im][NO₃]) (3b): White crystals, 96% yield; ^{1}H NMR (360 MHz, [D$_6$] DMSO) δ = 0.84 (t, 3H, -C<u>H3</u>), 1.81 (m, 2H, -C<u>H2</u>-CH$_3$), 4.15 (t, 3H, N-C<u>H2</u>-), 7.70 (s, 1H, C5-H), 7.90 (s, 1H, C4-H), 9.15 (s, 1H, C2-H); ^{13}C NMR (90 MHz, [D$_6$] DMSO) δ = 10.26 (-C<u>H3</u>), 22.72 (-C<u>H2</u>-CH$_3$), 49.86 (N-C<u>H2</u>-), 119.80, 121.84 (C4/C5), 135.13 (C2).

1-Butylimidazolium Nitrate ([1-Bu-3-H-Im][NO₃]) (4b): Colorless liquid, 99% yield; ^{1}H NMR (360 MHz, [D$_6$] DMSO) δ = 0.90 (t, 3H, -CH$_3$), 1.25 (sextet, 2H, -CH$_2$-), 1.80 (p, 2H, -CH$_2$-), 4.21 (t, 2H, N-CH$_2$-), 7.72 (s, 1H, C5-H), 7.82 (s, 1H, C4-H), 9.19 (s, 1H, C2-H); ^{13}C NMR (90 MHz, [D$_6$] DMSO) δ = 13.25, 18.84, 31.45 (alkyl), 48.23 (N-CH$_2$-), 120.08, 122.00 (C4/5), 135.35 (C2).

1-Butyl-2-methylimidazolium Nitrate ([1-Bu-2-Me-3-H-Im][NO₃]) (5b): White solid, 97% yield; ^{1}H NMR (360 MHz, [D$_6$] DMSO) δ = 0.90 (t, 3H, -C<u>H3</u>), 1.28 (m, 2H, -C<u>H2</u>-CH$_3$), 1.71 (p, 2H, -C<u>H2</u>-CH$_2$-), 2.58 (s, 3H, C2-C<u>H3</u>), 4.07 (t, 3H, N-C<u>H2</u>-), 7.57 (s, 1H, C5-H), 7.66 (s, 1H, C4-H); ^{13}C NMR (90 MHz, [D$_6$] DMSO) δ = 10.15 (-C<u>H3</u>), 13.33 (C2-C<u>H3</u>), 18.91 (-C<u>H2</u>-CH$_3$), 30.95 (-C<u>H2</u>-), 46.47 (N-C<u>H2</u>-), 117.93, 121.99 (C4/C5), 143.79 (C2).

1-Pentyl-2-methylimidazolium Nitrate ([1-Pent-2-Me-3-H-Im][NO₃]) (6b): White solid, 96% yield; ^{1}H NMR (360 MHz, [D$_6$] DMSO) δ = 0.87 (t, 3H, -C<u>H3</u>), 1.30 (m, 4H, -C<u>H2</u>-C<u>H2</u>-), 1.73

(p, 2H, -C$\underline{H_2}$-CH$_2$-), 2.58 (s, 3H, C2-C$\underline{H_3}$), 4.07 (t, 3H, N-C$\underline{H_2}$-), 7.57 (s, 1H, C5-H), 7.66 (s, 1H, C4-H); ^{13}C NMR (90 MHz, [D$_6$] DMSO) δ = 10.16 (-C$\underline{H_3}$), 13.71 (C2-C$\underline{H_3}$), 21.55 (-C$\underline{H_2}$-CH$_3$), 27.73 (-C$\underline{H_2}$-), 28.63 (-C$\underline{H_2}$-), 46.67 (N-C$\underline{H_2}$-), 117.94, 121.78 (C4/C5), 143.79 (C2).

1-Hexylimidazolium Nitrate ([1-Hex-3-H-Im][NO$_3$]) (7b): White solid, 98% yield; ^{1}H NMR (360 MHz, [D$_6$] DMSO) δ = 0.84 (t, 3H, -C$\underline{H_3}$), 1.25 (m, 6H, -C$\underline{H_2}$-C$\underline{H_2}$-C$\underline{H_2}$-), 1.79 (p, 2H, -C$\underline{H_2}$-CH$_2$-), 4.18 (t, 3H, N-C$\underline{H_2}$-), 7.70 (s, 1H, C5-H), 7.81 (s, 1H, C4-H), 9.17 (s, 1H, C2-H); ^{13}C NMR (90 MHz, [D$_6$] DMSO) δ = 13.76 (-C$\underline{H_3}$), 21.82 (-C$\underline{H_2}$-CH$_3$), 25.13 (-C$\underline{H_2}$-), 29.32 (-C$\underline{H_2}$-), 30.46 (-C$\underline{H_2}$-), 48.45 (N-C$\underline{H_2}$-), 119.89, 121.93 (C4/C5), 135.22 (C2).

1-Methyl-2-nitroimidazolium Nitrate ([1-Me-2-NO$_2$-3-H-Im][NO$_3$]) (8b): White solid, 82% yield; ^{1}H NMR (360 MHz, [D$_6$] DMSO) δ = 4.00 (s, 3H, N-CH$_3$), 7.17 (s, 1H, C5-H), 7.65 (s, 1H, C4-H), 11.49 (b, N-H); ^{13}C NMR (90 MHz, [D$_6$] DMSO) δ = 37.07 (N-CH$_3$), 127.49, 128.51 (C4/5), 141.31 (C2).

1,2-Dimethyl-5-nitroimidazolium Nitrate ([1,2-diMe-5-NO$_2$-3-H-Im][NO$_3$]) (9b): White solid, 84% yield; ^{1}H NMR (360 MHz, [D$_6$] DMSO) δ = 2.52 (s, 3H, C2-CH$_3$), 3.87 (s, 3H, N-CH$_3$), 8.36 (s, 1H, C4-H), 12.1 (b, N-H); ^{13}C NMR (90 MHz, [D$_6$] DMSO) δ = 12.81 (C2-CH$_3$), 33.62 (N-CH$_3$), 122.87 (C4), 138.55 (C2), 149.82 (C5).

1-Ethyl-2-nitroimidazolium Nitrate ([1-Et-2-NO$_2$-3-H-Im][NO$_3$]) (10b): Colorless liquid, 85% yield; ^{1}H NMR (360 MHz, [D$_6$] DMSO) δ = 1.38 (t, 3H, -CH$_3$), 4.39 (q, 2H, N-CH$_2$-), 7.17 (d, 1H, C5-H), 7.70 (d, 1H, C4-H); ^{13}C NMR (90 MHz, [D$_6$] DMSO) δ = 15.57 (-CH$_3$), 44.72 (N-CH$_2$), 127.08, 127.88 (C4/5), 149.16 (C2).

1-Ethyl-4-nitroimidazolium Nitrate ([1-Et-4-NO$_2$-3-H-Im][NO$_3$]) (11b): Colorless liquid, 89% yield; ^{1}H NMR (360 MHz, [D$_6$] DMSO) δ = 1.39 (t, 3H, -CH$_3$), 4.08 (q, 2H, N-CH$_2$-), 7.89 (s, 1H, C5-H), 8.46 (s, 1H, C2-H); ^{13}C NMR (90 MHz, [D$_6$] DMSO) δ = 15.70 (-CH$_3$), 42.50 (N-CH$_2$), 121.20 (C5), 136.95 (C2), 145.86 (C4).

1-Isopropyl-4-nitroimidazolium Nitrate ([1-*i*-Pr-4-NO$_2$-3-H-Im][NO$_3$]) (12b): White solid, 89% yield; ^{1}H NMR (360 MHz, [D$_6$] DMSO) δ = 1.44 (d, 6H, -C$\underline{H_3}$), 4.52 (m, 1H, N-C$\underline{H}$-), 7.95 (s, 1H, C5-H), 8.52 (s, 1H, C2-H); ^{13}C NMR (90 MHz, [D$_6$] DMSO) δ = 22.71 (-C$\underline{H_3}$), 50.33 (N-C$\underline{H}$-), 119.64 (C5), 135.75 (C4), 146.93 (C2).

1-Butyl-2-methyl-4-nitroimidazolium Nitrate ([1-Bu-2-Me-4-NO$_2$-3-H-Im][NO$_3$]) (13b): White solid, 93% yield; ^{1}H NMR (360 MHz, [D$_6$] DMSO) δ = 0.90 (t, 3H, -CH$_3$), 1.28 (m, 2H, -C$\underline{H_2}$-CH$_3$), 1.69 (p, 2H, -C$\underline{H_2}$-), 2.35 (s, 3H, C2-CH$_3$), 3.97 (t, 2H, N-C$\underline{H_2}$-), 8.33 (s, 1H, C5-H); ^{13}C NMR (90 MHz, [D$_6$] DMSO) δ = 12.49 (-C$\underline{H_3}$), 13.32 (C2-C$\underline{H_3}$), 18.97 (-C$\underline{H_2}$-CH$_3$), 31.43 (-C$\underline{H_2}$-), 46.07 (N-C$\underline{H_2}$-), 122.07 (C5), 144.71 (C4), 145.11 (C2).

1-Pentyl-2-methyl-4-nitroimidazolium Nitrate ([1-Pent-2-Me-4-NO$_2$-3-H-Im][NO$_3$]) (14b): Colorless viscous liquid, 97% yield; ^{1}H NMR (360 MHz, [D$_6$] DMSO) δ = 0.86 (t, 3H, -C$\underline{H_3}$), 1.30 (m, 4H, -C$\underline{H_2}$-C$\underline{H_2}$-), 1.71 (p, 2H, -C$\underline{H_2}$-), 2.35 (s, 3H, C2-C$\underline{H_3}$), 3.96 (t, 2H, N-C$\underline{H_2}$-), 8.34 (s, 1H, C5-H); ^{13}C NMR (90 MHz, [D$_6$] DMSO) δ = 12.28 (-C$\underline{H_3}$), 13.50 (C2-C$\underline{H_3}$), 21.33 (-

$\underline{CH_2}$-CH$_3$), 27.63 (-$\underline{CH_2}$-), 28.88 (-$\underline{CH_2}$-), 46.07 (N-$\underline{CH_2}$-), 121.79 (C5), 144.55 (C4), 145.10 (C2).

1-Hexyl-4-nitroimidazolium Nitrate ([1-Hex-4-NO$_2$-3-H-Im][NO$_3$]) (15b): Colorless viscous liquid, 95% yield; ^{1}H NMR (360 MHz, [D$_6$] DMSO) δ = 0.85 (t, 3H, -$\underline{CH_3}$), 1.25 (m, 6H, -$\underline{CH_2}$-$\underline{CH_2}$-$\underline{CH_2}$-), 1.75 (p, 2H, -$\underline{CH_2}$-), 4.03 (t, 2H, N-$\underline{CH_2}$-), 7.85 (d, 1H, C5-H), 8.44 (s, 1H, C2-H); ^{13}C NMR (90 MHz, [D$_6$] DMSO) δ = 13.76 (-$\underline{CH_3}$), 21.82 (-$\underline{CH_2}$-CH$_3$), 25.26, 29.79, 30.47 (-$\underline{CH_2}$-), 47.26 (N-$\underline{CH_3}$-), 121.44, (C5), 125.10 (C2), 137.29 (C4).

1-Methyl-2,4-dinitroimidazolium Nitrate ([1-Me-2,4-diNO$_2$-3-H-Im][NO$_3$]) (16b): No product was observed, only a mixture of reactants.

1-Methyl-4,5-dinitroimidazolium Nitrate ([1-Me-4,5-diNO$_2$-3-H-Im][NO$_3$]) (17b): No product was observed, only a mixture of reactants.

1-Methyl-4,5-dicyanoimidazolium Nitrate ([1-Me-4,5-diCN-3-H-Im][NO$_3$]) (18b): No product was observed, only a mixture of reactants.

General Protocol for the Synthesis of Alkylated Imidazolium Salt Derivatives
1,3-Dimethylimidazolium chloride (1,3-diMe-IM][Cl]) (**19c**) and 1,2,3-trimethylimidazolium chloride ([1,2,3-triMe-Im][Cl]) (**20c**) were prepared by purging chloromethane gas through an EtOH solution of either 1-methylimidazole or 1,2-dimethylimidazole at 0 °C similar to a protocol presented in the literature.[113] 1-Butyl-3-methylimidazolium chloride (1-Bu-3-Me-Im][Cl]) (**21c**) was prepared using the standard literature protocol by reacting 1-methylimidazole with a 30% excess of chlorobutane at 70 °C and later removal of unreacted substrates under vacuum.[114]

1,3-Dimethylimidazolium nitrate ([1,3-diMe-Im][NO$_3$]) (**19b**), 1,2,3-trimethyl imidazolium nitrate ([1,2,3-triMe-Im][NO$_3$]) (**20b**), and 1-butyl-3-methylimidazolium nitrate ([1-Bu-3-Me-Im][NO$_3$]) (**21b**) were prepared from their chloride precursors by the anion exchange reaction of the chloride salt with silver nitrate (1:1 molar ratio) in aqueous solution utilizing a previously reported protocol.[115] Equimolar amounts of silver nitrate, dissolved in water, and imidazolium chloride salt, dissolved in water, were mixed together by dropwise addition of silver nitrate solution into a stirred solution of chloride salt. After the solution was stirred in the dark for 24 h, the silver chloride was removed by filtration, and the filtrate checked for the presence of silver ions using HCl. The solvent was then evaporated at 80 °C under vacuum. A final purification step involved dissolution of the obtained nitrate salt in dry ethanol in order to separate it from any solid, inorganic by-product. The salts were then dried under high vacuum at 60 °C for an additional 5 h.

1,3-Dimethylimidazolium, 1,2,3-trimethylimidazolium, and 1-butyl-3-methylimidazolium picrate salts ware prepared from their chloride precursors by an anion exchange reaction of the chloride salt with sodium picrate (1:1 molar ratio) in a mixture of EtOH/H$_2$O. Solvent was evaporated using high vacuum, the samples were re-dissolved in water, and the picrate salts were extracted from the aqueous phase using chloroform. Following this, the salts were dried under high vacuum at 60 °C for an additional 5 h. The possible presence of chloride anions was tested using aqueous solution of silver nitrate.

1,3-Dimethylimidazolium Nitrate ([1,3-diMe-Im][NO₃]) (19b): White solid, 65% yield; ^{1}H NMR (360 MHz, [D$_6$] DMSO) δ = 3.83 (s, 6H, N-CH$_3$), 7.69 (d, 2H, C4/C5-H), 9.03 (s, 1H, C2-H); ^{13}C NMR (90 MHz, [D$_6$] DMSO) δ = 35.59 (N-CH$_3$), 123.33 (C4/C5), 136.99 (C2).

1,2,3-Trimethylimidazolium Nitrate ([1,2,3-triMe-Im][NO₃]) (20b): White crystalline solid, 70% yield; ^{1}H NMR (500 MHz, [D$_4$] MeOH) δ = 2.58 (s, 3H, C2-CH$_3$), 3.85 (s, 6H, N-CH$_3$), 7.43 (s, 2H, C4/C5-H); ^{13}C NMR (125 MHz [D$_4$] MeOH) δ = 10.02 (C2-CH$_3$), 35.33 (N-CH$_3$), 123.26 (C4/C5), 146.42 (C2).

1-Butyl-3-methylimidazolium Nitrate ([1-Bu-3-Me-Im][NO₃]) (21b): Colorless liquid, 69% yield; ^{1}H NMR (500 MHz, [D$_6$] DMSO) δ = 0.91 (t, 3H, -CH$_3$), 1.33 (m, 2H, -CH$_2$-CH$_3$), 1.87 (m, 2H, -CH$_2$-), 4.05 (s, 3H, N-CH$_3$), 4.29 (t, 2H, N-CH$_2$-), 7.59 (s, 1H, C5-H), 7.77 (s, 1H, C4-H), 9.06 (s, 1H, C2-H); ^{13}C NMR (125 MHz [D$_6$] DMSO) δ = 13.45 (-CH$_3$), 20.10 (-CH$_2$-CH$_3$), 32.59 (-CH$_2$-CH$_2$-), 37.00 (N-CH$_3$), 49.93 (N-CH$_2$-), 122.23, 123.87 (C4/C5), 138.67 (C2).

1,3-Dimethylimidazolium Picrate ([1,3-diMe-Im][Pic]) (19a): Yellow solid, 78% yield; ^{1}H NMR (360 MHz, [D$_6$] DMSO) δ = 3.82 (s, 6H, N-CH$_3$), 7.68 (d, 2H, C4/C5-H), 8.60 (s, 2H, picrate), 9.02 (s, 1H, C2-H); ^{13}C NMR (90 MHz, [D$_6$] DMSO) δ = 35.58 (N-CH$_3$), 123.32 (C4/C5), 124.07 (picrate), 125.10 (picrate), 136.95 (C2), 141.74 (picrate), 160.73 (picrate).

1,2,3-Trimethylimidazolium Picrate ([1,2,3-triMe-Im][Pic]) (20a): Yellow crystalline solid, 85% yield; ^{1}H NMR (500 MHz, [D$_4$] MeOH) δ = 2.56 (s, 3H, C2-CH$_3$), 3.75 (s, 6H, N-CH$_3$), 7.59 (s, 2H, C4/C5-H), 8.59 (s, 2H, picrate); ^{13}C NMR (125 MHz [D$_4$] MeOH) δ = 9.47 (C2-CH$_3$), 34.54 (N-CH$_3$), 121.81 (C4/C5), 124.03 (picrate), 125.09 (picrate), 141.70 (picrate), 144.57 (C2), 160.70 (picrate).

1-Butyl-3-methylimidazolium Picrate ([1-Bu-3-Me-Im][Pic]) (21a): Yellow viscous liquid, 84% yield; ^{1}H NMR (360 MHz, [D$_6$] DMSO) δ = 0.93 (t, 3H, -CH$_3$), 1.36 (m, 2H, -CH$_2$-CH$_3$), 1.81 (m, 2H, -CH$_2$-), 4.00 (s, 3H, N-CH$_3$), 4.33 (t, 2H, N-CH$_2$-), 7.50 (s, 1H, C5-H), 7.71 (s, 1H, C4-H), 8.57 (s, 2H, picrate), 9.02 (s, 1H,C2-H); ^{13}C NMR (125 MHz [D$_6$] DMSO) δ = 13.22 (-CH$_3$), 20.90 (-CH$_2$-CH$_3$), 33.02 (-CH$_2$-CH$_2$-), 37.28 (N-CH$_3$), 49.15 (N-CH$_2$-), 122.21, 123.65 (C4/C5), 124.15 (picrate), 125.11 (picrate), 138.55 (C2), 141.38 (picrate), 160.76 (picrate).

A7. **Azolium azolates from reactions of neutral azoles with 1,3-diemethyl-imidazolium-2-carboxylate, 1,2,3-trimethyl-imidazolium hydrogen carbonate, and N,N dimethyl-pyrrolidinium hydrogen carbonate**

General Protocol for the Preparation of Azolate Base Salts

The IL precursors were prepared according to literature protocols. The precursors were prepared at 2-3 g scale and used as obtained. 5 mmol of the appropriate IL precursor ([1,3-diMe-Im-2-COO], [1,2,3-triMe-Im][HCO$_3$]•H$_2$O, or[*N,N*-diMe-Pyr][HCO$_3$]) was placed into a 10 mL volumetric flask and dissolved in 50% aqueous ethanol (*v/v*). Similarly, 2.5 mmol of the appropriate neutral azole (4-NO$_2$-Im, 2-Me-5-NO$_2$-Im, 4,5-diNO$_2$-Im, 4-NO$_2$-Tri, 3-NH$_2$-1,2,4-Tri, and 5-NH$_2$-Tetr) was placed into a 5 mL volumetric flask and dissolved in 50% aqueous ethanol (*v/v*). Next, 1mL of each prepared solution of IL precursor (0.5 mmol) was placed in the

reaction vial and 1 mL of the solution of neutral azole (0.5 mmol) was added dropwise. Upon mixing of the reagents, in reactions involving 4,5-diNO$_2$-Im, 4-NO$_2$-tri, and 5-NH$_2$-tetr, evolution of the gas from the solution was observed. In the reactions involving [1,3-diMe-Im-2-COO], 0.1 mL of DMSO was added to each reaction to facilitate the decarboxylation process.

The reaction mixtures were kept under moderate heating (40 °C) for 48 h. After 48 h, the solvent was removed on the rotary evaporator under vacuum at 90 °C. The successful reactions were identified by disappearance of the carboxylate (in the case of the zwitterion) or carbonate (in the case of the [HCO$_3$]$^-$ salts) signature in the ^{13}C NMR spectra. The characteristic carbonate or carboxylate peaks were not observed, after the completion of the reaction, in any of the analyzed samples. Only in the case of salts with [3-NH$_2$-1,2,4-Tri]$^-$ and [5-NH$_2$-Tetr]$^-$, another peak at ~160 ppm appeared on the ^{13}C NMR spectra resulting from the carbon atom in the anion directly bound to the amine group.

1,3-Dimethyl-imidazolium 4-Nitro-imidazolate ([1,3-diMe-Im][4-NO$_2$-Im], 1a): Yellow, crystalline solid, hygroscopic, mp 78 °C, $T_{5\%dec}$ 182 °C; ^{1}H NMR (360 MHz, [D$_6$] DMSO) δ =3.79 (s, 6H, N-CH$_3$), 7.11 (s, 1H, C5'-H), 7.60 (s, 2H, C4/C5-H), 9.02 (s, 1H, C2-H); ^{13}C NMR (90 MHz, [D$_6$] DMSO) δ = 35.69 (N-CH$_3$), 123.47 (C4/C5), 131.07 (C5'), 137.15 (C2'), 145.66 (C4'), 148.11 (C2).

1,3-Dimethyl-imidazolium 2-Methyl-5-nitro-imidazolate ([1,3-diMe-Im][2-Me-5-NO$_2$-Im], 1b): Yellow, crystalline solid, hygroscopic, mp 112 °C, $T_{5\%dec}$ 178 °C; ^{1}H NMR (360 MHz, [D$_6$] DMSO) δ =2.10 (s, 3H, C2'-CH$_3$), 3.79 (s, 6H, N-CH$_3$), 7.64 (s, 1H, C4'-H), 7.64 (s, 2H, C4/C5-H), 9.09 (s, 1H, C2-H); ^{13}C NMR (90 MHz [D$_6$] DMSO) δ = 17.31 (C2'-CH$_3$), 35.59 (N-CH$_3$), 123.40 (C4/C5), 132. 69 (C4'), 137.13 (C2'), 147.36 (C2), 154.12 (C5').

1,3-Dimethyl-imidazolium 4,5-Dinitro-imidazolate ([1,3-diMe-Im][4,5-diNO$_2$-Im], 1c): Yellow, crystalline solid, mp 96 °C, $T_{5\%dec}$ 215 °C; ^{1}H NMR (360 MHz, [D$_6$] DMSO) δ =3.84 (s, 6H, N-CH$_3$), 6.94 (C2'-H), 7.67 (s, 2H, C4/C5-H), 9.02 (s, 1H, C2-H); ^{13}C NMR (90 MHz [D$_6$] DMSO) δ = 35.55 (N-CH$_3$), 123.33 (C4/C5), 136.92 (C2), 139.25 (C2'), 140.16 (C4'/5').

1,3-Dimethyl-imidazolium 4-Nitro-1,2,3-triazolate ([1,3-diMe-Im][4-NO$_2$-1,2,3-Tri], 1d): Yellow, crystalline solid, mp 85 °C, $T_{5\%dec}$ 187 °C; ^{1}H NMR (360 MHz, [D$_6$] DMSO) δ = 3.86 (s, 6H, N-CH$_3$), 7.69 (d, 2H, C4/C5-H), 8.04 (s, 1H, C4'-H), 9.08 (s, 1H, C2-H); ^{13}C NMR (90 MHz [D$_6$] DMSO) δ = 35.57 (N-CH$_3$), 123.34 (C4/C5), 129.39 (C5'), 136.99 (C2), 154.1 (C4').

1,3-Dimethyl-imidazolium 3-Amino-1,2,4-triazolate ([1,3-diMe-Im][3-NH$_2$-1,2,4-Tri], 1e): Yellow, viscous liquid, no mp observed, $T_{5\%dec}$ 190 °C; ^{1}H NMR (360 MHz, [D$_6$] DMSO) δ =3.75 (s, 6H, N-CH$_3$), 5.25 (b, C3'-NH$_2$), 7.29 (s, 2H, C4/5), 7.64 (s, 1H, C5'-H), 9.21 (s, 1H, C2-H); ^{13}C NMR (90 MHz [D$_6$] DMSO) δ = 35.59 (N-CH$_3$), 123.40 (C4/C5), 137.40 (C2), 147.80 (C5'), 159.74 (C3').

1,3-Dimethyl-imidazolium 5-Amino-tetrazolate ([1,3-diMe-Im][5-NH$_2$-Tetr], 1f): White solid, hygroscopic, mp 84 °C, T$_{5\%dec}$ 206 °C; ^{1}H NMR (360 MHz, [D$_6$] DMSO) δ = 3.77 (s, 6H, N-CH$_3$), 4.08 (b, C5'-NH$_2$), 7.58 (s, 2H, C4/C5-H), 8.87 (s, 1H, C2-H); ^{13}C NMR (90 MHz [D$_6$] DMSO) δ = 36.11 (N-CH$_3$), 123.83 (C4/C5), 137.38 (C2), 164.53 (C5').

1,2,3-Trimethyl-imidazolium 4-Nitro-imidazolate ([1,2,3-triMe-Im][4-NO$_2$-Im], 2a): Yellow viscous liquid, no mp observed, $T_{5\%dec}$ 171 °C; ^{1}H NMR (500 MHz, [D$_4$] MeOH) δ =2.60 (s, 3H, C2-C$\underline{H}_3$), 3.82 (s, 6H, N-C$\underline{H}_3$), 7.31 (s, 1H, C4'-H), 7.44 (s, 2H, C4/C5-H), 7.81 (s, 1H, C2'); ^{13}C NMR (125 MHz [D$_4$] MeOH) δ = 9.43 (C2-C$\underline{H}_3$), 35.52 (N-C$\underline{H}_3$), 123.44 (C4/C5), 126.30 (C5'), 129.64 (C2), 145.07 (C2'), 148.46 (C4').

1,2,3-Trimethyl-imidazolium 2-Methyl-5-nitro-imidazolate ([1,2,3-triMe-Im][2-Me-5-NO$_2$-Im], 2b): Yellow, crystalline solid, mp 126 °C, $T_{5\%dec}$ 182 °C; ^{1}H NMR (500 MHz, [D$_4$] MeOH) δ =2.41 (s, 3H, C2'-C$\underline{H}_3$), 2.60 (s, 3H, C2-C$\underline{H}_3$), 3.80 (s, 6H, N-C$\underline{H}_3$), 7.37 (s, 2H, C4/C5-H), 8.00 (s, 1H, C4'); ^{13}C NMR (125 MHz [D$_4$] MeOH) δ = 9.51 (C2-C$\underline{H}_3$), 14.17 (C2'-C$\underline{H}_3$), 35.56 (N-C$\underline{H}_3$), 121.47 (C4'), 123.08 (C4/C5), 147.52 (C2), 148.46 (C2'), 151.22 (C5').

1,2,3-Trimethyl-imidazolium 4,5-Dinitro-imidazolate ([1,2,3-triMe-Im][4,5-diNO$_2$-Im], 2c): Yellow solid, mp 86 °C, $T_{5\%dec}$ 198 °C; ^{1}H NMR (500 MHz, [D$_4$] MeOH) δ = 2.59 (s, 3H, C2-C$\underline{H}_3$), 3.80 (s, 6H, N-C$\underline{H}_3$), 7.15 (s, 1H, C2'-H), 7.43 (s, 2H, C4/C5 H); ^{13}C NMR (125 MHz [D$_4$] MeOH) δ = 9.31 (C2-C$\underline{H}_3$), 35.41 (N-C$\underline{H}_3$), 123.33 (C4/C5), 139.10 (C2'), 148.95 (C2).

1,2,3-Trimethyl-imidazolium 4-Nitro-1,2,3-triazolate ([1,2,3-triMe-Im][4-NO$_2$-1,2,3-Tri], 2d): Yellow, crystalline solid, mp 107 °C, T$_{5\%dec}$ 195 °C; ^{1}H NMR (500 MHz, [D$_4$] MeOH) δ =2.59 (s, 3H, C2-C$\underline{H}_3$), 3.80 (s, 6H, N-C$\underline{H}_3$), 7.42 (s, 2H, C4/C5-H), 8.33 (s, 1H, C5'-H); ^{13}C NMR (125 MHz [D$_4$] MeOH) δ = 9.35 (C2-C$\underline{H}_3$), 35.42 (N-C$\underline{H}_3$), 123.37 (C4/C5), 128.47 (C5'), 146.43 (C2), 155.42 (C4').

1,2,3-Trimethyl-imidazolium 3-Amino-1,2,4-triazolate ([1,2,3-triMe-Im][3-NH$_2$-1,2,4-Tri], 2e): Yellow solid, very hygroscopic, no mp observed, $T_{5\%dec}$ 179 °C; ^{1}H NMR (500 MHz, [D$_4$] MeOH) δ =2.58 (s, 3H, C2-C$\underline{H}_3$), 3.79 (s, 6H, N-C$\underline{H}_3$), 7.42 (s, 2H, C4/C5-H), 7.53 (s, 1H, C5'-H); ^{13}C NMR (125 MHz [D$_4$] MeOH) δ = 9.29 (C2-C$\underline{H}_3$), 34.30 (N-C$\underline{H}_3$), 123.20 (C4/C5), 148.59 (C2), 146.28 (C5'), 160.11 (C3').

1,2,3-Trimethyl-imidazolium 5-Amino-tetrazolate ([1,2,3-triMe-Im][5-NH$_2$-Tetr], 2f): White solid, hygroscopic, mp 160 °C, $T_{5\%dec}$ 202 °C; ^{1}H NMR (500 MHz, [D$_4$] MeOH) δ =2.55 (s, 3H, C2-C$\underline{H}_3$), 3.77 (s, 6H, N-C$\underline{H}_3$), 7.39 (s, 2H, C4/C5-H); ^{13}C NMR (125 MHz [D$_4$] MeOH) δ = 9.33 (C2-C$\underline{H}_3$), 35.41 (N-C$\underline{H}_3$), 123.39 (C4/C5), 146.25 (C2), 163.40 (C5').

***N,N*-Dimethyl-pyrrolidinium 4-Nitro-imidazolate ([*N,N*-diMe-Pyr][4-NO$_2$-Im], 3a):** Yellow, viscous liquid, no mp observed, $T_{5\%dec}$ 175 °C; ^{1}H NMR (500 MHz, [D$_4$] MeOH) δ =2.23 (t, 4H, -C$\underline{H}_2$-), 3.15 (s, 6H, N-C$\underline{H}_3$), 3.51 (t, 4H, N-C$\underline{H}_2$), 7.32 (s, 1H, C4'-H), 7.82 (s, 1H, C2'-H); ^{13}C NMR (125 MHz [D$_4$] MeOH) δ = 23.09 (-C$\underline{H}_2$-), 52.58 (N-C$\underline{H}_3$), 69.07 (N-C$\underline{H}_2$), 129.16(C5'), 144.80 (C2'), 149.06 (C4').

***N,N*-Dimethyl-pyrrolidinium 2-Methyl-5-nitro-imidazolate ([*N,N*-diMe-Pyr][2-Me-5-NO$_2$-Im], 3b):** Yellow, crystalline solid, mp 128 °C, $T_{5\%dec}$ 179 °C; ^{1}H NMR (500 MHz, [D$_4$] MeOH) δ = 2.22 (t, 4H, -C$\underline{H}_2$-), 2.26 (s, 3H, C2'-C$\underline{H}_3$), 3.14 (s, 6H, N-C$\underline{H}_3$), 3.51 (t, 4H, N-C$\underline{H}_2$), 7.75 (s, 1H, C5'-H); ^{13}C NMR (125 MHz [D$_4$] MeOH) δ = 16.49 (C2'-C$\underline{H}_3$), 23.07 (-C$\underline{H}_2$-), 52.58 (N-C$\underline{H}_3$), 67.05 (N-C$\underline{H}_2$), 131.12 (C4'), 148.29 (C2'), 154.82 (C5').

N,N-Dimethyl-pyrrolidinium 4,5-Dinitro-imidazolate ([N,N-diMe-Pyr][4,5-diNO₂-Im], 3c): Yellow, crystalline solid, mp at $T_{5\%dec}$ (hot stage apparatus) ~220 °C, $T_{5\%dec}$ 221 °C; ¹H NMR (500 MHz, [D₄] MeOH) δ =2.25 (t, 4H, -CH₂-), 3.17 (s, 6H, N-CH₃), 3.53 (t, 4H, N-CH₂), 7.06 (s, 1H, C2'); ¹³C NMR (125 MHz [D₄] MeOH) δ = 23.00 (-CH₂-), 52.51 (N-CH₃), 67.00 (N-CH₂), 139.85 (C2').

N,N-Dimethyl-pyrrolidinium 4-Nitro-1,2,3-triazolate ([N,N-diMe-Pyr][4-NO₂-1,2,3-Tri], 3d): Yellow, viscous liquid, mp 57 °C, $T_{5\%dec}$ 173 °C; ¹H NMR (500 MHz, [D₄] MeOH) δ =2.24 (t, 4H, -CH₂-), 3.16 (s, 6H, N-CH₃), 3.52 (t, 4H, N-CH₂), 8.23 (s, 1H, C5'-H); ¹³C NMR (125 MHz [D₄] MeOH) δ = 22.99 (-CH₂-), 52.49 (N-CH₃), 66.98 (N-CH₂), 129.12 (C5'), 155.12 (C4').

N,N-Dimethyl-pyrrolidinium 3-Amino-1,2,4-triazolate ([N,N-diMe-Pyr][3-NH₂-1,2,4-Tri], 3e): Yellow, viscous liquid, no mp observed, $T_{5\%dec}$ 143 °C; ¹H NMR (500 MHz, [D₄] MeOH) δ =2.23 (t, 4H, -CH₂-), 3.12 (s, 6H, N-CH₃), 3.49 (t, 4H, N-CH₂), 7.52 (s, 1H, C5'-H); ¹³C NMR (125 MHz [D₄] MeOH) δ = 22.98 (-CH₂-), 52.47 (N-CH₃), 66.93 (N-CH₂), 148.87 (C5'), 159.94 (C3').

N,N-Dimethyl-pyrrolidinium 5-Amino-tetrazolate ([N,N-diMe-Pyr][5-NH₂-Tetr], 3f): White solid, hygroscopic, mp 138 °C, $T_{5\%dec}$ 178 °C; ¹H NMR (500 MHz, [D₄] MeOH) δ =2.23 (t, 4H, -CH₂-), 3.14 (s, 6H, N-CH₃), 3.51 (t, 4H, N-CH₂); ¹³C NMR (125 MHz [D₄] MeOH) δ = 22.99 (-CH₂-), 52.47 (N-CH₃), 66.96 (N-CH₂), 163.50 (C5').

A8.   Hypergolic Ionic Liquids to Mill, Suspend, and Ignite Boron Nanoparticles

Synthesis of 1-Butyl-3-methylimidazolium chloride ([1-Bu-3-Me-Im]Cl)
1-methylimidazole (150.00 g, 1.83 mol) was distilled directly into the reaction flask and a 1.1 molar excess of 1-chlorobutane (204.64 g, 2.00 mol) was added and the reaction was refluxed under Argon through Schlenk-line techniques. The reaction was monitored by NMR until all traces of 1-methylimidazole were no longer visible, or 96 h. The remaining excess of 1-chlorobutane was removed under reduced pressure and the product was slowly cooled to a white crystalline solid. ¹H NMR (360 MHz, *DMSO-d₆*) δ ppm: 9.124 (1H, s), 7.929 (1H, s), 7.847 (1H, s), 4.223 (2H, t, *J* = 7.132 Hz), 3.898 (3H, s), 1.773 (2H, quintet, *J* = 7.427 Hz), 1.250 (2H, sextet, *J* = 7.538 Hz), 0.890 (3H, t, *J* = 7.310 Hz).

Synthesis of 1-Methyl-4-amino-1,2,4-triazolium iodide ([1-Me-4-NH₂-Tri]I)
4-amino-1,2,4-triazole (400 g, 4.76 mol) was weighed out and piecewise added into a 6 L jacketed filter reaction flask containing 2 L of reagent grade acetonitrile while agitating with a glass stir shaft and Teflon paddle. The jacket was slowly heated to 35 °C during the addition. When the 4-amino-1,2,4-triazole was inside the reactor an additional 2 L - 2.5 L of acetonitrile was added with continued stirring at 35 °C until all of the solids dissolved (3 h to achieve dissolution). The reactor was covered to minimize light exposure. While at 35 °C, the methyl iodide was added slowly dropwise 1688 g (11.9 mol) over ~ 2 h, keeping the temperature of the solution under 40 °C during the addition. At the end of the methyl iodide addition, the chiller was turned off, and the reaction mixture allowed to cool down while agitating overnight. The

reaction was monitored by TLC (7:3; ethyl acetate/methanol). When the reaction was complete, the jacket was cooled (chiller set to 0 °C) with ensuing solid precipitation. The solids were then filtered directly through the reactor filter via nitrogen pressure (< 5 psi) and removed to obtain 1300 g crude product. The crude solids were divided into 600 g − 700 g quantities and each recrystallized in 3000 mL quantities of absolute ethanol to yield a white crystalline solid. Melting point 98 °C; ^{1}H NMR (360 MHz, DMSO-$d6$) δ ppm: 10.115 (1H, s), 9.161 (1H, s), 6.938 (2H, s), 4.024 (3H, s); ^{13}C NMR (125 MHz, DMSO-$d6$) δ ppm: 145.109 (s), 143.002 (s), 39.107 (s).

Synthesis of Silver dicyanamide (Ag[DCA])

Sodium dicyanamide (13.35 g, 150 mmol) was dissolved in 20 mL DI water and added dropwise to a solution of silver nitrate (25.48 g, 150 mmol) in a 100 mL round bottom flask with a Teflon stirbar. The mixture was stirred overnight in darkness at room temperature, and the resulting white solid was vacuum filtered and washed with DI water followed by methanol. The solid was dried in a vacuum oven at 70 °C for 24 h.

Metathesis Reactions

1-Butyl-3-methylimidazolium dicyanamide ([1-Bu-3-Me-Im][DCA]):   [1-Bu-3-Me-Im]Cl (12.482 g, 71.46 mmol) stored in separate vials was dissolved in 25 mL of dry methanol and transferred to a 250 mL round bottom flask containing a 1.1 molar excess of Ag[DCA] (13.670 g, 78.61 mmol) as synthesized above containing 175 mL of dried methanol. An excess of Ag[DCA] was used to ensure complete conversion due to the limited solubility in methanol. The flask was covered with aluminum foil and stirred for 3 days. AgCl and remaining Ag[DCA] was filtered and the solvent removed through reduced pressure. The resulting clear oil was dissolved in the minimum amount of methanol and filtered again to remove trace amounts of AgCl dissolved in the IL. The methanol was removed through reduced pressure. The IL was dried by high vacuum drying and freeze thawed to remove remaining gas. A clear nonviscous liquid was obtained. TGA: $T_{dec5\%}$ = 257 ^{o}C; ^{1}H NMR (360 MHz, $DMSO$-$d6$) δ ppm: 9.082 (1H, s), 7.737 (1H, s), 7.670 (1H, s), 4.164 (2H, s), 3.853 (3H, s), 1.775 (2H, quintet (triplet of triplets)), 1.267 (2H, sextet), 0.898 (3H, t); ^{13}C NMR (125 MHz, $DMSO$-d_6) δ ppm: 136.950 (s), 124.028 (s), 122.691 (s), 119.550 (s), 49.065 (s), 36.183 (s), 31.813 (s), 19.255 (s), 13.647 (s).

1-Methyl-4-amino-1,2,4-triazolium dicyanamide ([1-Me-4-NH$_2$-Tri][DCA]): [1-Me-4-NH$_2$-Tri]I (50.0 g, 221 mmol) was dissolved in methanol with a 1.1 molar equivalent of Ag[DCA] (42.27 g, 243.1 mmol). An excess of Ag[DCA] was used to ensure complete conversion due to the limited solubility in methanol. AgCl and any remaining Ag[DCA] was filtered and the solvent removed through reduced pressure to yield a colorless liquid. TGA: $T_{dec5\%}$ = 161 ^{o}C; ^{1}H NMR (500 MHz, neat liquid) δ ppm: 10.67 (1H, s), 9.74 (1H, s), 7.39 (2H, s, NH$_2$), 5.00(3H, s, CH$_3$); ^{13}C NMR (125 MHz, neat liquid) δ ppm: 146.2 (s), 144.0 (s), 120.1 (s), 40.4 (s); ^{15}N NMR(400 MHz, neat liquid) δ ppm: 86.3 (s), -169.3 (s), -189.5 (s), -305.4(t, $^1J_{Hz}$ 72), -218.5(s), -368.2 (s).

Preparation of Boron Nanoparticles. Following a modified protocol developed by Anderson et al.,[116,117] boron with an average diameter of 2 μm was ball-milled using a planetary ball mill (Spex-CertiPrep 800 M, Metuchen, NJ) with tungsten carbide milling jar and 1/8" diameter spherical balls to create B nanoparticles (60 nm in diameter). The boron feedstock (2 g) was first

milled for a total of 12 h (80:1 ball-to-powder mass ratio; 300 rpm) to break the particles and expose more reactive surfaces. Subsequently the B was milled in the presence of surfactant or IL for an additional 6 h, and then another 6 h with acetonitrile (200 mL) as a dispersive solvent. Boron feedstock was milled with either no ligand, a combination of oleic acid and oleyl amine (1.5 mL, 1:1 v/v), or [1-Me-4-NH$_2$-Tri][DCA] (1.5 mL). In the case where B was milled without ligand, the surfactant milling step was omitted from the procedure. Acetonitrile was added in the last milling step to help reduce viscosity, disperse the particles, and to allow easy transfer the newly milled nanoparticles.

A9. **Tuning azolate ionic liquids to promote surface interactions with titanium nanoparticles leading to increased suspension stability and passivation**

Metathesis Reactions

1-Butyl-3-methylimidazoloum 5-amino-tetrazolate ([1-Bu-3-Me-Im][5-NH$_2$-Tetr]): 5-NH$_2$-Tetrazole (6.447 g, 50 mmol) was combined with K$_2$CO$_3$ (13.8205 g, 100 mmol) in 250 mL of anhydrous acetone and stirred for 2 h to deprotonate the azole. [1-Bu-3-Me-Im][Cl] (8.734 g, 50 mmol) was added piecewise maintaining anhydrous conditions and stirred for 72 h. The mixture was filtered and the acetone was removed under reduce pressure. The resulting oil was dissolved in anhydrous acetone and filtered again and the acetone was removed under reduced pressure and high vacuum techniques. The resulting liquid was freeze thawed with liquid N$_2$ under high vacuum to remove excess dissolved gas. The resulting red viscous liquid was stored under argon. ^{1}H NMR (360 MHz, *DMSO-d6*) δ ppm: 9.580 (1H, s), 7.892 (1H, s), 7.814 (1H, s), 4.212 (2H, t), 3.891 (3H, s), 1.771 (2H, quintet), 1.254 (2H, sextet), 0.883 (3H, s); ^{13}C NMR (125 MHz, *DMSO-d$_6$*) δ ppm: 164.681 (s), 137.366 (s), 124.099 (s), 122.828 (s), 48.917 (s), 36.175 (s), 31.873 (s), 19.233 (s), 13.711 (s). T_g: -67 ^{o}C

1-Butyl-3-methylimidazoloum 4,5-dicyano-imidazolate ([1-Bu-3-Me-Im][4,5-DiCN-Im]): 4,5-Dicyano-imidazole (5.96 g, 50 mmol) was combined with K$_2$CO$_3$ (13.8205 g, 100 mmol) in 250 mL of anhydrous acetone and stirred for 2 h. [1-Bu-3-Me-Im][Cl] (8.734 g, 50 mmol) was added piecewise maintaining anhydrous conditions and stirred for 72 h. The mixture was filtered and the acetone was removed under reduce pressure. The resulting oil was dissolved in anhydrous acetone and filtered again and the acetone was removed under reduced pressure and high vacuum techniques. The resulting liquid was freeze thawed with liquid N$_2$ under high vacuum to remove excess dissolved gas. The resulting yellowing non-viscous liquid was stored under argon. ^{1}H NMR (360 MHz, *DMSO-d6*) δ ppm: 9.618 (1H, s), 7.735 (1H, s), 7.675 (1H, s), 7.312 (1H, s), 4.165 (2H, t), 3.876 (3H, s), 1.780 (2H, quintet), 1.280 (2H, sextet), 0.889 (3H, t); ^{13}C NMR (125 MHz, *DMSO-d$_6$*) δ ppm: 149.226 (s), 136.985 (s), 124.127 (s), 122.788 (s), 117.986 (s), 117.352 (s), 49.130 (s), 36.230 (s), 31.786 (s), 31.786 (s), 19.529 (s), 13.602 (s). T_g: -74 ^{o}C

1-Butyl-3-methylimidazolium 4-nitro-imidazolate ([1-Bu-3-Me-Im][4-NO$_2$-Im]): 4-NO$_2$-imidazole (5.829 g, 50 mmol) was combined with K$_2$CO$_3$ (13.8205 g, 100 mmol) in 250 mL of anhydrous acetone and stirred for 2 h. [1-Bu-3-Me-Im][Cl] (8.734 g, 50 mmol) was added piecewise maintaining anhydrous conditions and stirred for 72 h. The mixture was filtered and the acetone was removed under reduce pressure. The resulting oil was dissolved in anhydrous

acetone and filtered again and the acetone was removed under reduced pressure and high vacuum techniques. The resulting liquid was freeze thawed with liquid N_2 under high vacuum to remove excess dissolved gas. The resulting yellow-orange non-viscous liquid was stored under argon. ^{1}H NMR (360 MHz, *DMSO-d6*) δ ppm: 9.381 (1H, s), 7.835 (1H, s), 7.773 (1H, s), 7.758 (1H, s), 7.171 (1H, s), 4.177 (2H, s), 3.891 (3H, s), 1.757 (2H, quintet), 1.242 (2H, sextet), 0.873 (3H, t); ^{13}C NMR (125 MHz, *DMSO-d₆*) δ ppm: 146.512 (s), 137.152 (s), 132.058 (s), 131.951 (s), 124.112 (s), 122.773 (s), 49.060 (s), 36.088 (s), 31.862 (s), 19.219 (s), 13.459 (s). T_g: -72 °C

1-Butyl-3-methylimidazolium 2-methyl-4-nitro-imidazolate ([1-Bu-3-Me-Im][2-Me-4-NO₂-Im]): 2-Me-4-NO₂-imidazole (9.349 g, 72.8 mmol) was combined with K_2CO_3 (20.1277 g, 145.6 mmol) in 250 mL of anhydrous acetone and stirred for 2 h. [1-Bu-3-Me-Im][Cl] (12.719 g, 72.8 mmol) was added piecewise maintaining anhydrous conditions and stirred for 72 h. The mixture was filtered and the acetone was removed under reduce pressure. The resulting oil was dissolved in anhydrous acetone and filtered again and the acetone was removed under reduced pressure and high vacuum techniques. The resulting liquid was freeze thawed with liquid N_2 under high vacuum to remove excess dissolved gas. The resulting dark orange non-viscous liquid was stored under argon. ^{1}H NMR (360 MHz, *DMSO-d6*) δ ppm: 9.308 (1H, s), 7.827 (1H, s), 7.748 (1H, s), 7.660 (1H, s), 4.165 (2H, t), 3.869 (3H, s), 2.138 (3H, s), 1.752 (2H, quintet), 1.243 (2H, sextet), 0.876 (3H, t). ^{13}C NMR (125 MHz, *DMSO-d₆*) δ ppm: 154.895 (s), 147.984 (s), 137.175 (s), 133.801 (s), 124.084 (s), 122.751 (s), 48.997 (s), 36.145 (s), 31.852 (s), 19.264 (s), 18.022 (s), 13.666 (s).

A10. <u>Graphene and Graphene Oxide Can 'Lubricate' Ionic Liquids based on Specific Surface Interactions Leading to Improved Low Temperature Hypergolic Performance</u>

Metathesis Reactions

1-Butyl-3-methylimidazolium dicyanamide ([1-Bu-3-Me-Im][DCA]): [1-Bu-3-Me-Im]Cl (12.482 g, 71.46 mmol) stored in separate vials was dissolved in 25 mL of dry methanol and transferred to a 250 mL round bottom flask containing a 1.1 molar excess of Ag [DCA] (13.670 g, 78.61 mmol) as synthesized above containing 175 mL of dried methanol. An excess of Ag [DCA] was used to ensure complete conversion due to the limited solubility in methanol. The flask was covered with aluminum foil and stirred for 3 days. AgCl and remaining Ag [DCA] was filtered and the solvent removed through reduced pressure. The resulting clear oil was dissolved in the minimum amount of methanol and filtered again to remove trace amounts of AgCl dissolved in the IL. The methanol was removed through reduced pressure. The IL was dried by high vacuum drying and freeze thawed to remove remaining gas. A clear nonviscous liquid was obtained. TGA: $T_{dec5\%}$ = 257 °C; ^{1}H NMR (360 MHz, *DMSO-d6*) δ ppm: 9.082 (1H, s), 7.737 (1H, s), 7.670 (1H, s), 4.164 (2H, s), 3.853 (3H, s), 1.775 (2H, quintet (triplet of triplets)), 1.267 (2H, sextet), 0.898 (3H, t); ^{13}C NMR (125 MHz, *DMSO-d₆*) δ ppm: 136.950 (s), 124.028 (s), 122.691 (s), 119.550 (s), 49.065 (s), 36.183 (s), 31.813 (s), 19.255 (s), 13.647 (s).

1-Methyl-4-amino-1,2,4-triazolium dicyanamide ([1-Me-4-NH₂-Tri][DCA]): [1-Me-4-NH₂-Tri]I (50.0 g, 221 mmol) was dissolved in methanol with a 1.1 molar equivalent of Ag[DCA] (42.27 g, 243.1 mmol). An excess of Ag[DCA] was used to ensure complete conversion due to

the limited solubility in methanol. AgCl and any remaining Ag[DCA] was filtered and the solvent removed through reduced pressure to yield a colorless liquid. TGA: $T_{dec5\%} = 161\,^{\circ}C$; ^1H NMR (500 MHz, neat liquid) δ ppm: 10.67 (1H, s), 9.74 (1H, s), 7.39 (2H, s, NH_2), 5.00(3H, s, CH_3); ^{13}C NMR (125 MHz, neat liquid) δ ppm: 146.2 (s), 144.0 (s), 120.1 (s), 40.4 (s); ^{15}N NMR(400 MHz, neat liquid) δ ppm: 86.3 (s), -169.3 (s), -189.5 (s), -305.4(t, $^1J_{Hz}$ 72), -218.5(s), -368.2 (s).

Appendix B – Analytical Data

B1. A General Design Platform for Ionic Liquid Ions Based on Bridged Multi-Heterocycles With Flexible Symmetry and Charge

Thermal Analysis

Table B1.1 Thermal Data of Reported Major products

Compound	$T_{5\%onset}$ (°C)	T_{onset} (°C)	T_g/T_m (°C)
1-(2-(5-tetrazolidyl)ethyl)-3-(5-1*H*-tetrazolyl)-methylimidazolium, (**10**)	237.54	247.43	49.44
1-(2-(5-1*H*-tetrazolyl)ethyl)-3-(5-1*H*-tetrazolyl)-methylimidazolium bis(trifluoromethanesulfonyl)amide, (**11**)	245.58	345.01	10.50
1,3-dimethylimidazolium 1-(2-(5-tetrazolidyl)ethyl)-3-(5-tetrazolidyl)methylimidazolium, (**12**)	224.37	235.69	-24.45

B2. Catalytic Ignition of Ionic Liquids for Propellant Applications

Thermal Analysis

Table B2.1. Thermal Analysis Data

Material	TGA (°C)	DSC (°C)	Thermal Stability
HEH (neutral)	$T_{5\%dec} = 102.10$ $T_{onset} = 181.98$ $T_{dec} = 195.94$	T_g -72.11	- 88.1% weight loss
[HEH][NO$_3$]	$T_{5\%dec} = 193.63$ $T_{onset} = 214.10$ $T_{dec} = 259.67$	$T_g = -56.91$	-23.8% weight loss
[HEH][NO$_3$]$_2$	$T_{5\%dec} = 62.71$ $T_{onset} = 91.51$ $T_{dec} = 101.01$	$T_g = -47.89$	-43.8% weight loss

Decomposition temperatures shown were determined by TGA, heating at 5 °C min-1 under dried air atmosphere and are reported as (a) onset to 5 wt% mass loss ($T_{5\%dec}$); (ii) onset to total mass loss (T_{onset}); and (iii) peak temperature (T_{dec}). Glass transition (Tg) points (°C) were measured from the transition onset temperature and determined by DSC from the second heating cycle at 5 °C min-1, after cooling samples to -100 °C. The longer term stability was measured by heating each sample to 75 °C for 24 h.

Reactivity Experiments

Table B2.1. Reactivity Data

Comp.		50 °C	100 °C	150 °C	200 °C
HEH **1st drop**	Observation	NR	a	a	a
	Delay to Smoke	--	126 ms	48 ms	24 ms
	Smoke Longevity	--	2904 ms	3012 ms	2838 ms
	Delay to flame[a]	--	--	--	--
	Flame Longevity[b]	--	--	--	--
	Residue[c]	100%	0%	0%	0%
[HEH][NO$_3$] **1st drop**	Observation	NR	a	b	b
	Delay to Smoke	--	1166 ms	90 ms	114 ms
	Smoke Longevity	--	4558 ms	1826 ms	2556 ms
	Delay to flame[a]	--	--	722 ms	958 ms
	Flame Longevity[b]	--	--	1826 ms	1064 ms
	Residue[c]	100%	0%	0%	0%
2nd drop	Observation	NR	a	b	d
	Delay to Smoke	--	--	242 ms	
	Smoke Longevity	--	--	2834 ms	
	Delay to flame[a]	--	--	1898 ms	
	Flame Longevity[b]	--	--	1216 ms	
	Residue[c]	100%	60%	0%	
3rd drop	Observation	NR	c	b	d
	Delay to Smoke	--	--	2594 ms	
	Smoke Longevity	--	--	4042 ms	
	Delay to flame[a]	--	--	4302 ms	
	Flame Longevity[b]	--	--	2294 ms	
	Residue[c]	100%	98%	0%	
[HEH][NO$_3$]$_2$ **1st drop**	Observation	NR	b	b	b
	Delay to Smoke	--	582 ms	28 ms	162 ms
	Smoke Longevity	--	4690 ms	5614 ms	1242 ms
	Delay to flame[a]	--	1158 ms	78 ms	966 ms
	Flame Longevity[b]	--	3652 ms	1716 ms	244 ms
	Residue[c]	100%	0%	0%	0%
2nd drop	Observation	NR	a	b	d
	Delay to Smoke	--	7801 ms	312 ms	
	Smoke Longevity	--	13503 ms	6180 ms	
	Delay to flame[a]	--	--	2854 ms	
	Flame Longevity[b]	--	--	516 ms	
	Residue[c]	100%	35%	0%	
3rd drop	Observation	NR	c	b	d
	Delay to Smoke	--	--	688 ms	
	Smoke Longevity	--	--	5920 ms	
	Delay to flame[a]	--	--	1832 ms	
	Flame Longevity[b]	--	--	642 ms	
	Residue[c]	100%	73%	0%	

All times ± 2 ms; NR – no observable reaction, visible slow bubbling; [a]Smoke evolution after delay, no ignition; [b]Smoke evolution after delay followed by ignition; [c]Slow bubbling observed, no smoke, no flame;

B3. **Synthesis of N-cyanoalkyl-functionalized imidazolium nitrate and dicyanamide ionic liquids with a comparison of their thermal properties for energetic applications**
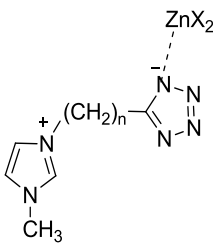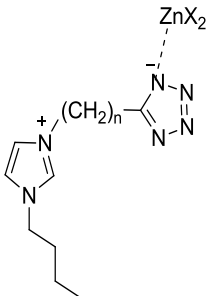
Thermal Analysis

Table B3.1 Combined thermal data for *N*-cyanoalkyl-functionalized imidazolium halide precursors (**2a-q**), nitrates, **3(a-d,h-l)**, and dicyanamides, **4(a,c-g,m-q)**

R	R′	Halide			Nitrate			Dicyanamide			
		Prod	$T_{5\%onset}$ (°C)^a	T_g/T_m (°C)^b	Prod	$T_{5\%onset}$ (°C)	T_g/T_m (°C)	Prod	$T_{5\%onset}$ (°C)	T_g/T_m (°C)	Impact (kg·cm)
Me	C1CN	2a	221	178 (Lit.= 170)	3a	189	109	4a	186	67	>200
	C2CN	2b	222	149	3b	184	-58	4b	158	-66	172
	C3CN	2c	247 (Lit. = 254)[34]	96 (Lit. = 90.3)	3c	280	-52	4c	243	-77	170
	C4CN	2d	239	-23 (Lit. = 32)[33]	3d	279	-55	4d	238	-73	170
	C5CN	2e	250	-34	3e	---	---	4e	260	-75	170
	C6CN	2f	247	-44	3f	---	---	4f	263	-77	174
	C1(CH₃)CN	2g	220	138	3g	192	-43	4g	---	---	---
Bu	C1CN	2h	200	-7.1	3h	177	-43	4h	---	---	---
	C2CN	2i	241	91	3i	191	-30	4i	---	---	---
	C3CN	2j	260	-31	3j	273	-59	4j	---	---	---
	C4CN	2k	310	-38	3k	276	-58	4k	---	---	---
	C1(CH₃)CN	2l	224	-7.6	3l	190	-50	4l	---	---	---
C2CN	C1CN	2m	196	49	3m	---	---	4m	144	60	176
	C3CN	2n	196	-23	3n	---	---	4n	161	-61	176
	C4CN	2o	189	-34	3o	---	---	4o	167	-60	174
	C5CN	2p	201	-39	3p	---	---	4p	162	-65	164
	C6CN	2q	178	-38	3q	---	---	4q	154	-66	170

a) Obtained by TGA for 5 °C·min⁻¹ from ambient temperature to 600 °C with a 30 minute isothermal hold at 75 °C under air atmosphere. $T_{5\%decomp}$ is temperature for which first 5% material weight is lost upon heating.

b) Obtained by DSC from last 2 of 3 heating cycles, where heating cycle was taken to near 50 °C less than $T_{5\%onset}$ at a ramp rate of 5 °C·min⁻¹ with 5 min isotherms at end of heating cycle. Cooling cycles were taken down to -100 °C at 5 °C·min⁻¹ with 5 min isothermal hold at end of cooling cycle. All glass transitions and melting points are recorded at the onset of the event.

c) Impact sensitivity measurements recorded by Dr. Tommy Hawkins and coworkers at Edwards AFB using a drop-hammer apparatus [see Appendix C for more information].

B5. Zinc-assisted synthesis of imidazolium-tetrazolate bi-heterocyclic zwitterions with variable alkyl bridge length

Table B5.1. Thermal data summary for Click products **9-16**.

Structure	#	n	[X]	T_g (°C)[a]	T_m (°C)[a]	$T_{5\%}$ (°C)[c]
	9	1	Cl⁻/Br⁻	64	---	295 (303)
	10	2	Br⁻	40	---	281 (307)
	11	3	Cl⁻/Br⁻	91	196[b]	298 (311)
	12	4	Cl⁻/Br⁻	72	---	286 (303)
	13	1	Cl⁻/Br⁻	46	40[b]	290 (301)
	14	2	Br⁻	53	44[b]	244 (263)
	15	3	Cl⁻/Br⁻	81	---	260 (319)
	16	4	Cl⁻/Br⁻	66	---	290 (312)

[a]Melting point (T_m) and/or glass transition temperatures (T_g) were taken from the onset of observed transition and determined by DSC during the second heating cycle at a ramp rate of 5 °C·min⁻¹ after initially melting then cooling all samples to -100 °C. [b]All melting transitions were observed for the initial heating cycle only, where dashed lines (---) indicated that no T_m was observed. Thermal decomposition temperatures were obtained by TGA using a heating ramp of 5 °C min⁻¹ under a dried air atmosphere. All values are reported as (i) onset to 5 weight % loss of mass ($T_{5\%onset}$) and (ii) onset to total mass loss (T_{onset}) (parentheses).

B6. **Synthesis, limitations, and thermal properties of energetically-substituted, protonated imidazolium picrate and nitrate salts and further comparison with their methylated analogs**

Thermal analysis

Table B6.1 Melting point transitions of the protonated substituted imidazolium salts.[a]

Cation	[Cation]⁺	Thermal transitions (°C)					
		[Picrate Anion]⁻ (a)			[Nitrate]⁻ (b)		
1	[1-Me-3-H-Im]⁺	--	--	159^f	--	--	**60^f**
2	[1,2-diMe-3-H-Im]⁺	--	--	182^f	--	--	**79^f**
3	[1-Pr-3-H-Im]⁺	-24^b	--	**97^e**	-81^b	64^c	--
4	[1-Bu-3-H-Im]⁺	-38^b	**34^c**	--	-76^b	--	**6^d**
5	[1-Bu-2-Me-3-H-Im]⁺	--	--	104^f	-76^b	66^c	--
6	[1-Pent-2-Me-3-H-Im]⁺	--	--	127^f	-68^b	48^c	--
7	[1-Hex-3-H-Im]⁺	-44^b	--	**41^d**	-72^b	--	**79^d**
8	[1-Me-2-NO$_2$-3-H-Im]⁺	-25^b	38^c	**42^e**	--	--	**98^f**
9	[1,2-diMe-5-NO$_2$-3-H-Im]⁺	--	--	165^f	--	--	**88^f**
10	[1-Et-2-NO$_2$-3-H-Im]⁺	-33^b	**51^c**	--	-60^b	38^c	--
11	[1-Et-4-NO$_2$-3-H-Im]⁺	-26^b	**42^c**	--	-51^b	--	**40^f**
12	[1-*i*-Pr-4-NO$_2$-3-H-Im]⁺	-28^b	--	**57^e**	-51^b	63^c	--
13	[1-Bu-2-Me-4-NO$_2$-3-H-Im]⁺	-28^b	**71^c**	--	--	--	**67^f**
14	[1-Pent-2-Me-4-NO$_2$-3-H-Im]⁺	-30^b	**67^c**	--	--	--	**-31^f**
15	[1-Hex-4-NO$_2$-3-H-Im]⁺	-33^b	--	**79^d**	-63^b	--	**11^d**

[a] Salts meeting the definition of ILs, with melting point < 100 °C, are shown in **bold**. All transitions are presented as the onset temperature for that thermal transition. [b]Glass transition (T_g) on heating, as result of initial melting and cooling of the sample, with no crystallization occurring on cooling, and formation of the glass; [c]Secondary liquid-liquid transitions (T_{l-l}); [d]Melting point of the sample (mp) where the crystallization event occurs on heating prior to the melting point; [e]Melting event occurring only during the first heating cycle (for the rest of the experiment the sample remained as a supercooled liquid); [f]Reproducible melting point.

Table B6.2 Thermal stabilities.[a]

Cation Precursor	Cation	Thermal stabilities (°C)	
		Picrates (a)	Nitrates (b)
1	[1-Me-3-H-Im]$^+$	184	137
2	[1,2-diMe-3-H-Im]$^+$	209	131
3	[1-Pr-3-H-Im]$^+$	177	143
4	[1-Bu-3-H-Im]$^+$	198	150
5	[1-Bu-2-Me-3-H-Im]$^+$	224	121
6	[1-Pent-2-Me-3-H-Im]$^+$	226	137
7	[1-Hex-3-H-Im]$^+$	188	138
8	[1-Me-2-NO$_2$-3-H-Im]$^+$	112	82
9	[1,2-diMe-5-NO$_2$-3-H-Im]$^+$	145	123
10	[1-Et-2-NO$_2$-3-H-Im]$^+$	107	69
11	[1-Et-4-NO$_2$-3-H-Im]$^+$	157	83, 141[b]
12	[1-*i*-Pr-4-NO$_2$-3-H-Im]$^+$	137	87, 192[b]
13	[1-Bu-2-Me-4-NO$_2$-3-H-Im]$^+$	188	102, 213[b]
14	[1-Pent-2-Me-4-NO$_2$-3-H-Im]$^+$	176	104, 203[b]
15	[1-Hex-4-NO$_2$-3-H-Im]$^+$	175	102, 231[b]

[a]All transitions are presented as the onset temperature for the 5% decomposition ($T_{5\%dec}$). [b]Sample with two distinguishable decomposition slopes; the given value is the onset temperature for the second decomposition step

B7. <u>Azolium azolates from reactions of neutral azoles with 1,3-diemethyl-imidazolium-2-carboxylate, 1,2,3-trimethyl-imidazolium hydrogen carbonate, and N,N dimethyl-pyrrolidinium hydrogen carbonate</u>

Thermal Analysis

Table B7.1 Melting point transitions (°C) and decomposition temperatures(°C) of [1,3-diMe-Im]$^+$, [1,2,3-triMe-Im]$^+$, and [*N,N*-diMe-Pyr]$^+$ azolate salts.[a]
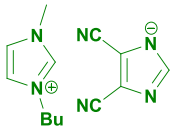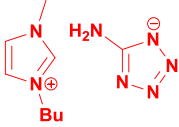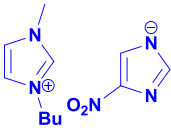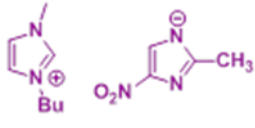
Anion/Cation	[1,3-diMe-Im]$^+$ (1)		[1,2,3-triMe-Im]$^+$(2)		[*N,N*-diMe-Pyr]$^+$ (3)		[1-Bu-3-Me-Im]$^+$(4)Error! Bookmark not defined.	Bookmark
	mp	$T_{5\%dec}$	mp	$T_{5\%dec}$	mp	$T_{5\%dec}$	mp	$T_{5\%dec}$
[4-NO$_2$-Im]$^-$ (a)	**78**	182 480[b]	--[c]	171 434[b]	--[c]	175	**-63**[d]	200
[2-Me-5-NO$_2$-Im]$^-$ (b)	112	178 485[b]	126	182 420[b]	128	179 391[b]	--	--
[4,5-diNO$_2$-Im]$^-$ (c)	**96**	215	**86**	198 442[b]	mp at $T_{5\%dec}$ (~220)	221 445[b]	**-64**[d]	241
[4-NO$_2$-1,2,3-Tri]$^-$(d)	**85**	187	107	195 379[b]	**57**	173 382[b]	**-73**[d]	219
[3-NH$_2$-1,2,4-Tri]$^-$(e)	--[c]	190	--[c]	179	--[c]	143	--	--
[5-NH$_2$-Tetr]$^-$(f)	**84**	206	160	202	138	178	**-74**Error! Bookmark not	248Error! Bookmark

^{a}*Salts meeting the definition of ILs (mp < 100 °C) are in **bold**; ^{b}Observed second decomposition step; ^{c}Due to the extremely hygroscopic character of the sample, the determination of melting point was not possible by DSC or by a visual method; ^{d}Glass transitions on heating.*

B9.   <u>Tuning azolate ionic liquids to promote surface interactions with titanium nanoparticles leading to increased suspension stability and passivation</u>

Colloidal Stability

Table B9.1 First observable and complete sedimentation times for 100 nm Ti(0) Nanoparticles in AzAz ILs.

Ionic Liquids	IL:Ti Molar Ratio	[Ti] (wt%)	T_s/T_f (h)
 [1-Bu-3-Me-Im][4,5-DiCN-Im] η =31.56 cP; ρ =1.080 g/cm^3	100:1	0.186	24/36
	150:1	0.124	24/36
	200:1	0.093	24/36
	250:1	0.075	24/36
 [1-Bu-3-Me-Im][5-NH$_2$-Tetr] η =245.3 cP; ρ =1.096 g/cm^3	100:1	0.214	24/72
	150:1	0.143	24/72
	200:1	0.107	36/120
	250:1	0.086	36/120
 [1-Bu-3-Me-Im][4-NO$_2$-Im] η =42.52 cP; ρ =1.201 g/cm^3	100:1	0.190	36/144
	150:1	0.127	48/144
	200:1	0.095	48/168
	250:1	0.076	48/168
 [1-Bu-3-Me-Im][2-Me-4-NO$_2$-Im] η =150.2 cP; ρ =1.134 g/cm^3	100:1	0.180	36/168
	150:1	0.120	48/168
	200:1	0.090	72/168
	250:1	0.072	120/336

^{a} Viscosity and Density were determined at 40 ^{o}C

B10. Graphene and Graphene Oxide Can 'Lubricate' Ionic Liquids based on Specific Surface Interactions Leading to Improved Low Temperature Hypergolic Performance

Full Hypergolic Results

Table B10.1 Results of all hypergolic tests performed

Ionic Liquid	Additive And Concentration	Ambient Temp (ID)	0°C	-10°C	-20°C	- 40°C
[1-Bu-3-Me-Im] [DCA]	Neat	78, 116, 85 = 93 ms	Ignition ~300 ms	No ignition	No ignition	No ignition
	GO 0.030%	295, 94, 118 = 169 ms	267, 290 = 278.5 ms	No ignition	No ignition	No ignition
	Pristine Graphene 0.029%	X, 95, 94 = 94.5 ms	375, 209 =292 ms	253, X 253 ms	No ignition	No ignition
[1-Me-4-NH$_2$-Tri] [DCA]	Neat	31, 58, 26 = 38.3	62, 65, 74 = 67 ms	61, 69 = 65 ms	105, 203 = 154 ms	No ignition
	GO 0.026%	43, 38, 47 = 42.7	92, 102, 86 = 93.3 ms	125, 80 = 102.5 ms	246, 210 = 228 ms	Ignition
	Pristine Graphene 0.029%	59, 28, 31 = 39.33	Ignition (can't see)	89, 75 = 82 ms	141, 224 = 182.5 ms	Ignition
[N-Bu-N-Me-Pyr] [DCA]	Neat	70, 65, 56 = 63.7				
	GO 0.029%	X, 120, 287				
	Pristine Graphene 0.032%	166, 130, 125				

Appendix C – Protocols and Equipment

Differential Scanning Calorimetry (DSC) Protocol A. Melting point/glass transition analyses were performed by Differential Scanning Calorimetry (DSC) using a DSC 2920 Modulated DSC, TA Instruments, Inc. (New Castle, DE) cooled with a liquid nitrogen cryostat. The calorimeter was calibrated for temperature and cell constants using indium (melting point 156.61 ^{o}C; H = 28.71 J g^{-1}). Data were collected at constant atmospheric pressure, with heating at a rate of 5 ^{o}C min^{-1} using samples between 5-15 mg in aluminum sample pans (sealed then perforated with a pin-hole to equilibrate pressure from potential expansion of evolved gases). The DSC was adjusted so that zero heat flow was between 0 and -0.5 mW, and the baseline drift was less than 0.1 mW over the temperature range of 0-180 ^{o}C. An empty sample pan served as the reference.

Differential Scanning Calorimetry (DSC) Protocol B. Some experiments to determine thermal transitions were done on a Mettler-Toledo (Columbus, OH) Differential Scanning Calorimeter (DSC), DSC 1. The calorimeter was calibrated for temperature and cell constants using In, Zn, H_2O, and *n*-octane. Samples were weighed and sealed in aluminum pans (5–15 mg) and heated at a rate of 5 ^{o}C/min to 100 ^{o}C. Following the initial heating cycle the samples were cooled to -80 ^{o}C *via* a recirculating chiller followed by a heating cycle to 100 ^{o}C at a rate of 5 ^{o}C/min. After each dynamic temperature ramp, a 15 min isotherm was employed to ensure equilibration of the temperature in the cell. The entire cycle was repeated three times and the values for phase changes were analyzed. Each sample was referenced to an empty aluminum pan.

Thermogravimetric Analysis (TGA) Protocol A. Thermogravimetric analyses (TGA) was performed using a TGA 2950, TA Instruments, Inc. (New Castle, DE). These experiments were conducted under air atmosphere and measured in the dynamic heating regime. Samples between 5-15 mg were heated from 30-600 ^{o}C under constant heating ramp of 5 ^{o}C min^{-1} with a 30 minute isotherm at 75 ^{o}C.

Thermogravimetric Analysis (TGA) Protocol B. Thermal decompositions experiments for some hypergolic ILs were conducted with a Mettler-Toledo (Columbus, OH) TGA/DSC 1. The instrument's internal temperature was calibrated by observing the melting point of Au, Zn, and In. Samples of 2–15 mg were analyzed on a 70 μL alumina pan under a stream of nitrogen. Samples were heated from room temperature to 75 ^{o}C at 5 ºC/min and with a 30 min isotherm at 75 ^{o}C in order to ensure excess volatiles or residual solvents were removed. Following the isotherm, samples were heated to 800 ^{o}C at 5 ^{o}C/min. The 5% onset temperature for decomposition (or $T_{5\%onset}$) was evaluated as the onset temperature where 5% of the sample had decomposed.

Nuclear Magnetic Resonance Spectroscopy. All Nuclear Magnetic Resonance (NMR) spectra were recording utilizing a Bruker Avance Spectrometer Bruker/Magnex UltraShield 500 MHz magnet (Madison, WI) or a Bruker Spectrospin DRX 400 MHz UltrashieldTM spectrometer (Madison, WI). ^{1}H (500 MHz) and ^{13}C (125 MHz) were collected using DMSO-*d6*, CDCl$_3$, D_2O, or acetone-*d6* as the solvent with TMS as the standard and shifts reported in δ (ppm).

Infrared Spectroscopy Protocol A. Infrared (IR) analyses were obtained by direct measurement of the neat samples by utilizing a Perkin-Elmer 100 FT-IR instrument featuring an ATR force gauge, and spectra were obtained in the range of $\nu_{max} = 650 - 4000$ cm^{-1}.

Infrared Spectroscopy Protocol B. Infrared (IR) spectra were collected using a Bruker α-FTIR by direct measurement *via* attenuated total reflection of the neat samples (or loaded with boron nanoparticles) on a diamond crystal.

Water Content Determination Protocol A. Parts per million quantities of water were determined via coulometric Karl Fischer (KF) titration using a Metrohm 684 KF Coulometer from Brinkmann Instruments, Inc. (Westbury, NY). Each sample was titrated three times and if found in good correlation, the values were averaged to obtain the water content.

Density Protocol A. The density of [HEH][NO$_3$] was determined by mass to volume ratio. Density of each sample was determined five times and if found in good correlation, the values were averaged to obtain the actual density value.

Density Protocol B. Density measurements were taken at 40 ℃ with an Anton Paar USA (Ashland, VA) density meter, DMA 500. Samples of IL (~1 mL) were inserted *via* a syringe directly into the instrument. The value for density was recorded and the sample was washed out with methanol and water.

Viscosity Protocol A. Viscosity measurements were taken at 40 ℃ with a Cambridge Viscosity (Medford, MA) Viscometer, VISCOlab 3000. Approximately 1 mL of each IL was placed in the sample chamber. The correct sized piston corresponding to the expected viscosity range was added and the measurement was taken.

Viscosity Protocol B. Viscosity measurements were taken at various temperatures with a Cambridge Viscosity (Medford, MA) Viscometer, VISCOlab 3000. Approximately 1 mL of IL, either neat or as a dispersion of either pristine graphene or GO, were placed in the sample chamber. The correct sized piston corresponding to the expected viscosity range was added and the measurement was taken. The value for viscosity was not recorded until the error had averaged out to be less than 3%. The sample chamber was cooled by using a VWR (West Chester, PA) recirculating chiller filled with a 50% (v/v) mixture of ethylene glycol in water. The coolant mixture was recirculated in Tygon^{TM} tubing that was wrapped around the stainless steel exterior of the viscometer to cool the chamber to 0 ℃. The viscosity measurements were taken as the chamber heated up as the movement of the piston heated up the colloids during sample measurements.

Combustion Microcalorimetry. The heat of combustion was determined using a Parr (Moline, IL) (series 1425) semimicro oxygen bomb calorimeter. The substances were burned in an oxygen atmosphere at a pressure of 30 atm. Each sample was loaded into a crucible and placed in the bomb with a 5 five turn nichrome wire dipped into the liquid sample. The energy

equivalent of the calorimeter was determined with a standard reference sample of benzoic acid. Each sample was run twice and the values averaged.

Ignition Delay and Burn Duration. A Redlake Motion Pro® HS 4 (Tallahassee, FL) was utilized to capture the hypergolic process at 1000 fps at a 512 X 512 resolution. The ignition delay was determined by counting the frames from which the fuel hit the oxidizer until the first signs of a visible flame. Each sample was run three times and averaged. The ignition delay was determined by counting the frames from which the fuel hit the oxidizer until the first signs of a visible flame. Burn duration was determined to be the time from the first signs of visible ignition until the last visible flame. Each sample was run three times and averaged.

X-Ray Photoelectron Spectroscopy (XPS). All XPS analyses were run on a Kratos Axis 165 XPS/Auger (Manchester, UK) containing an Al X-ray source. Samples were prepared neat by applying droplets of either neat IL or dispersions of Ti in an IL to a copper stub with a depression to allow the liquid to reside. Samples were brought under high vacuum (~1 X 10^{-8} torr) in the antechamber before allowed to enter the sampling chamber (~1 X 10^{-9} torr).

Scanning Electron Microscopy. Dispersions of pristine graphene and GO in [1-Me-4-NH$_2$-Tri][DCA] were filtered through a 0.45 µm cellulose acetate filter to remove excess IL, leaving larger aggregated graphene-based material on the filter which were then subjected scanning electron microscopy (SEM). The filter was placed on a pin-mount aluminum stub and brought under high vacuum to be brought into the sample chamber. Scanning measurements were taken with an accelerating voltage of 10 kV with a Hitachi S-2500 SEM (Tokyo, Japan).

Appendix D – Single Crystal X-ray Diffraction

Suitable single crystals were examined under an optical polarizing microscope, selected, and mounted on a glass fiber using silicone grease. Single crystal X-ray diffraction data was measured on a Bruker diffractometer equipped with a PLATFORM goniometer and an Apex II CCD area detector (Bruker-AXS, Inc., Madison, WI) using graphite-monochromated Mo-Kα radiation. Crystals were cooled during collection under a cold nitrogen stream using an N-Helix cryostat (Oxford Cryosystems, Oxford, UK). A hemisphere of data was collected for each crystal using a strategy of omega scans with 0.5° frame widths. Unit cell determination, data collection, data reduction, integration, absorption correction, and scaling were performed using the Apex2 software suite.[118]

The SHELXTL-97 software suite was used for space group determination, structure solution, model adjustment, and generation of ellipsoid plots.[119] SHELXD was used for dual space solution.[120] Refinement was performed with SHELXL 2013.[121] Short contact analysis and packing diagrams were done using the CCDC program Mercury.

D1. **A General Design Platform for Ionic Liquid Ions Based on Bridged Multi-Heterocycles With Flexible Symmetry and Charge**
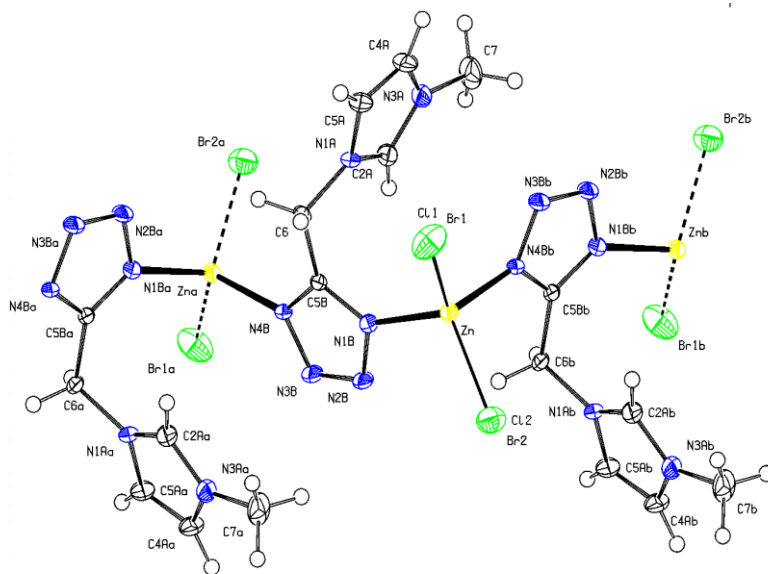
Figure D1.1 *catena*-poly[(bromochlorozinc)-*μ*-[1-(5-tetrazolato)methyl-3-methylimidazolium]-N^1:N^4], **2**.
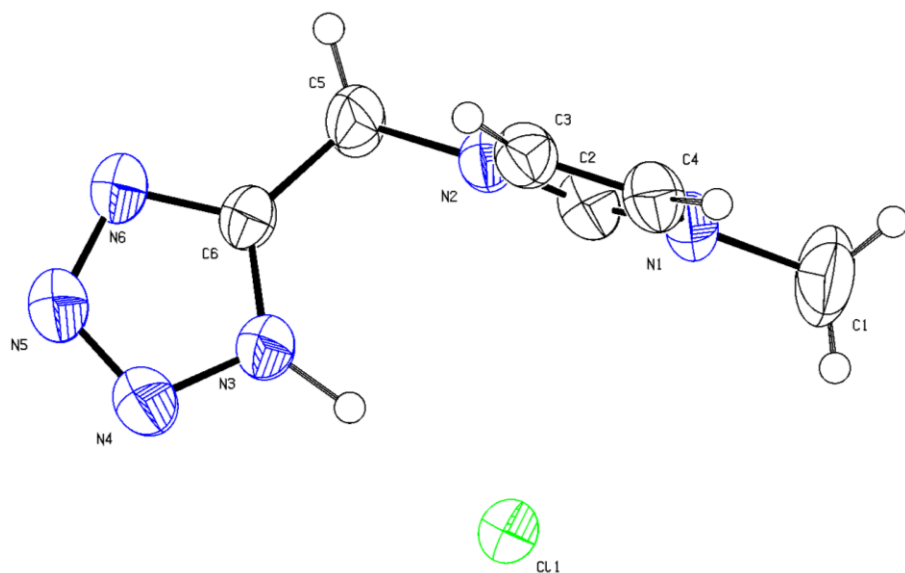
Figure D1.2 1-(5-1*H*-tetrazolyl)methyl-3-methylimidazolium chloride, **3**.
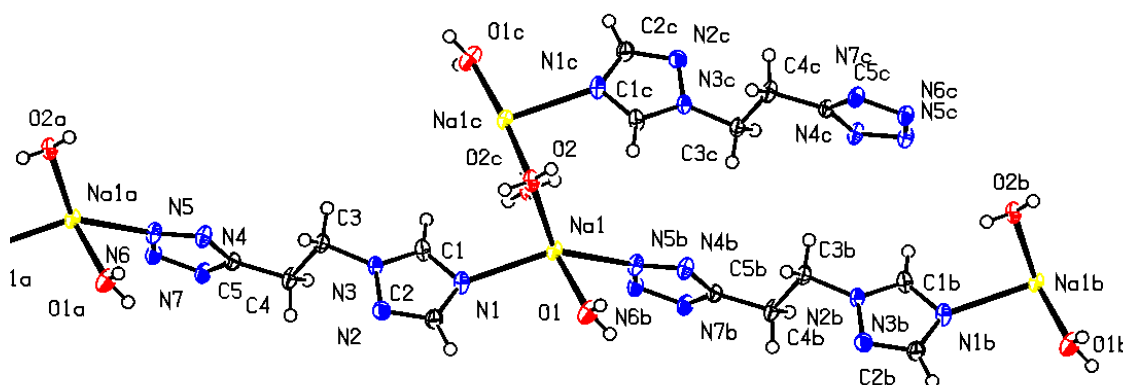
Figure D1.3 Sodium 5-(2-(1,2,4-triazol-1-yl)ethyl)tetrazolate, **7**.
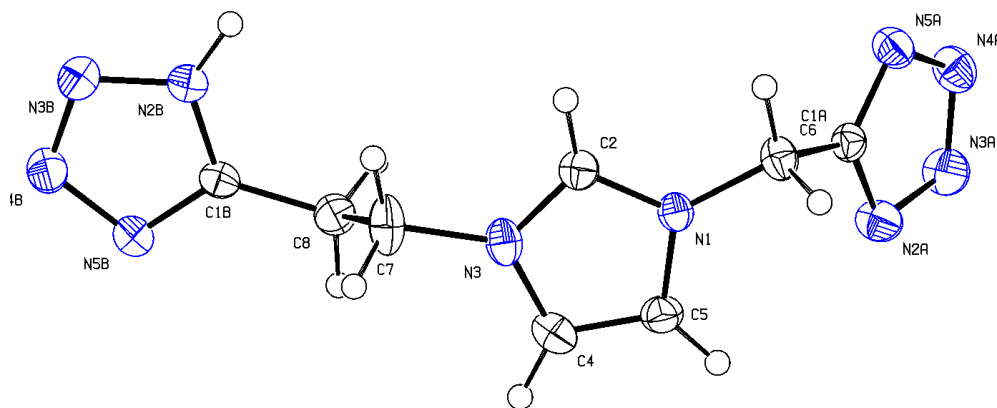
Figure D1.4 1-(2-(5-tetrazolidyl)ethyl)-3-(5-1*H*-tetrazolyl)methylimidazolium, **10**.

Synthesis of N-cyanoalkyl-functionalized imidazolium nitrate and dicyanamide ionic liquids with a comparison of their thermal properties for energetic applications
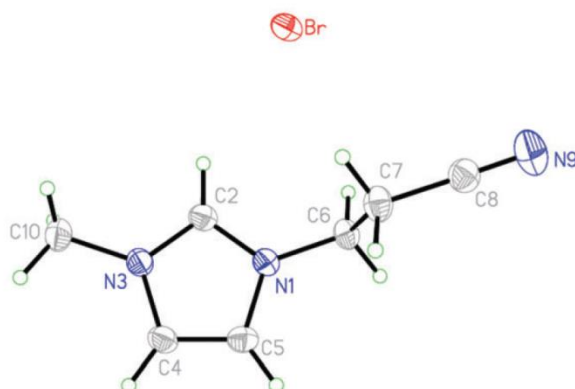
Figure D3.1 1-(2-cyanoethyl)-3-methylimidazolium bromide, 5[Br]
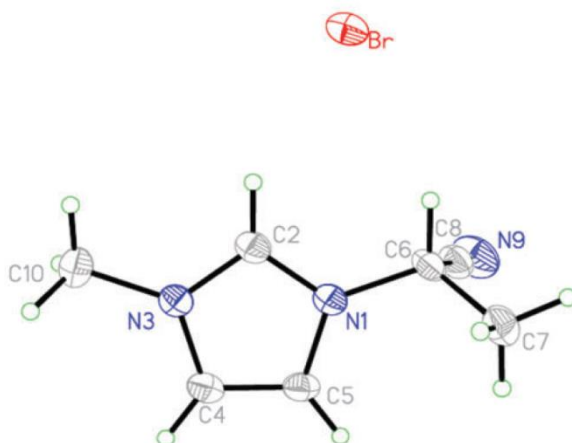
Figure D3.2 ,1-(1-Cyanoethyl)-3-methylimidazoium bromide, 10[Br]
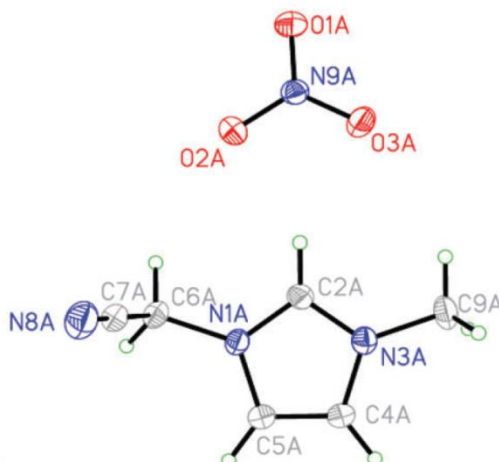
Figure D3.3 1-Cyanomethyl-3-methylimidazolium nitrate, 4[NO₃]
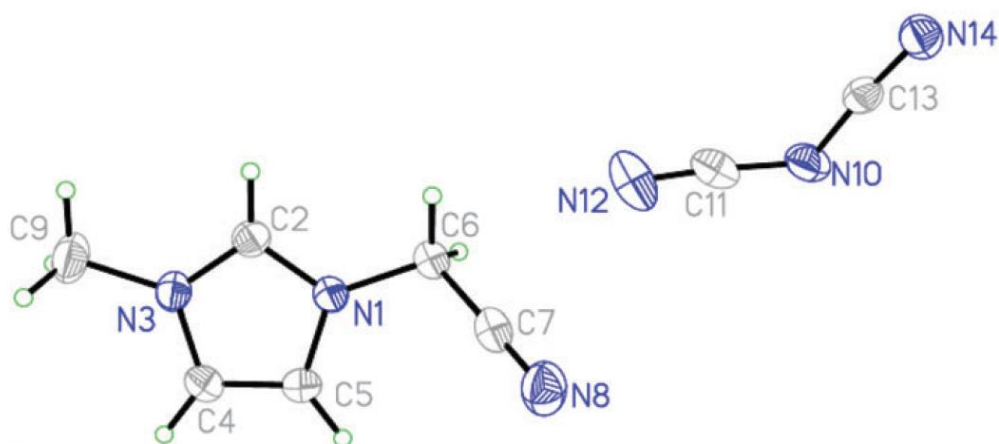
Figure D3.3 1-Cyanomethyl-3-methylimidazolium dicyanamide, 4[DCA]

D4. **Reactivity of N-cyanoalkyl-substituted imidazolium halide salts by simple elution through an azide anion exchange resin**
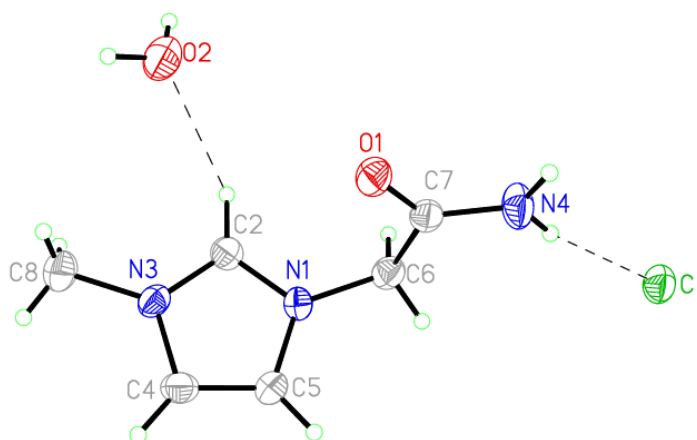
Figure D4.1 1--(acetamido)methyl -3-methylimidazolium chloride, 5[Cl]

D5. **Zinc-assisted synthesis of imidazolium-tetrazolate bi-heterocyclic zwitterions with variable alkyl bridge length**
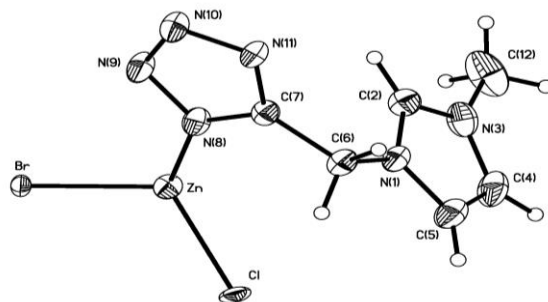
Figure D5.1 *catena*-poly[(bromochlorozinc)-*μ*-[1-(5-tetrazolato)-methyl-3-methylimidazolium]-N_1:N_4], 9

D6. <u>Synthesis, limitations, and thermal properties of energetically-substituted, protonated imidazolium picrate and nitrate salts and further comparison with their methylated analogs</u>
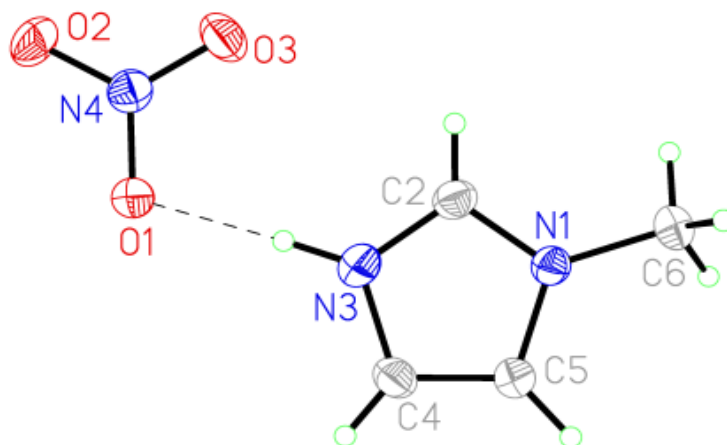
Figure D6.1 1-Methyl-3-H-imidazolium nitrate, 1b
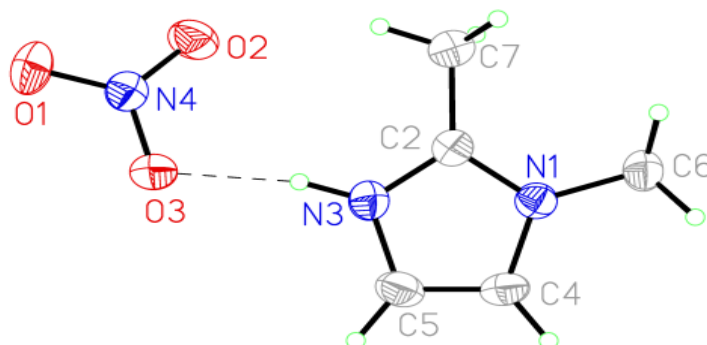
Figure D6.2 1,2-Dimethyl-3-H-imidazolium nitrate, 2b
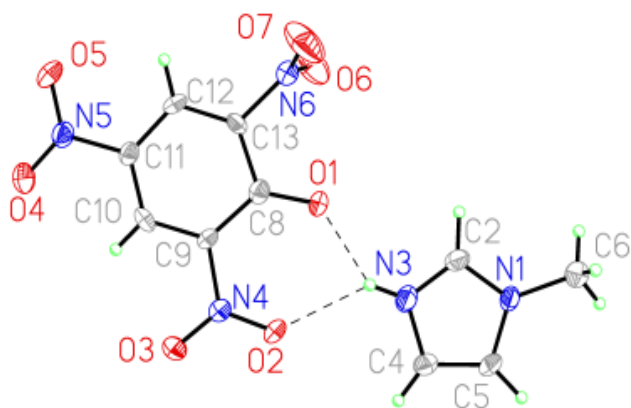
Figure D6.3 1-Methyl-3-H-imidazolium picrate, 1a
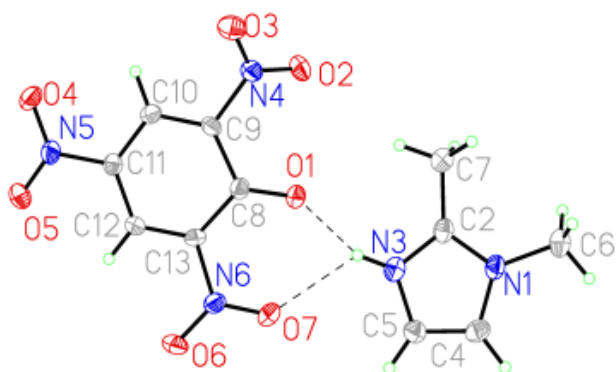
Figure D6.4 1,2-Dimethyl-3-H-imidazolium picrate, 2a
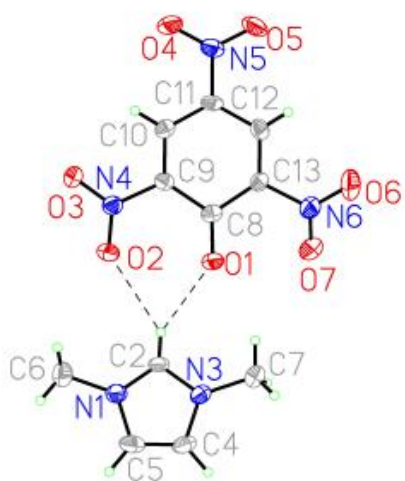
Figure D6.5 1,3-Dimethylimidazolium picrate, 19a
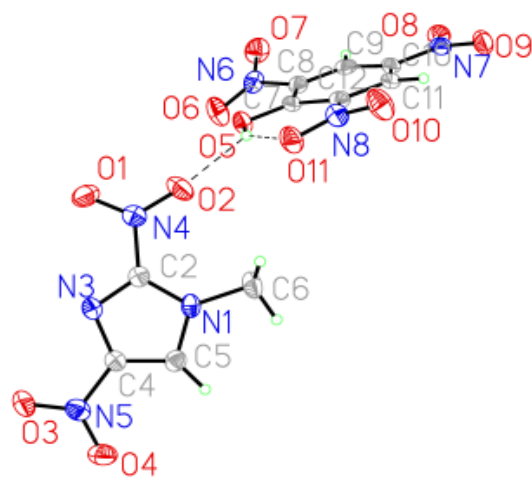
Figure D6.6 Co-crystal of 1-methyl-2,4-dinitroimidazole (16) and picric acid.
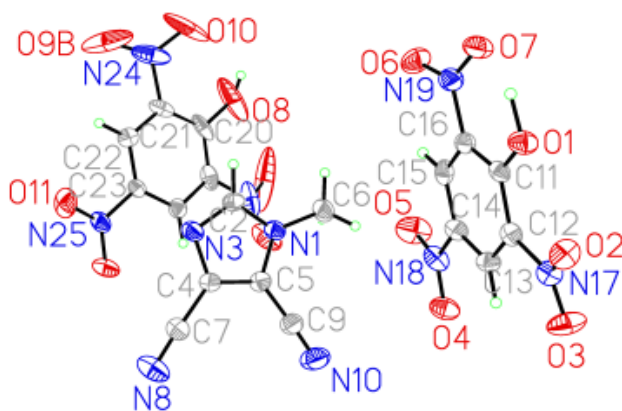

Figure D6.7 Co-crystal of 1-methyl-4,5-dicyanoimidazole (18) and two equivalents of picric acid.
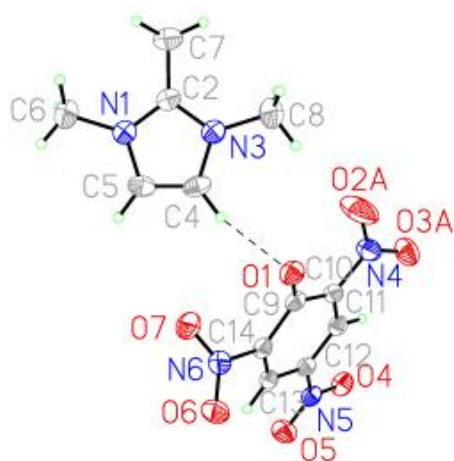
Figure D6.8 1,2,3-Trimethylimidazolium picrate, 20a

D7. **Azolium azolates from reactions of neutral azoles with 1,3-diemethyl-imidazolium-2-carboxylate, 1,2,3-trimethyl-imidazolium hydrogen carbonate, and N,N dimethyl-pyrrolidinium hydrogen carbonate**
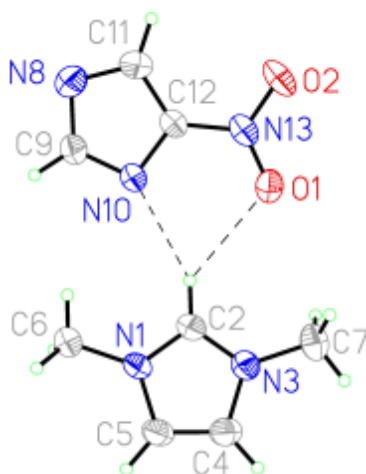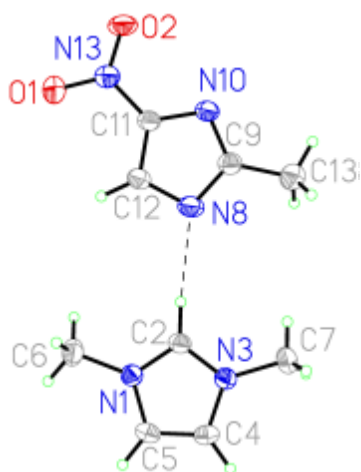

Figure D7.1 [1,3-diMe-Im][4-NO$_2$-Im], (1a)
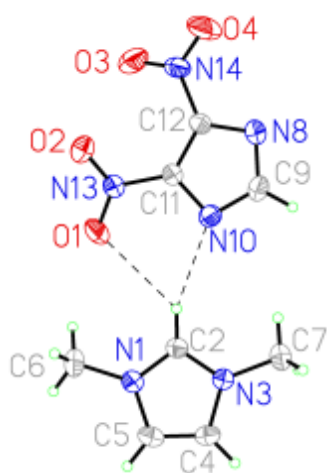
Figure D7.2 [1,3-diMe-Im][2-Me-5-NO₂-Im] (1b)
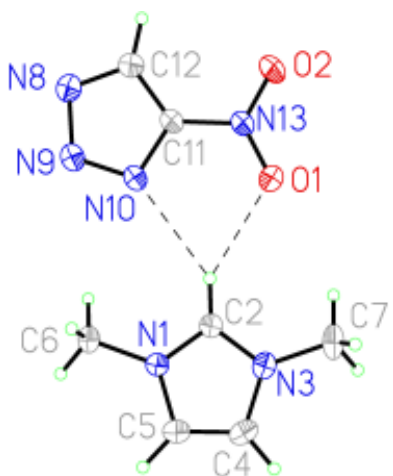

Figure D7.3 [1,3-diMe-Im][4,5-diNO₂-Im] (1c)

Figure D7.4 [1,3-diMe-Im][4-NO₂-Im] (1c)

Appendix E – Commonly Used Abbreviations

Cations

[1-R-3-R-Im]	1-R-3-R-Imidazolium salts where R is a substituted functional group. Definitions for commonly used R groups are defined within.
[1-R-3-R-4-R-Tri]	1-R-3-R-4-R-1,2,4-Triazolium based salts
[*N*-R-*N*-R-Pyr]	*N*-R-*N*-R-Pyrrolidinium based salts
[HEH]	Hydroxyethylhydrazinium
[1,3-diMe-Im-2-COO]	1,3-diMethyl-2-Carboxylate-Imidazolium

Anions

[Cl]	Chloride
[Br]	Bromide
[I]	Iodide
[NO_3]	Nitrate
[DCA]	Dicyanamide
[Pic]	Picrate
[HCO_3]	Hydrogen Carbonate
[5-NH_2-Tetr]	5-Amino-Tetrazolate
[4,5-DiCN-Im]	4,5-Dicyano-Imidazolate]
[4-NO_2-Im]	4-Nitro-Imidazolate
[2-Me-4-NO_2-Im]	2-Methyl-4-Nitro-Imidazolate
[4,5-diNO_2-Im]	4,5-Dinitro-Imidazolate
[4-NO_2-1,2,3-Tri]	4-Nitro-1,2,3-Triazolate
[3-NH_2-1,2,3-Tri]	3-Amino-1,2,3-Triazolate

Functional Groups – R

H	Proton
Me	Methyl
Et	Ethyl
Pr	Propyl
i-Pr	Isopropyl
Bu	Butyl
Pent	Pentyl
Hex	Hexyl
NO_2	Nitro
NH_2	Amino
CN	Cyano

References

1   M. A. Petrie, J. A. Sheehy, J. A. Boatz, G. Rasul, G. K. S. Prakash, G. A. Olah and K. O. Christie, *J. Am. Chem. Soc.*, 1997, **119**, 8802.
2   A. R. Katritzky, H. Yang, D. Zhang, K. Kirichenko, J. D. Holbrey, W. M. Reichert, M. Smiglak and R. D. Rogers, *New J. Chem.*, 2006, **30**, 349.
3   A. R. Katritzky, S. Singh, K. Kirichenko, J. D. Holbrey, M. Smiglak, W. M. Reichert and R. D. Rogers, *Chem. Commun.*, 2005, 868.
4   A. R. Katritzky, S. Singh, K. Kirichenko, M. Smiglak, J. D. Holbrey, W. M. Reichert, S. K. Spear and R. D. Rogers, *Chem. Eur. J.*, 2006, **12**, 4630.
5   M. Smiglak, W. M. Reichert, J. D. Holbrey, J. S. Wilkes, L. Sun, J. S. Thrasher, K. Kirichenko, S. Singh, A. R. Katritzky and R. D. Rogers, *Chem. Commun.*, 2006, 2554.
6   J. G. Huddleston, A. E. Visser, W. M. Reichert, H. D. Willauer, G. A. Broker and R. D. Rogers, *Green Chem.*, 2001, **3**, 156.
7   M. Smiglak, J. D. Holbrey, S. T. Griffin, W. M. Reichert, R. P. Swatloski, A. R. Katritzky, H. Yang, D. Zhang, K. Kirichenko and R. D. Rogers, *Green Chem.*, 2007, **9**, 90.
8   T. V. Artamonova, M. V. Zatsepina and, G. I. Koldobskii, *Russ. J. Org. Chem.*, 2004, **40**, 1318.
9   Z. P. Demko and K. B. Sharpless, *J. Org. Chem.,* 2001, **66**, 7945.
10   S. Schneider, T. Hawkins, M. Rosander, J. Mills, G. Vaghjiani and S. Chambreau, *Inorg. Chem.*, 2008, **47**, 6082.
11   E. W. Schmidt in *Hydrazine and Its Derivatives—Preparation, Properties, Applications*, Wiley, New York, 2nd edn., 1984, p.376.
12   S. Chambreau, C. Gallegos and G. Vaghjiani, *Abstracts of Papers*, 235th National ACS Meeting, New Orleans, LA, April 6-10, 2008; ACS: Washington DC, 2008; PHYS-312.
13   E. Blumenthal and E. Guth, U.S. Patent 3732694, 15 May, 1973.
14   T. N. Hubbuch, J. A. Murfree, Jr., W. A. Duncan, B. J. Sandlin and H. A. Nappier, U.S. Patent 3710573, 16 January 1973.
15   I. P. Contour and I. P.; Pannetier. *J. Catal.*, 1972, **24**, 434.
16   S. Hussain, D. Mattie and J. Frazier, *CPIA Publication*, 2002, 709.
17   K. E. Gutowski, B. Gurkan, S. Jayaraman and E. Maginn, *Abstracts of Papers*, 236th National ACS Meeting, Philadelphia, PA, August 17-21, 2008; ACS: Washington DC, 2008; IEC-146.
18   K. O. Knollmueller, S. Manke, F. W. Migliaro and E. F. Rothgery, U.S. Patent 5433802, 18 July, 1995.
19   Drake reports the synthesis of HEH nitrate salts in a patent1, but only NMR characterization is provided.
20   W. E. Armstrong, L. B. Ryland and H. H. Voge, U.S. Patent 4124538, 7 November, 1978.
21   T. W. Hawkins and G. W. Drake, private communication.
22   A. Lum and S. Tannenbaum, U.S. Patent 3658609, 25 April, 1972.
23   K. M. Johansson, E. I. Izgorodina, M. Forsyth, D. R. MacFarlane and K. R. Seddon, *Phys. Chem. Chem. Phys.*, 2008, **10**, 2972.
24   K. Bica and R. D. Rogers, *Chem. Commun.*, 2010, **46**, 1215.
25   A. R. Katritzky, S. Singh, K. Kirichenko, J. D. Holbrey, M. Smiglak, W. M. Reichert and R. D. Rogers, *Chem. Commun.*, 2005, 868.
26   A. R. Katritzky, S. Singh, K. Kirichenko, M. Smiglak, J. D. Holbrey, W. M. Reichert, S. K. Spear and R. D. Rogers, *Chem.–Eur. J.*, 2006, **12**, 4630.
27   A. R. Katritzky, H. Yang, D. Zhang, K. Kirichenko, M. Smiglak, J. D. Holbrey, W. M. Reichert and R. D. Rogers, *New J. Chem.*, 2006, **30**, 349.
28   M. Smiglak, N. J. Bridges, M. Dilip and R. D. Rogers, *Chem.–Eur. J.*, 2008, **36**, 11314.
29   M. Smiglak, C. C. Hines, T. B. Wilson, S. Singh, A. S. Vincek, K. Kirichenko, A. R. Katritzky and R. D. Rogers, *Chem.–Eur. J.*, 2010, **16**, 1572.
30   Y. Gao, H. Gao, C. Piekarski and J. M. Shreeve, *Eur. J. Inorg. Chem.*, 2007, 4965.
31   J. G. Huddleston, A. E. Visser, W. M. Reichert, H. D. Willauer, G. A. Broker and R. D. Rogers, *Green Chem.*, 2001, **3**, 156.
32   J. D. Holbrey and K. R. Seddon, *J. Chem. Soc., Dalton Trans.*, 1999, 2133.
33   C. Oommen and S. R. Jain, *J. Hazard. Mater.*, 1999, **67**, 253.
34   D. R. MacFarlane, J. Golding, S. Forsyth, M. Forsyth and G. B. Deacon, *Chem. Commun.*, 2001, 1430.

35 D. M. Drab, J. L. Shamshina, M. Smiglak, C. C. Hines, D. B. Cordes and R. D. Rogers, *Chem. Commun.*, 2010, **46**, 3544.

36 P. B. Hitchcock, K. R. Seddon and T. Welton, *J. Chem. Soc., Dalton Trans.*, 1993, 2639.

37 H. Olivier-Bourbigou and F. Favre, in *Ionic Liquids in Synthesis*, ed. P. Wasserscheid and T. Welton, Wiley-VCH, New York, 2008, 2nd edn, pp. 490–491.

38 I. M. Dinarès, C. G. Ibáñez, N. Mesquida and E. Alcalde E. *Green Chem.,* 2009, **11**, 1507.

39 D. M. Drab, M. Smiglak, J. L. Shamshina, S. P. Kelley, S. Schneider, T. W. Hawkins and R. D. Rogers, *New J. Chem.,* 2011, **35**, 1701.

40 H. Hassner and M. Ster, *Angew. Chem. Int. Ed.*, 1986, **25**, 478.

41 (*a*) A. R. Cherkasov, V. I. Galkin and R. A. Cherkasov, *J. Phys. Org. Chem.,* 1998, **11**, 437; (*b*) O. Exner, *J. Phys. Org. Chem.,* 1999, **12**, 265.

42 F. Himo, Z. P. Demko, L. Noodleman and K. B. Sharpless, *J. Am. Chem. Soc.,* 2002, **124**, 12210.

43 M. Adcock and T. C. Khor, *J. Org. Chem.,* 1978, **43**, 1272.

44 G. J. Loew, S. Chang and D. Berkowitz, *J. Mol. Evol.,* 1975, **5**, 131.

45 J. Lee, M. Kim, S. Chang and H. Y. Lee, *Org. Lett.,* 2009, **11**, 5598.

46 M. Lakshman, D. V. Nadkarni and R. E. Lehr, *J. Org. Chem.,* 1990, **55**, 4892.

47 Z. P. Demko and K. B. Sharpless, *J. Org. Chem.,* 2001, **66**, 7945.

48 D. M. Drab, J. L. Shamshina, M. Smiglak, C. C. Hines, D. B. Cordes and R. D. Rogers, *Chem. Commun.,* 2010, **46**, 3544.

49 A. R. Katritzky, S. Singh, K. Kirichenko, M. Smiglak, J. D. Holbrey, W. M. Reichert, S. K. Spear and R. D. Rogers, *Chem. – Eur. J.,* 2006, **12**, 4630.

50 M. Smiglak, C. C. Hines, T. B. Wilson, S. Singh, A. S. Vincek, K. Kirichenko, A. R. Katritzky and R. D. Rogers, *Chem. – Eur. J.,* 2010, **16**, 1572.

51 G. I. Koldobskii, *Russ. J. Org. Chem.,* 2006, **42**: 469.

52 D. M. Drab, M. Smiglak, J. L. Shamshina, S. P. Kelley, S. Schneider, T. W. Hawkins and R. D. Rogers, *New J. Chem.,* 2011, **35**, 1701.

53 F. Himo, Z. P. Demko, L. Noodleman, K. B. Sharpless, *J. Am. Chem. Soc.,* 2002, **124**, 12210.

54 D. Amantini, R. Beleggia, F. Fringuelli, F. Pizzo and L. Vaccaro, *J. Org. Chem.,* 2004, **69**, 2896.

55 B. Schmidt, D. Meid and D. Kieser, *Tetrahedron*, 2007, **63**, 492.

56 F. Himo, Z. P. Demko, L. Noodleman and K. B. Sharpless, *J. Am. Chem. Soc.,* 2003, **125**, 9983.

57 Q. Zhang, Z. Li, J. Zhang, S. Zhang, L. Zhu, J. Yang, X. Zhang and Y. Deng, *J. Phys. Chem. B,* 2007, **111**, 2864.

58 T. J. Wooster, K. M. Johanson, K. J. Fraser, D. R. MacFarlane and J. L. Scott, *Green Chem.,* 2006, **8**, 691.

59 D. R. MacFarlane, S. A. Forsyth, J. Golding and G. B. Deacon, *Green Chem.,* 2002, **4**, 444.

60 A. M. Golub, H. Kohler and V. V. Skopenko, In *Chemistry of Pseudohalides*; Elsevier: Berlin, 1986.

61 A. R. Katritzky, H. Yang, D. Zhang, K. Kirichenko, M. Smiglak, J. D. Holbrey, W. M. Reichert and R. D. Rogers, *New J. Chem.*, 2006, **30**, 349.

62 S. Schneider, T. Hawkins, M. Rosander, G. Vaghjiani, S. Chambreau and G. W. Drake, *Energy Fuels,* 2008, **22**, 2871.

63 L. He, G. Tao, D. A. Parrish and J. M. Shreeve, *Chem. Eur. J.,* 2010, **16**, 5736.

64 S. Schneider, T. Hawkins, Y. Ahmed, M. Rosander, L. Hudgens and J. Mills, *Angew. Chem. Int. Ed.*, 2011, **50**, 5886.

65 L. G. Sanchez, J. R. Espel, F. Onink, G. W. Meindersma and A. B. de Haan, *J. Chem. Eng. Data,* 2008, **54**, 2803.

66 V. N. Emel'yanenko, S. P. Verevkin and A. Heintz, *J. Am. Chem. Soc.,* 2007, **129**, 3930.

67 J. D. Clark, *Ignition: An Informal History of Liquid Rocket Propellants*; Rutgers University Press: New Brunswick, NJ, 1972.

68 J. Dupont, G. S. Fonseca, A. P. Umpierre, P. F. P. Fichtner and S. R. Teixeira, *J. Am. Chem. Soc.,* 2002, **124**, 4228.

69 A. S. Pensado and A. A. H. Padua, *Angew. Chem. Int. Ed.,* 2011, **50**, 8683.

70 J. C. Rubim, F. A. Trindade, M. A. Gelesky, R. F. Aroca, J. Dupont,. *J. Phys. Chem. C*, 2008, **112**, 19670.

71 N. J. Bridges, A. E. Visser and E. B. Fox, *Energy Fuels*, 2011, **25**, 4852.

72 A. Macek and J. M. Semple, *Combust. Sci. Technol.,* 1969, **1**, 181.

73 G. Young, K. Sullivan, M. R. Zachariah and K. Yu, *Combust. Flame,* 2009, **156**, 322.

74 D. Dreizin, D. G. Keil and W. Felder, *Combust. Flame,* 1999, **119**, 272.

75   B. Van Devener, J. P. L. Perez and S. L. Anderson, *J. Mater. Res.,* 2009, **24**, 3462.

76   B. Van Devener, J. P. L. Perez, J. Jankovich and S. L. Anderson, *Energy Fuels,* 2009, **23**, 6111.

77   Y. Zhang, H. Gao, Y.Joo and J.M. Shreeve, *Angew. Chem. Int. Ed.*, 2011, **50**, 9554.

78   K. K. Kuo, G. A. Risha, B. J. Evans and E. Boyer, *Mat. Res. Soc. Symp. Proc.*, 2004, **800**, 3.

79   J. Dupont and J. D. Scholten, *Chem. Soc. Rev.*, 2010, **39**, 1780

80   H. Itoh, K. Naka and Y. Chujo, *J. Am. Chem. Soc.*, 2004, **126**, 3026.

81   F. Endres, A. P. Abbott, and D. MacFarlane in *Electrodeposition from Ionic Liquids*, ed. F. Endres, D. MacFarlane and A. Abbott, Wiley-VCH Verlag GmbH & Co. KGaA, Weinheim, Germany, 2008, ch.13, 369-377.

82   N. J. Bridges, A. E. Visser and E. B. Fox, *Energy Fuels*, 2011, **25**, 4862.

83   J. Dupont, G. S. Fonseca, A. P. Umpierre, P. F. P. Fichtner and S. R. Teixeira, *J. Am. Chem. Soc.*, 2002, **124**, 4228.

84   P. D. McCrary, P. A. Beasley, O. A. Cojocaru, S. Schneider, T. W. Hawkins, J. P. L. Perez, B. W. McMahon, M. Pfeil, J. A. Boatz, S. L. Anderson, S. F. Son and R. D. Rogers, *Chem. Commun.*, 2012, **48**, 4311.

85   S. A. Stratton, K. L. Luska and A. Moores, *Catalysis Today*, 2012, **183**, 96.

86   K. L. Luska and A. Moores, *Adv. Synth. Catal.*, 2011, **353**, 3167.

87   M. Smiglak, C. C. Hines, T. B. Wilson, S. Singh, A. S. Vincek, K. Kirichenko, A. R. Katritzky and R. D. Rogers, *Chem. Eur. J.*, 2010, **16**, 1572.

88   (a) T. L. Cottrell, *The Strengths of Chemical Bonds,* 2nd ed., Butterwoth, London, 1958.; (b) B. deB. Darwent, National Standard Reference Data Series, National Bureau of Standards, no. 31, Washington, 1970; (c) S. W. Benson, *J. Chem. Educ.,* 1965, **42**, 502.

89   E. F. Smith, I. J. Villar-Garcia, D. Briggs and P. License, *Chem. Commun.*, 2005, 5633.

90   E. F. Smith, F. J. M. Rutten, I. J. Villar-Garcia, D. Briggs and P. License, *Langmuir*, 2006, **22**, 9386.

91   F. Bernardi, J. D. Scholten, G. H. Fecher, J. Dupont and J. Morais, *Chem. Phys. Lett.*, 2009, **479**, 113.

92   J. F. Moulder, W. F. Stickle, P. E. Sobol and K. D. Bomben, Handbook of X-ray Photoelectron Spectroscopy, 2nd ed. Perkin-Elmer Corp., Eden Prairie, MN, 1992.

93   Y. Shi and L.-J. Li, *J. Mater. Chem.,* 2011, **21**, 3277.

94   J. L. Sabourin, R. A. Yetter and V. S. Parimi, *J. Prop. Power*, 2010, **26**, 1006.

95   J. L. Sabourin, D. M. Dabbs, R. A. Yetter, F. L. Dryer and I. A. Aksay, *ACS Nano,* 2009, **3**, 3945.

96   "Exfoliation of Graphite using Ionic Liquids": R. M. Frazier, D. T. Daly, S. K. Spear and R. D. Rogers, U.S. Provisional Patent, November 25, 2008; PCT Int. Appl. WO, 2010065346 A1, June 10, 2010.

97   X. Wang, P. F. Fulvio, G. A. Baker, G. M. Veith, R. R. Unocic, S. M. Mahurin, M. Chi and S. Dai, *Chem. Commun.,* 2010, **46**, 4487.

98   X. Zhou, T. Wu, K. Ding, B. Hu, M. Hou and B. Han, *Chem. Commun.,* 2010, **46**, 386.

99   J. D. Clark, *Ignition: An Informal History of Liquid Rocket Propellants*; Rutgers University Press, New Brunswick, NJ, **1972**.

100   C. K. Law, *AIAA J.,* 2012, **50**, 19.

101   K. C. Back, V. L. Carter, Jr. and A. A. Thomas, *Aviat. Space Envir. Md.*, 1978, **49**, 591.

102   D. R. MacFarlane, J. Golding, S. Forsyth, M. Forsyth and G. B. Deacon, *Chem. Commun.,* 2001, 1430.

103   J. Pu, S. Wan, W. Zhao, Y. Mo, X. Zhang , L. Wang and Q. Xue, *J. Phys. Chem. C,* 2011, **115**, 13275.

104   P. D. McCrary, P. A. Beasley, O. A. Cojocaru, S. Schneider, T. W. Hawkins, J. P. L. Perez, B. W. McMahon, M. Pfeil, J. A. Boatz, S. L. Anderson, S. F. Son and R. D. Rogers, *Chem. Commun.*, 2012, **48**, 4311.

105   S. Stankovich, D. A. Dikin, R. D. Piner, K. A. Kohlhaas, A. Kleinhammes, Y. Jia, Y. Wu, S. T. Nguyen and R. S. Ruoff, *Carbon,* 2007, **45**, 1558.

106   G. Kamath and G. A. Baker, *Phys. Chem. Chem. Phys.,* 2012, **14**, 7929.

107   S. Park and R. S. Ruoff, *Nat. Nanotechnol.,* 2009, **4**, 217.

108   M. Acik, D. R. Dreyer, C. W. Bielawaski and Y. J. Chabal, *J. Phys. Chem. C*, 2012, **116**, 7867.

109   F. Macaev, K. Gavrilov, V. Muntyanu, E. Styngach, L. Vlad, L. Bets, S. Pogrebnoi and A. Barba, *Chem. Nat. Compd.,* 2007, **43**, 136.

110   C. G. Begg, M. R. Grimmett and P. D. Wethey, *Aust. J. Chem.*, 1973, **11**, 2435.

111   B. Lenarcik and P. Ojczenasz, *J. Het. Chem.*, 2002, **39**, 287.

112   H. Ohno, M. Yoshizawa and W. Ogihara, *Electrochim. Acta,* 2004, **50**, 255.

113   Z. Szulc and J. Mlochowski, *Pol. J. Chem.,* 1986, **60**, 615.

114   J. G. Huddleston, A. E. Visser, W. M. Reichert, H. D. Willauer, G. A. Broker and R. D. Rogers, *Green Chem.,* 2001, **3**, 156.

115   L. Cammarata, S. G. Kazarian, P. A. Salter and T. Welton, *Phys. Chem. Chem. Phys.,* 2001, **3**, 5192.

116 B. Van Devener, J. P. L. Perez, S. L. Anderson, *J. Mater. Res.* 2009, **24**, 3462.

117 B. Van Devener, J. P. L. Perez, J. Jankovich, S. L. Anderson, *Energy Fuels* 2009, **23**, 6111.

118 *SHELXTL, structure determination software suite,* v.6.14., G. M. Sheldrick, Bruker AXS Inc: Madison, WI., 2003 (Accessed September 18th 2013).

119 *SHELXL,* version 2013/4, G. M. Sheldrick, 2013 (accessed September 18th 2013).

120 *SHELXD,* version 2013/2, G. M. Sheldrick, 2013 (accessed September 16th 2013).

121 F. Macrae, I. J. Bruno, J. A. Shisholm, P. R. Edgington, P. McCabe, E. Picock, L. Rodriguez-Monge, R. Taylor, J. van de Streek, and P. A. Wood, *J. Appl. Cryst.*, 2008, **41**, 4660.